Canada

STUDENT FIELD EXCURSION

Sudbury Igneous Complex

July 25 - August 10, 2019

ETH Zürich, Switzerland

Abitibi Greenstone Belt

SEG Student Chapter
ETH Zürich

Photo of mine: tunnel of a Sudbury mine; https://www.northeasternontario.com/partner/dynamic-earth/
Photo of sample: gold from Lamaque mine; https://www.mindat.org/loc-14001.html

Canada Field Trip Guide

Contributions

The contributions to the field guide were compiled from the literature by the students of the society of economic geologists (SEG) student chapter of ETH Zürich, who take responsibility for correct referencing of data sources, to the best of their knowledge. There is no own research beyond the literature study involved.

Editing by Alina Fiedrich and Michael Schirra, formatting by Alina Fiedrich, front page design by Julian Reyes.

Support

We gratefully acknowledge the financial support by Glencore, the Institute of Geochemistry and Petrology of ETH Zürich, and the Society of Economic Geologists, and we appreciate the logistical and scientific support of the SEG student chapter of Laurentian University, Richard James and Shirley Péloquin, Ed van Hees, Jean Goutier, Pierre Bedeaux, and the many helpful employees of Glencore, Agnico Eagle, and Eldorado Gold.

Table of Contents

Participants

Name	Association	E-mail address
Benz, Jean-Marc [2]	MSc student, ETHZ	jbenz@student.ethz.ch
Bulcewicz, Kamil	BSc student, University of Wroclaw	kamil.bulcewicz@gmail.com
Castellanos, Maria Paula [2]	MSc student, ETHZ	casmaria@student.ethz.ch
Dmitrovskii, Andrei	MSc student, ETHZ	dmandrei@student.ethz.ch
Etter, Andreas	BSc student, ETHZ	aetter@student.ethz.ch
Fiedrich, Alina [1]	PhD student, ETHZ	alina.fiedrich@erdw.ethz.ch
Halter, William [2]	MSc student, ETHZ	william_halter@hotmail.com
Khan, Dean	PhD student, ETHZ	dean.khan@erdw.ethz.ch
Klimentyeva, Dina	PhD student, ETHZ	dina.klimentyeva@erdw.ethz.ch
Reyes, Julian [1,2]	MSc student, ETHZ	rejulian@student.ethz.ch
Roodpeyma, Taraneh	PhD student, ETHZ	taraneh.roodpeyma@erdw.ethz.ch
Schirra, Michael [1,2]	PhD student, ETHZ	michael.schirra@erdw.ethz.ch
Velojic, Milos	PhD student, University of Belgrade	milos.velojic@rgf.bg.ac.rs
Viher, Florian [2]	MSc student, ETHZ	viherf@student.ethz.ch
Zabihian, Farid	research associate, ETHZ	faridzabihian69@gmail.com

[1] organizers, [2] drivers

General Information

Do not forget:

☐ field guide
☐ valid passport
☐ Ausländerausweis - to return to Switzerland
☐ (international) student card - for discounts
☐ driver‘s license (European or Swiss)
☐ international driver‘s license (if available)
☐ credit card for personal purchases
☐ info about health & accident insurance (must be valid in Canada!) in case of emergency

☐ solid shoes (e.g. hiking boots)
☐ safety boots (steel-cap) if available
☐ high-visibility vest if available
☐ comfortable shoes (sneakers)
☐ field clothes (long sleeves, nothing fancy)
☐ rain gear
☐ sunscreen, bug spray
☐ towel (for hostels and mines)

☐ field note book & pencils
☐ camera
☐ hand lens
☐ hammer, pocket knife, magnet, etc.
☐ sampling bags, sharpie
☐ water bottle
☐ small present for the people who will guide and help us during the field trip

In case of emergency:

911 - police, ambulance, fire brigade

Climate in Ontario / Québec

Sudbury:

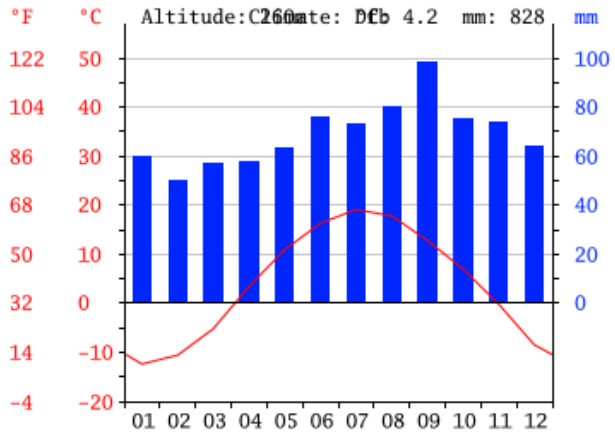

Val-d‘Or:

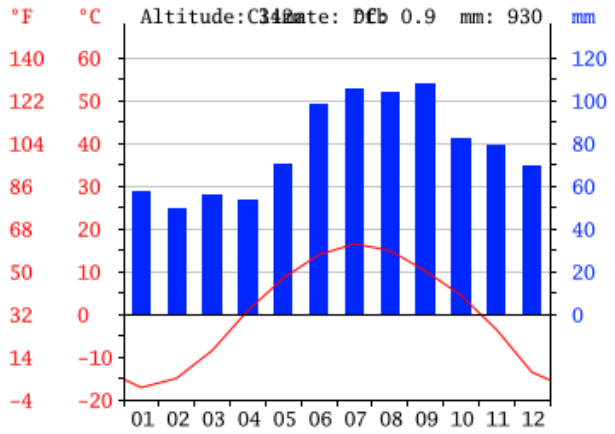

https://en.climate-data.org/north-america/canada/...

Field trip program

Date	Program	Guide	Accommodation
Thu, 25.07.	Arrival in Toronto	-	Humber College North Campus Residence, Toronto
Fri, 26.07.	Drive to Sudbury (ca. 11 am - 4 pm); meeting with Laurentian student chapter & geology club (6 pm); dinner with Laurentian students and alumni (7 pm)	1	Residence & Conference Centre Sudbury West
Sat, 27.07.	Outcrops around Sudbury, focus on Sudbury Igenous Complex (8:30 am); dinner with S. Yarrow (6:30 pm)	2	
Sun, 28.07.			
Mon, 29.07.	Presentation & underground tour at Nickel Rim South (6:30 am); drillcore at Norman West exploration project (1 pm); dinner with S. Yarrow (7 pm)	3, 4	
Tue, 30.07.	Smelter tour (8:15 am); Onaping Depth presentation (11:45 am); core-logging exercise (1:30 pm)	5, 4	
Wed, 31.07.	Mill tour and remediation (7:30 am); XPS facilities visit (12 pm); surface visit to Barnet Showing with mapping exercise (1 pm) including filming with Glencore	6, 7	The Senator Hotel & Conference Center, Timmins *
Thu, 01.08.	Kidd Creek underground mine visit (6:30 am); dinner with Y. Jost (6 pm)	8	
Fri, 02.08.	Kidd Creek mine visit, drillcore and presentations (7:30 am); presentation about the Porcupine Camp geology (6 pm); dinner with E. Archibald and Kidd Creek team (7 pm)	8, 9	
Sat, 03.08.	Outcrops around Timmins (8 am)	9	Comfort Inn Rouyn-Noranda *
Sun, 04.08.	Geological hike around historic mining town Cobalt (optional); presentation about the Blake River Group geology (7 pm); dinner with J. Goutier (7 pm)	-, 10	
Mon, 05.08.	Outcrops of the Blake River group (8 am)	10	
Tue, 06.08.	Horne smelter visit (9 am); LaRonde mine visit - surface only (2 pm); dinner with P. Bedeaux (8 pm)	11, 12	
Wed, 07.08.	Outcrops of the Cadillac fault, Rouyn-Noranda (8:30 am)	13	Comfort Inn Val D'Or *
Thu, 08.08.	Outcrops of the Cadillac fault, Val-d'Or (8:30 am); Canadian Malartic open pit visit (1 pm)	13, 14	
Fri, 09.08.	Lamaque underground mine visit (8:30 am - 12 noon); drive back to Toronto (1 pm - 10 pm)	15	Humber College North Campus Residence, Toronto
Sat, 10.08.	Return flight	-	

* breakfast includ

mine visits
outcrops in the field
non-geological

Guides:

1 Charlotte Stone (student, Laurentian University)
2 Shirley Péloquin (Sudbury district geologist),
Richard James (professor em., Laurentian University)
3 Dave Richardson (geologist at NiRimS)
4 Brad Lazich (exploration geologist)
5 Mike Sweeny (exploration geologist),
Sari Muinonen (process technologist, smelter)
6 Leigh Allen (field geologist),
Julie Coffin (mill geologist, Strathcona Mill)
7 Paul Wawrzonkowski, Mike Sweeny (exploration geologists)
8 Eric Archibald (production engineer) and colleagues
9 Ed van Hees, Pierre Bousquet (Timmins district geologists)
10 Jean Goutier (retired geologist, Ministry of Energy and Natural Resources, Québec)
11 Yves Prévost (metallurgist)
12 Roxanne Jacobs, David Pitre (exploration geologists)
13 Pierre Bedeaux (researcher at UQAC)
14 Christian Tessier (mine geologist)
15 Émilie Gagnon (mine geologist)

Route

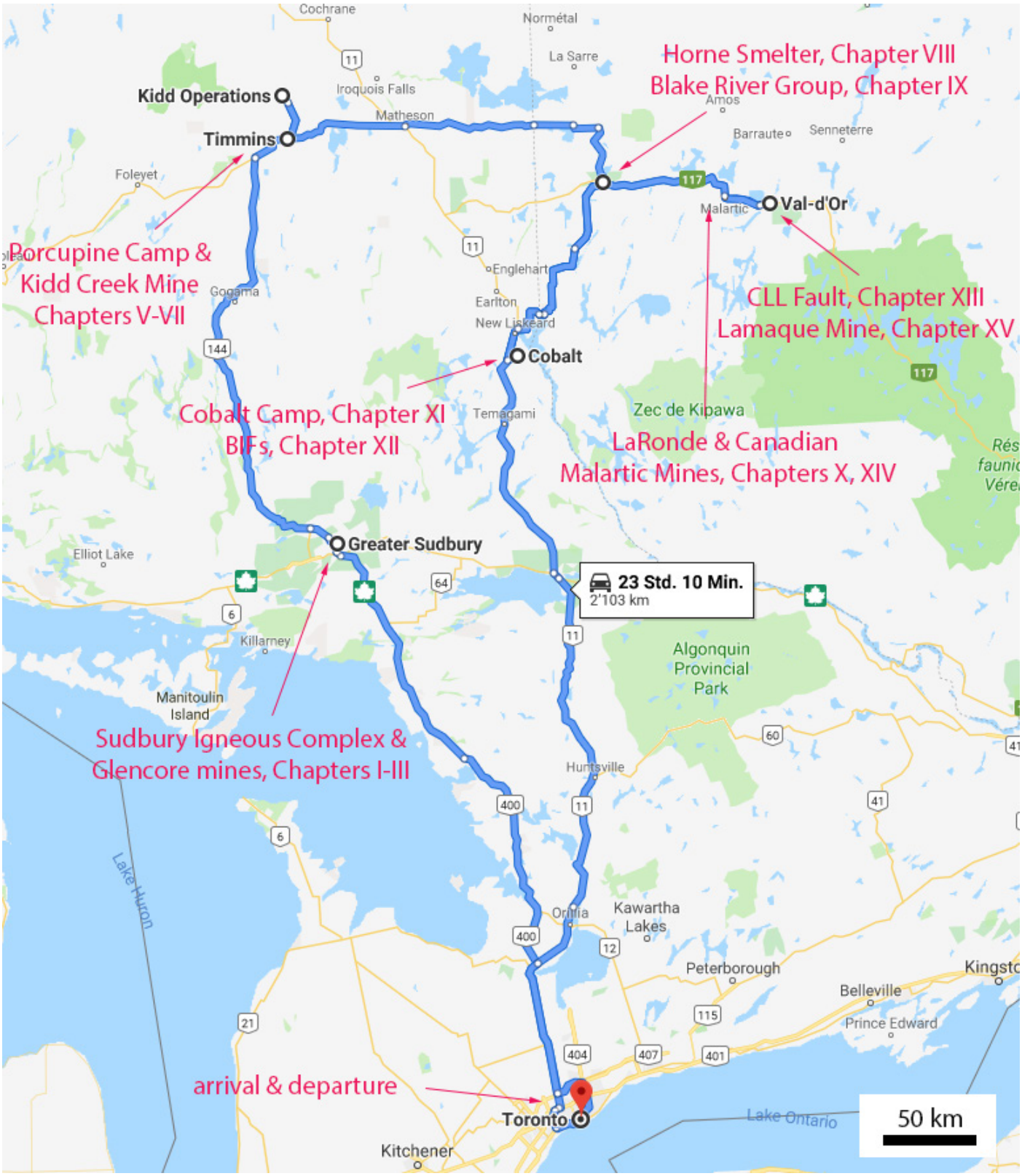
Horne Smelter, Chapter VIII
Blake River Group, Chapter IX
Porcupine Camp &
Kidd Creek Mine
Chapters V-VII
CLL Fault, Chapter XIII
Lamaque Mine, Chapter XV
Cobalt Camp, Chapter XI
BIFs, Chapter XII
LaRonde & Canadian
Malartic Mines, Chapters X, XIV
Sudbury Igneous Complex &
Glencore mines, Chapters I-III
arrival & departure
Kidd Operations
Timmins
Cobalt
Greater Sudbury
Toronto
Val-d'Or
23 Std. 10 Min.
2'103 km
50 km
Cochrane
Normétal
La Sarre
Iroquois Falls
Matheson
Amos
Barraute
Senneterre
Foleyet
Malartic
Englehart
Gogama
Earlton
New Liskeard
Temagami
Zec de Kipawa
Elliot Lake
Killarney
Manitoulin
Island
Algonquin
Provincial
Park
Huntsville
Lake Huron
Orillia
Kawartha
Lakes
Peterborough
Belleville
Prince Edward
Kingsto
Lake Ontario
Kitchener

Addresses

Hotels

Humber College North Campus Residence:
203 Humber College Boulevard, Etobicoke, Toronto, ON M9W 6V3
GPS: 43.726555, -79.606813

Residence & Conference Centre - Sudbury West:
21 Lasalle Boulevard, Sudbury ON P3A 6B1
GPS: 46.516399, -80.992074

The Senator Hotel & Conference Center:
14 Mountjoy St S, Timmins, ON P4N 1S4
GPS: 48.475759, -81.335610

Comfort Inn Rouyn-Noranda:
1295 Av Lariviere, Rouyn-Noranda, QC J9X 6M6
GPS: 48.223218, -78.990578

Comfort Inn Val-d'Or:
1665 3ième Av, Val-d'Or, QC J9P 1V9
GPS: 48.099457, -77.815158

Mines & others

Laurentian University, Harquail School of Mines
Willet Green Miller Centre, 935 Ramsey Lake Rd, Sudbury, ON P3E 2C6
GPS: 46.470443, -80.974554

Sudbury INO Nickel Rim South:
Garson, ON P3L 1V3, at Victor Mine Rd
GPS: 46.659164, -80.796946

Norman West Drill Site:
north of Capreol, at route 84
GPS: 46.757234, -80.928177

Onaping Levack Site / Strathcona Mill:
meet at First Aid Security northeast of Onaping
ON P0M 1R0
GPS: 46.633484, -81.381058 (Onaping)
GPS: 46.673034, -81.341812 (Mill)

Sudbury Smelter (Sudbury INO):
meet at smelter gate
1 Longyear Drive, Greater Sudbury, ON P0M 1S0
GPS: 46.576835, -80.808626

Barnet outcrops:
start from Strathcona Mill
GPS: 46.687918, -81.330484

Kidd Creek Mine:
11335 Highway 655 North, Timmins, ON P4N 7K1
GPS: 48.690016, -81.373248

Horne Smelter:
101 Avenue Portelance, C.P. 4000, Rouyn-Noranda, QC J9X 5B6
GPS: 48.252116, -79.016181

Cobalt Mining Museum:
24 Silver St, Cobalt, ON P0J 1C0
GPS: 47.395323, -79.686059

LaRonde Mine:
10 200 Route de Preissac, Rouyn-Noranda, QC J0Y 1C0
GPS: 48.247380, -78.438884

Canadian Malartic Mine:
100 Chemin du Lac Mourier, Malartic, QC J0Y 1Z0
GPS: 48.111738, -78.131734

Lamaque Mine:
1000 Voie de Service Goldex-Manitou, Val-d'Or, QC J9P 4P4
GPS: 48.076532, -77.742013

I Sudbury Igneous Complex: general geology

Maria Paula Castellanos

Introduction

The Sudbury Igneous Complex (SIC) is located in the Canadian Precambrian Shield at the boundary of the Archean Superior and the Proterozoic Southern Provinces. It formed as a result of a meteorite impact into Early Proterozoic meta-volcanic and –sedimentary rocks at 1850 Ma (Lightfoot & Zlotov, 2005 and references therein). Extreme temperature and pressure conditions during this impact event led to the production of a 2-2.5 km thick sheet of overheated crustal melt, which filled the crater and subsequently exsolved an immiscible sulphide melt (Marsh & Zieg, 1999; Riller, 2005). The original size of the crater has been estimated to be around 200-250 km^2. This well-preserved meteorite impact structure represents a unique ore-forming setting containing some of the biggest orthomagmatic Ni-Cu-PGE deposits on Earth (e.g. Lightfood, 2016).

Geological framework

The SIC consists mainly of deformed layered sheets and can be subdivided into three main components: the Main Massif, the Sublayer, and the Off-set dykes (Figures 1a and b).

The Main Massif comprises the main portion of the elliptically shaped outcrop of the SIC and varies significantly in its thickness from around 3000 to 300 m. Predominant rocks are norites at the base and granitic rocks at the top (termed granophyres or micro-pegmatites). The Main Massif can be further subdivided into the North and South Range, which differ in their lithological units due to a different differentiation history and variable degrees of deformation and metamorphism (Lightfoot & Zotov, 2005). In the North Range, the rock sequence from base to top consists of mafic norite, quartz-bearing gabbronorite, quartz gabbro and granophyre. Progressive magma evolution is displayed by the whole stratigraphic column as well as within the single units, like the norites that evolved from mafic Mg-rich (8-16 wt% MgO) to more felsic compositions (5-7 wt% MgO; Lightfoot & Zlotov, 2005). The norites are mainly fresh to weakly metamorphosed at greenschist facies conditions and the granophyres experienced hydrothermal alteration (Ripley et al., 2015). The lowermost mafic norite unit is not present in the South Range sequence where variably altered quartz norite represents the base of the sequence overlain by quartz gabbro and granophyre units similar to the North Range. The overall magmatic evolution from more mafic to more evolved rock compositions is also visible within the South Range in the norite units. For example, MgO concentrations vary independently of elevation, thus requiring more complex differentiation mechanisms (Lightfoot & Zlotov, 2005). Also here, the granophyre is hydrothermally altered while the norites‘ metamorphism at greenschist facies conditions was more intense. Darling et al. (2012) report variable Pb isotope compositions from the North and South Range, suggesting that variable degrees of local host-rock assimilation might explain the compositional differences and evolution trends.

The Sublayer is located below the Main Massif and represents the base of the SIC. It is discontinuous, commonly located within depressions (embayments and troughs) along the basal contact of the SIC and distinct from the overlying Main Massif rocks by hosting abundant (sub-) rounded mafic to felsic inclusions that range from centimetres to tens of meters in size and Ni-Cu-PGE mineralization (Wang et al., 2018). The majority of these inclusions come from the surrounding country rocks. In contrast, volumetrically important olivine-bearing ultramafic inclusions seem to have no equivalents in the vicinity of the SIC but are assumed to be derived from unexposed mafic to ultramafic intrusions in the upper to middle crust (Wang et al., 2018). Lithologically, the ultramafic inclusions can be described as dunite, feldspar peridotite, pyroxenite, amphibole pyroxenite, olivine melanorite, and olivine gabbro (Wang et al., 2018). The olivine-clinopyroxene-plagioclase barometer yields intermediate equilibration depths of these minerals between 7.7 ± 4.1 and 14.9 ± 5.7 km, consequently speaking against a very deep (Mungall et al., 2004) or a very shallow (Darling et al., 2010) excavation depth of the SIC.

The Off-sets are concentrically and radially arranged dykes that extend as far as 20 km from the main structure into the surrounding country rocks. They are geochemically akin to the Main Massif rocks and contain similar populations of inclusions as the Sublayer (Lightfoot, 2016). Some Off-set dykes host economic mineralization while others are barren (Ripley et al., 2015; Lightfoot, 2016).

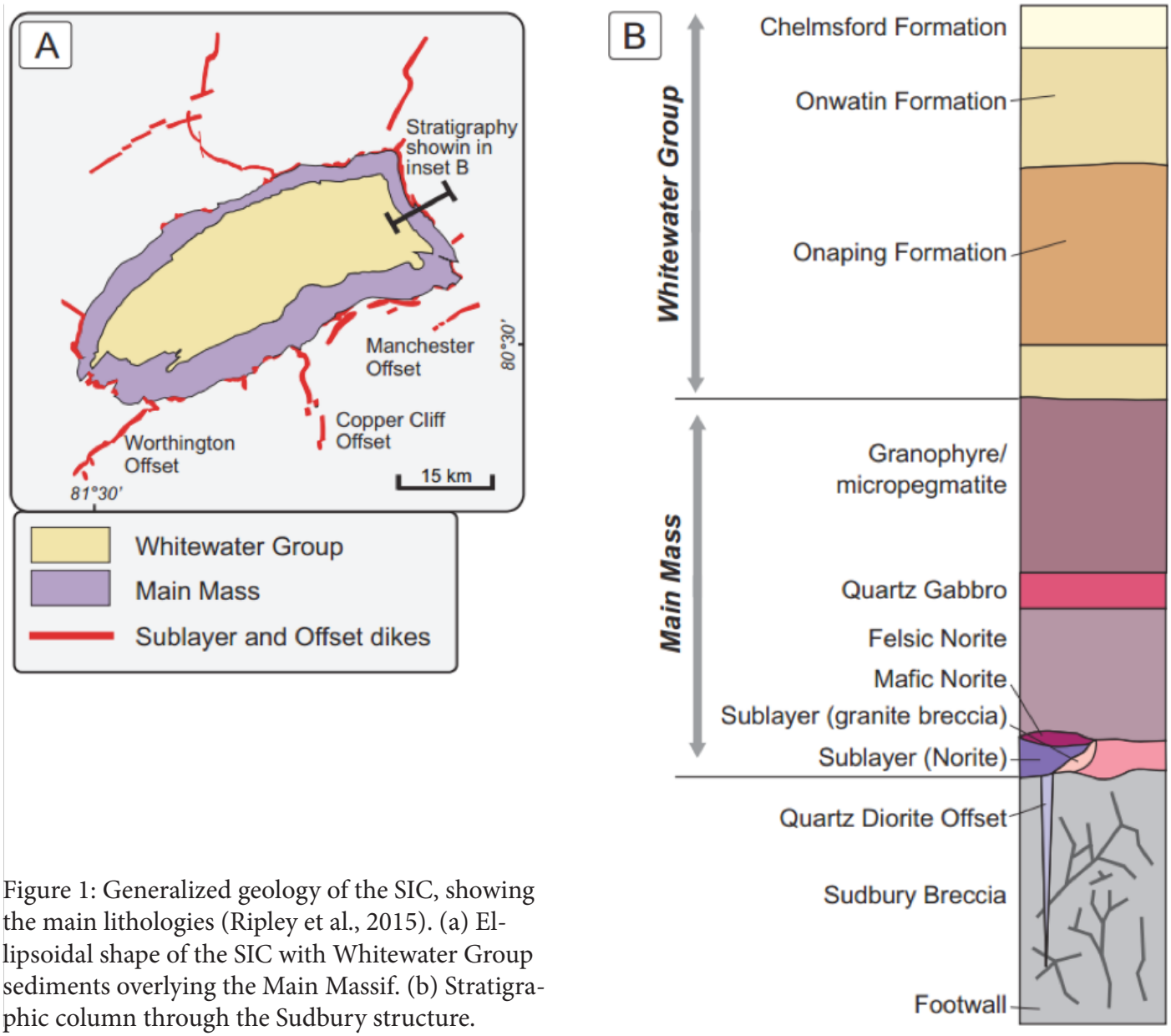

Figure 1: Generalized geology of the SIC, showing the main lithologies (Ripley et al., 2015). (a) Ellipsoidal shape of the SIC with Whitewater Group sediments overlying the Main Massif. (b) Stratigraphic column through the Sudbury structure.

The footwall rocks beneath the mineralized Sublayer of the SIC are mainly supracurstal rocks of the Huronian Supergroup and are heavily brecciated.

Overlying rock sequences are collectively termed Whitewater Group and consist of breccias and melt bodies (Onaping Formation) followed by progressively deeper water sedimentary rocks like laminated pelagic argillite and siltstone (Onwatin and Chelmsford Formation; Rousell, 1984).

Evidence for the meteorite impact

Despite the obstruction produced by orogenic deformation, several lines of evidence suggest a meteorite impact as the origin of the SIC, which is widely accepted nowadays. The most prominent macroscopic features are clast-rich pseudotachylites [cataclastic rocks with local melt] within the country rocks surrounding the SIC. Their aphanitic texture containing rounded clasts from surrounding lithologies of up to several meter in size indicate cataclastic flow during significant shear heating produced by the impact shock waves (Riller, 2005). Secondly, shatter-cones [usually conically shaped fracture planes with radial striae] and shattered country rocks, common in the footwall rocks of the SIC, are a typical feature of meteorite impact structures suggesting shock-metamorphism (Gibson & Spray, 1998). Minerals show intensive deformation features that require very high pressures. Especially mosaicism in olivine and strong fracturing and partial isotropization of plagioclase are other characteristic features of shock deformation at pressures in the range of 20 to 30 GPa (Figure 2; Wang et al., 2018). Such shock-metamorphosed minerals also occur in the Onaping Formation covering the SIC. This polymict breccia formation also contains melt inclusions as well as lithic fragments and was interpreted to represent a fall-back deposit or impact breccia (Riller, 2005, and references therein).

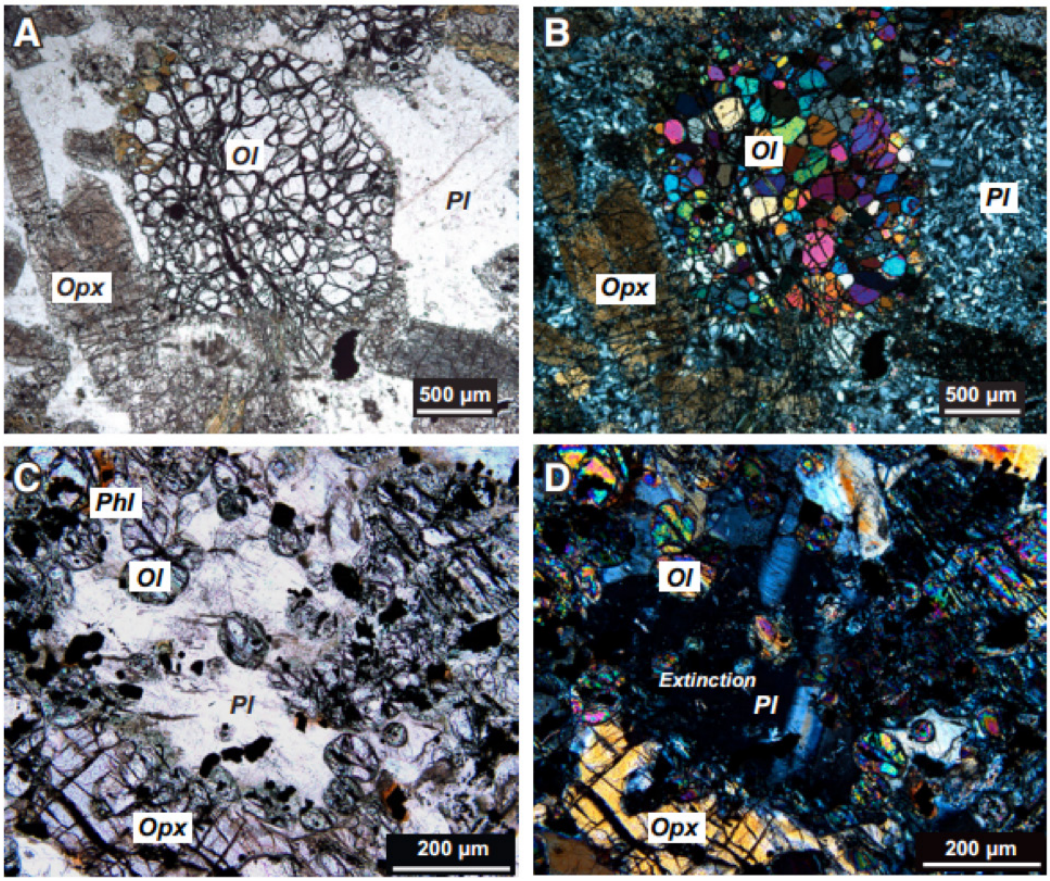

Figure 2: Impact features in olivine and plagioclase from ultramafic inclusions within the Sublayer of the SIC (Wang et al., 2018). (a) Mosaic olivine with persevered euhedral shape under plane-polarized light and (b) under cross-polarized light showing the subgrains with variable interference colors. (c) Plagioclase with multi-oriented fractures under plane-polarized light and (d) under cross-polarized light showing partial isotropization. Abbreviations: Ol – olivine, Opx – orthopyroxene, Pl – plagioclase; Phl – phlogopite.

Field Observations

The SIC constitutes an approximately 3-km-thick melt layer that crystallized and differentiated from norite-like to granodiorite-like compositions (Figure 3), the former one being the least abundant. The different rock varieties are easily found outcropping along the rims of the crater-like structure. Impact features such as impact breccia with clast-rich pseudotachylites within the country rock, shatter cones, and polymictic fall out breccia are also observed, providing evidence of a strong impact (Figures 4,5).

Figure 3. Equigranular granophyre with miarolitic cavities developed in melts pockets of more evolved compositions, cut by later epidote veinlets. This compositional variety represents one of the most abundants in the SIC. Photo: M. P. Castellanos

Figure 4. Clast-rich pseudotachylite in country rock. These features represent brecciated pieces of rocks cemented by glass that resulted from the local melting of the country rock during impact. Photo: M. P. Castellanos

Figure 5. Fall-out breccia of the Onaping Formation. This polymictic breccia contains clasts of the different occurring rocks that were impacted and that were re-deposited after the impact. Photo: M. P. Castellanos

References

Darling, J. R., Hawkesworth, C. J., Storey, C. D., and Lightfoot, P. C. (2010): Shallow impact: Isotopic insights into crustal contributions to the Sudbury impact melt sheet. Geochimica et Cosmochimica Acta 74, 5680-5696.

Darling, J. R., Storey, C. D., Hawkesworth, C. J., and Lightfoot, P. C. (2012): In-situ Pb isotope analysis of Fe-Ni-Cu-Zn sulfides by laser ablation multi-collector ICPMS: New insights into ore formation in the Sudbury impact melt sheet. Geochimica et Cosmochimica Acta 99, 1-17.

Gibson, H. M., and Spray, J. G. (1998): Shock-induced melting and vaporization of shatter cone surfaces: Evidence from the Sudbury impact structure. Meteoritics & Planetary Science 33, 329-336.

Golightly, J. P. (2009): The Ni-Cu-Pge deposits of the Sudbury Igneous Complex. In: A field guide to the geology of Sudbury, Ontario, Ontario geological survey open file report 6243.

Lightfoot, P. C. (2016): Nickel sulfide ores and impact melts: Origin of the Sudbury Igneous Complex. Elsevier.

Lightfoot, P. C., and Zotov, I. A. (2005): Geology and geochemistry of the Sudbury Igneous Complex, Ontario, Canada: Origin of nickel sulfide mineralization associated with an impact generated melt sheet. Geology of Ore Deposits 47, 349-381.

Marsh, B. D., and Zieg, M. (1999): Solidification fronts of the Sudbury melt sheet. Geological Association of Canada – Mineralogical Association of Canada Joint Annual Meeting, Field Trip Guidbook B9, 34 pp.

Mungall, J. M., Ames, D. E., and Hanley, J. J. (2004): Geochemical evidence from the Sudbury structure for crustal redistribution by large bolide impacts. Nature 429, 546-548.

Riller, U. (2005): Structural characteristics of the Sudbury impact structure, Canada: Impact-induced versus orogenic deformation – A review. Meteoritics & Planetary Science 40, 1723-1740.

Ripley, E. M., Lightfoot, P. C., Stifter, E. C., Underwood, B., Taranovic, V., Dunlop III., M., and Donoghue, K. A. (2015): Heterogeneity of S isotope compositions recorded in the Sudbury Igneous Complex, Canada: Significance to formation of Ni-Cu sulfide ores and the host rocks. Economic Geology 110, 1125-1135.

Rousell, D. H. (1984): Onwatin and Chelmsford Formations. In: The geology and ore deposits of the Sudbury structure, Pye, E.G., Naldrett, A.J., and Giblin, P.E. (eds), Special Publication 1.

Wang, Y., Lesher, M., Lightfood, P. C., Pattison, E. F., and Golightly, J. P. (2018): Shock metamorphic features in mafic and ultramafic inclusions in the Sudbury Igneous Complex: Implications for their origin and impact excavation. Geology 46, 443-446.

II Sudbury Igneous Complex: metallogeny

Florian Viher & Maria Paula Castellanos

Introduction

The Sudbury Igneous Complex (SIC) in northern Ontario, Canada, was produced by the impact of a meteorite (Dietz, 1964; Davis, 2008). The remnant of the deformed multi-ring impact basin is of such extraordinary economic significance, that the Sudbury Nickel Camp is the second largest (after Noril'sk Camp) producer of Ni in sulfide deposits in the world (Ames & Farrow, 2007; Lightfoot, 2017). Sudbury is Canada's largest mining camp with 79 producing and past-producing Ni-Cu-PGE deposits, as well as 10 Cu-Ni-PGE exploration projects with over 1.6 Gt past-production, reserves and resources (Ames & Farrow, 2007; Lightfoot, 2017). Figure 1 shows the distribution of the mines and mine complexes in the Sudbury region. The Sudbury Structure contains 14 Mt Ni in production with a high Ni grade between 1.5 and 2.5%, and it has produced 80% of the global Ni supply since 1920 (Lightfoot, 2017). By 1994, the district also produced more than 8 Mt of Cu as well as several hundred tons of Ag, Pd, Pt, and Au with significant amounts of Os, Ir, Rh, Ru, Se, Te and Fe from 116 deposits (Golightly, 2009).

History

The sulfides in Sudbury were first discovered in 1856 by Alexander Murray (Murray, 1856). The significance of this discovery was not realized until 1883 when Thomas Flanagan noticed Cu (Ni) sulfides and performed a detailed geological survey in an electromagnetic area which became the Murray Mine (Ames & Farrow, 2007; Lightfoot, 2017). Since this discovery,

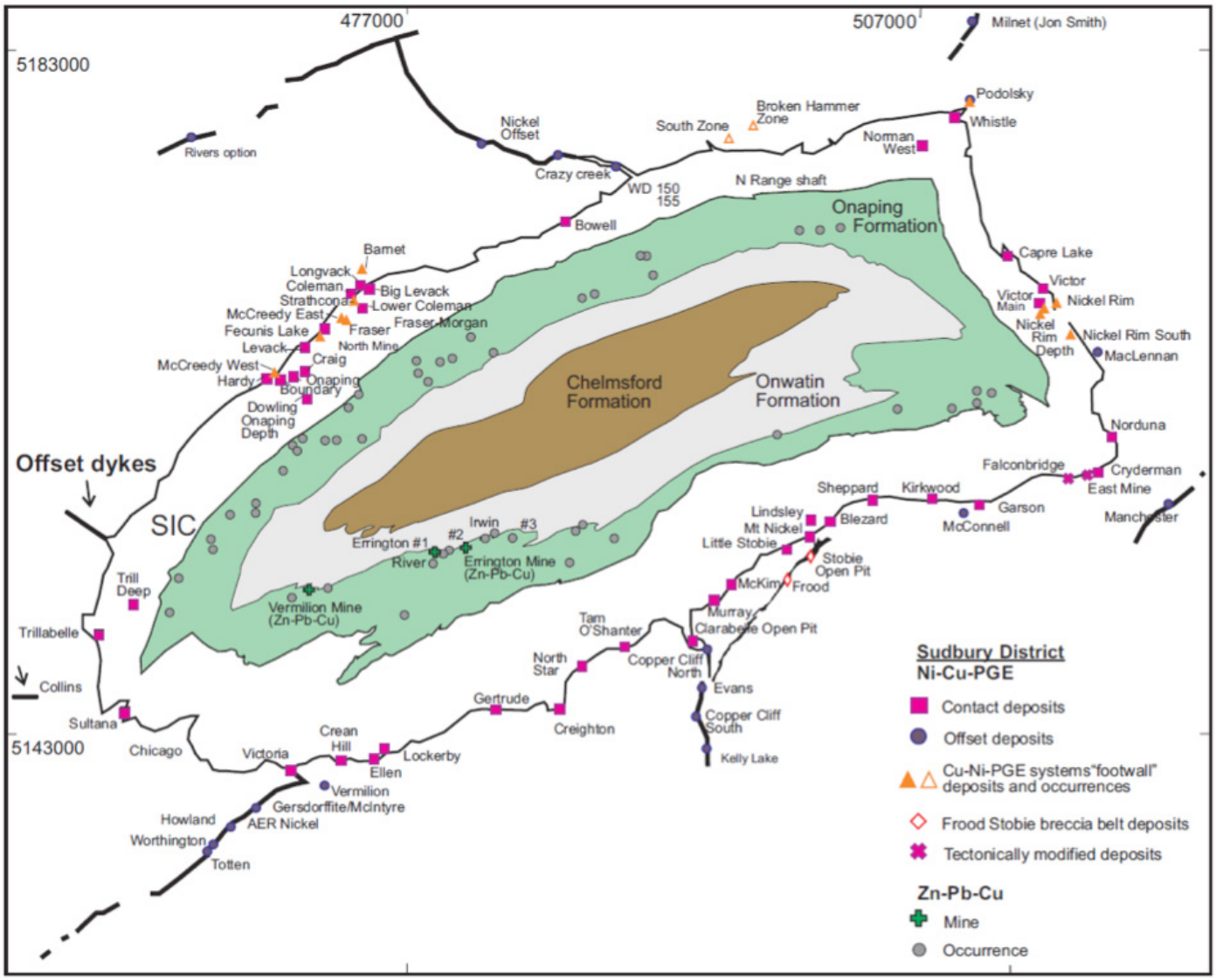

Figure 1: Map of the Ni-Cu-PGE deposit types and the hydrothermal Zn-Pb-Cu mineralization associated with the impact event; from Ames & Farrow (2007).

over 11.1 Mt of nickel and 10.8 Mt of copper with by-product of cobalt, silver, gold and platinum group elements (PGE) have been mined from the ore deposits (Lightfoot, 2017).

In 1946 airborne survey was used for the first time by Inco, developing these methods to explore for new deposits (Lightfoot, 2017). In the last years the majority of the produced metals have come from two principal companies: Vale and Glencore (Lightfoot, 2017). The production continues and as a result of exploration, new discoveries are made (Lightfoot, 2017). Increasingly deeper ore bodies are reached: The deepest operation in North America with over 2400 m depth is at the Creighton Mine (Lightfoot, 2017).

Ni-Cu-PGE deposit types

The majority of the world-class Ni-Cu-PGE deposits of Sudbury can be grouped into four different types, based on position within the SIC, mineralization style, and hosting lithologies: >50% are contact deposits, <10% are footwall deposits, ca. 25% are offset deposits and ca. 15% are Frood-Stobie-type breccia belt deposits (Ames et al., 2007; Figure 1). Mafic and ultramafic rocks of the Sublayer and Off-set dykes of Early to Middle Proterozoic age host most of Ni-Cu-PGE mineralization close to the basal contact of the SIC or within the footwall breccias (Lightfoot & Zotov, 2005; Golightly, 2009; Darling et al., 2012; Figure 2). Ore bodies are chemically zoned, ranging from Ni-rich cumulate at the contact to the foot-wall rock to more evolved Cu-rich ore within the brecciated foot-wall rock (Ballhaus et al., 2001 and references therein). The main ore minerals are pyrrhotite, pentlandite, and chalcopyrite. There also exists minor hydrothermal Zn-Pb-Cu mineralization, which is related to the SIC (Ames & Farrow, 2007).

Contact deposits (Figure 3 top): The contact deposits occur at the lower contact of the Main Mass with the footfall in relation with physical traps and structures (Lightfoot, 2017). Contact deposits are hosted in a basal igneous "sublayer norite" or "footwall breccia" and form disseminated or (semi-) massive sulfides (Ames & Farrow, 2007; Naldrett, 2009, and references therein). This deposit type is typically dominated by pyrrhotite (with 0.2-1% Ni), pentlandite, chalcopyrite, and magnetite (with some PGEs) and are rich in Ni-Ir-Rh with Cu/Ni ratios of ~0.7 and low values of <1 g/t of Pt+Pd+Au (Naldrett & Pessaran, 1992; Ames et al., 2007).

Footwall deposits: Footwall deposits are also termed "Cu-(Ni)-PGE" deposits to cover the more diverse deposit-types that were discovered in the environment of the footwall and offset (Farrow et al., 2005). Footwall deposits are hosted by brecciated country rocks (Sudbury breccia), which are distributed around the base of the SIC (Morrison et al., 1994) and typically occur near contact deposits (Golightly, 2009, and references therein). These deposits are chalcopyrite-rich and the Cu/Ni of the sulfides is >6.5 with correspondingly high Pt+Pd+Au value of >7.7 g/t (Farrow & Lightfoot, 2002; Ames & Farrow, 2007). The following mineralization types occur: (a) veins characterized by chalcopyrite, pentlandite, (millerite, cubanite,) (b)

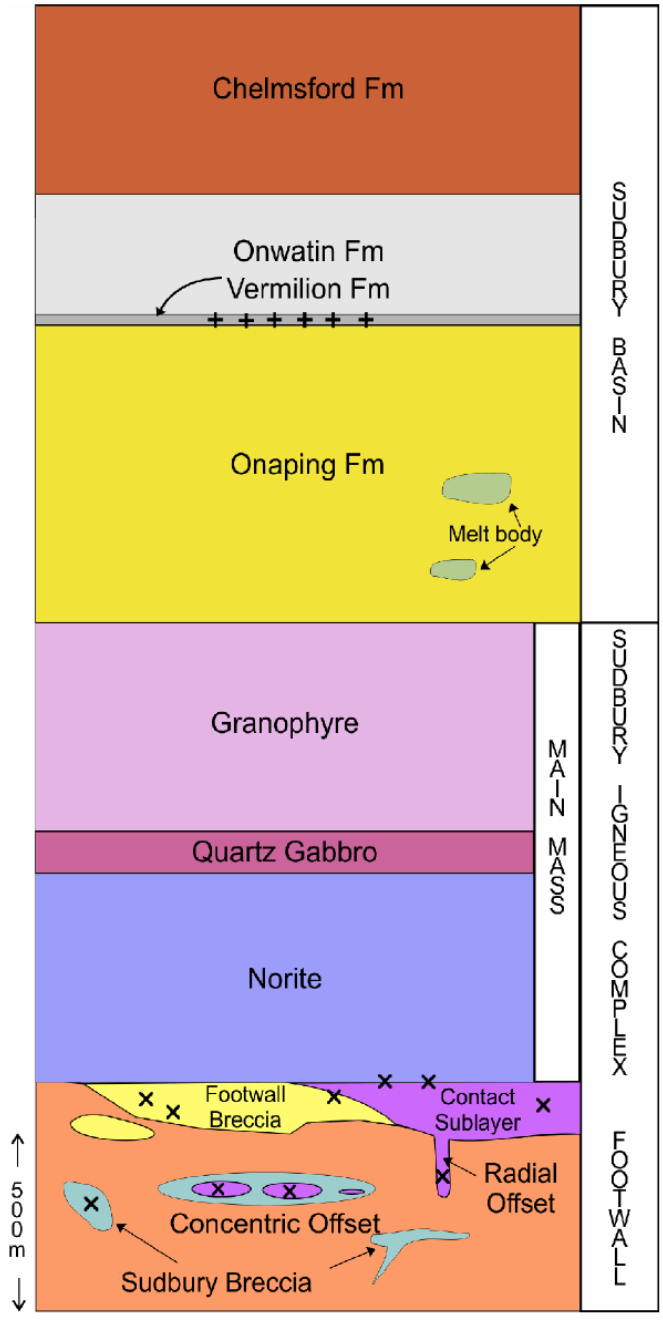

Figure 2: Stratigraphic section of the Sudbury Structure, from Rousell and Card (2009). x = Ni-Cu-PGE deposit, + = Zn-Pb-Cu deposit.

veins characterized by bornite, (millerite, pentlandite, quartz, carbonate,) (c) Au-PGE-rich, sulfide-poor disseminations, and (d) hybrid types of (a)-(c) (Golightly, 2009, and references therein). Hydrothermal activity around the footwall systems is attested by epidote-pyrite-quartz-chalcopyrite veins containing hypersaline fluid inclusions (Golightly, 2009, and references therein).

Offset deposits (Golightly, 2009, and references therein; Figure 3 bottom): The offset deposits are hosted in a radial or concentric quartz-diorite dykes. These dykes exhibit an early sulfide-free and a later sulfide-bearing phase, preserved in the margins and cores of the dykes, respectively. These deposits contain disseminated to massive sulfides (mainly pyrrhotite, pentlandite, and chalcopyrite). The Cu/Ni ratios are ~1 with Pt+Pd+Au values of 2.5 g/t (Ames et al., 2007).

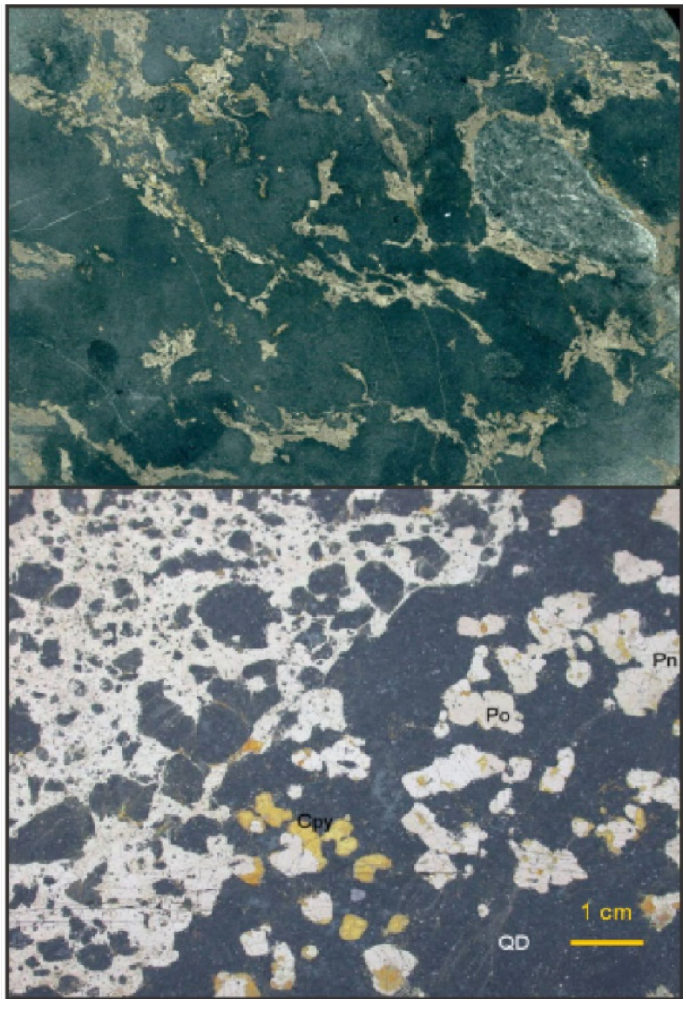

Figure 3: Mineralization textures from different mines within the SIC (Golightly, 2009). Top: Sublayer with sulfide matrix, the coarse-grained pyroxenite inclusion is around 10 cm wide. Bottom: Transition from massif (upper left) to disseminated ore (lower right) in fine-grained quartz diorite (QD). Abbreviations: Cpy – chalcopyrite, Po – pyrrhotite, Pn – pentlandite.

Ore genesis

In contrast to hydrothermally formed ore deposits, orthomagmatic ore formation is defined by direct segregation of Cu- and Ni-sulfides from a melt without significant contributions of hydrothermal fluid phases. Thus, fractionation of metals such as Fe, Ni and Cu, as well as S between silicate and sulphide melt is a crucial controlling factor. Temperature and metal/S ratios, which are dependent on the redox state of the melt (i.e. fS_2 vs. fO_2; oxidized melt: metal/S <1; reduced melt: metal/S > 1) were identified to be the main factors that determine the partition coefficients of Ni, Cu and Fe (Figure 4; Ballhaus et al., 2001). The higher density of sulphide melts relative to mafic melts fosters spatial separation, i.e. the formation of cumulates consisting either of monosulfide solid solution (mss; Fe-rich sulphide melt poor in Ni and Cu) or pooled sulphide melts (e.g. Barnes et al., 1997; Lightfoot & Zotov, 2005; Ripley et al. 2015). Primary features of magmatic sulphides, however, are never preserved due to exsolution of mss or iss into assemblages like pyrrhotite-pentlandite-chalcopyrite-pyrite at lower temperatures (Ballhaus et al., 2001).

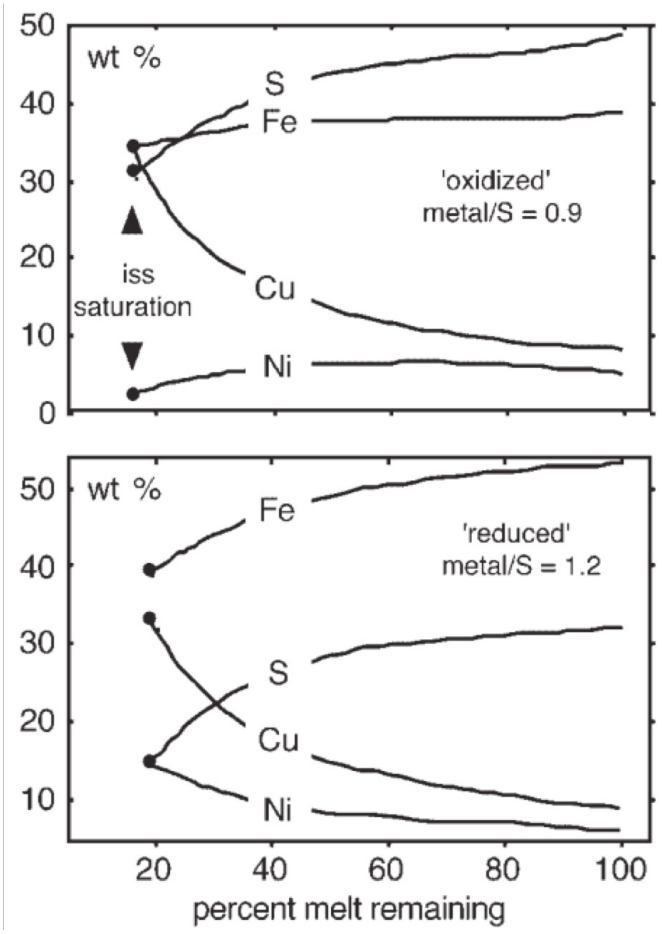

Figure 4: Fractionation paths of mss for oxidized (top) and reduced (bottom) compositions, modeled assuming batch fractionation; from Ballhaus et al. (2001).

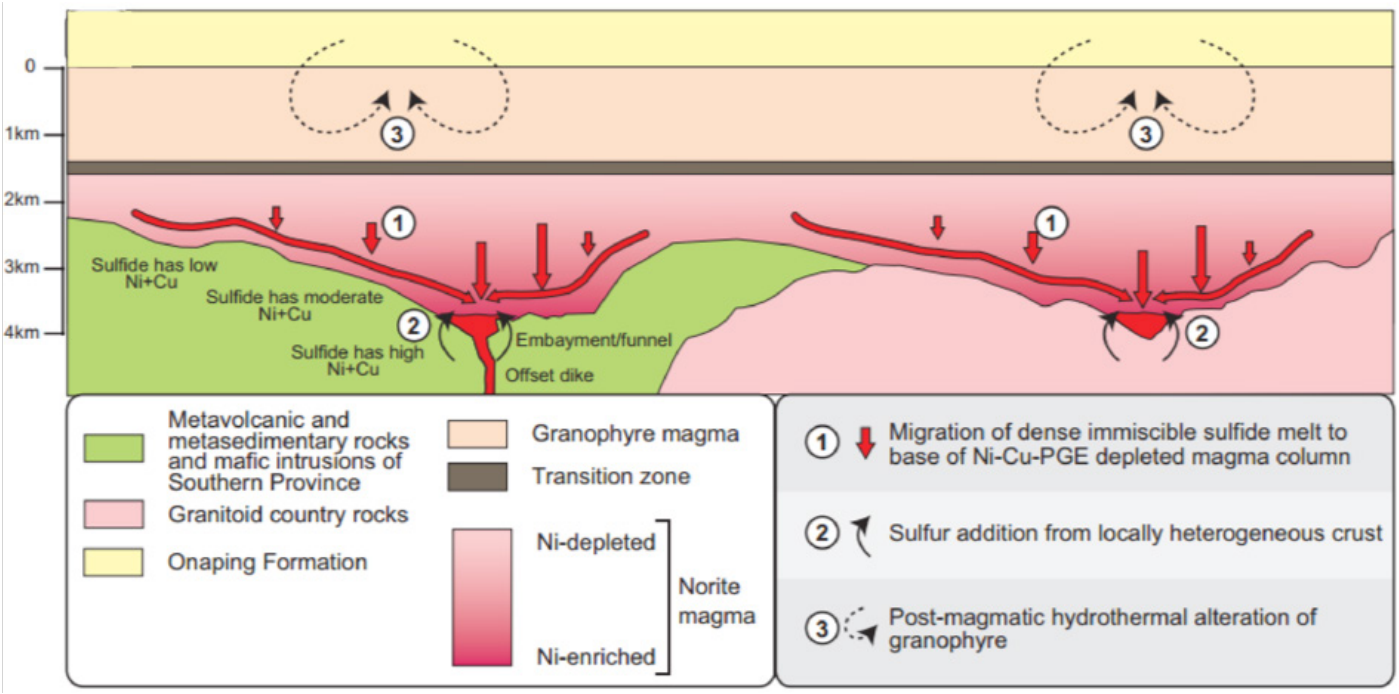

Figure 5: Conceptual model of sulfide melt segregation from the melt sheet and Ni-Cu-PGE ore formation by density-driven settling and accumulation of immiscible sulfide melt at the contact to the footwall rock and within the footwall rock and Off-set dykes (Ripley et al., 2015). Variations in thickness and fractionation time determine the final amount of metal enrichment, explaining why the deepest parts of the SIC contain the biggest ore deposits.

The chemical zoning of ore bodies in the SIC indicates that magmatic sulfide crystallization commenced by separation of mss, leaving behind a residual sulfide melt rich in Cu and PGE (Figure 4; Ripley et al., 2015). Continuous fractionation of the residual melt crystallized chalcopyrite-pentlandite ± millerite and in the extreme case bornite ± millerite assemblages within the brecciated footwall rocks. The norites, reflecting the lower portion of the initial melt sheet, show a uniform S isotope signature ($\delta 34S = 2.59 \pm 0.48‰$; Ripley et al., 2015) and metal depletion all around the SIC (Lightfoot & Zlotov, 2005), indicating a common S saturation history within the SIC and that metals were mainly derived from the noritic melts. The cumulate mineralization shows similar constant S isotope composition, while mineralization in the footwall rocks yields a wider range of S isotope ratios, demanding addition of S from local country rocks (Ripley et al., 2015). Crustal assimilation is also suggested by variable Pb isotope ratios (Darling et al., 2012). Consequently, the crustal host rocks of the SIC locally contributed S for ore formation within the footwall rocks (Fig. 5; Ripley et al., 2015). However, cumulate sulfide mineralization demonstrate that additional S was not necessary for ore formation but might have had an effect on tonnage or grade of the footwall mineralization. Distribution of ore deposits around the SIC seems to be governed by the geometry of the crater, with thicker portions of metal-depleted norites overlying bigger ore deposits and vice versa (Lightfoot & Zlotov, 2005). The degree of metal depletion indicates that enrichment processes occurred over extended periods of time and that gravitational sulfide melt segregation must have been very efficient to transport the required amount of metals to the lowermost parts of the crater. Fast settlement of sulfide melt implies that the initial crustal melt sheet was superheated (Lightfoot & Zlotov, 2005).

Hydrothermal Zn-Pb-Cu deposits

In addition to the orthomagmatic Ni-Cu-PGE deposits in the SIC, hydrothermal deposits developed in the Sudbury Basin due to circulation of basin fluids by heat conduction from the underlying SIC (Ames et al., 2006). These hydrothermal sulfide deposits are hosted by carbonates of the Vermilion Formation of the Whitewater Group (Rousell et al., 2009, and references therein). Replacement-type Zn-Pb-Cu (-Fe-Ag-Au) mineralization formed at temperatures between 250° and 300°C (Ames et al. 2006). Hydrothermal replacement took place in carbonate mounds and carbonaceous tuff in a subseafloor (Vermilion mine) or seafloor (Errington min) environment to

form stratiform to stratabound (semi-) massive sulfide lenses (Ames and Farrow, 2007; Rousell et al., 2009, and references therein). The basin-wide hydrothermal features are interpreted to represent a subaqueous hydrothermal vent complex and include silicification, albitization and carbonate-chlorite alteration (Ames et al. 2006). Typical ore minerals include pyrite, sphalerite, chalcopyrite, galena, marcasite, and pyrrhotite (Rousell et al., 2009, and references therein). The historic Errington and Vermilion deposits contain 6.9 and 2.7 Mt, respectively, with ore grades of ~4-5 wt% Zn, 1-1.5 wt% Cu, 1.3 wt% Pb, 55 g/t Ag and minor gold (Ames and Farrow, 2007).

Exploration

There are two approaches in Sudbury for the discovery of new ore bodies (Lightfoot, 2017). The first is done by following the known surface ore deposits to depth by drilling at the edges of the ore bodies along the trends of known mineralization (Lightfoot, 2017). This approach is used in very large deposits and has been successful in many cases because it pushed the closure of the mine complex well into the future (Lightfoot, 2017).

The other exploration work is often challenging and harder to conduct, because it is not obviously attached to a known ore body (Lightfoot, 2017). Therefore, the expenditure and risk of the company has to be minimized by a combination of geological information, geophysical methods and geochemistry (Lightfoot, 2017). Like a solid understanding of the 3-D geology followed by EM/RIM (radio imaging) geophysical methods which increases the sampling radius of drillholes is key to effective exploration (Ames & Farrow, 2007).

The exploration success is crucial, because it shows the value of better datasets and new ideas to find new discoveries like Kelly Lake, Onaping Depth, McCreedy East 153, Podolsky, Capre, Victor, Nickel Rim South and Victoria Deposits (Lightfoot, 2017). These mentioned discoveries, the un-mined deposits and the yet unfound deposits are the future of the Sudbury camp (Lightfoot, 2017).

References

Ames, D. E. (2002): Sudbury Targeted Geoscience Initiative (TGI: 2000-2003): Overview and Update, in Summary of Field Work and Other Activities, 6100, 17-1 to 17-10.

Ames, D. E., and Farrow, C. E. G., (2007): Metallogeny of the Sudbury mining camp, Ontario. Mineral Deposits of Canada: A Synthesis of Major Deposit-Types, District Metallogeny, the Evolution of Geological Provinces, and Exploration Methods, 5, 329-350.

Ames, D. E., Jonasson, I. R., Gibson, H. L., and Pope, K. O. (2006): Impact-generated hydrothermal system – constraints from the large Paleoproterozoic Sudbury Crater, Canada. Biological Processes Associated with Impact Events.

Ballhaus, C., Tredoux, M., and Späth, A. (2001): Phase relations in the Fe-Ni-Cu-PGE-S system at magmatic temperature and application to massive sulfide ores of the Sudbury Igneous Complex. Journal of Petrology 42, 1911-1926.

Barnes, S. J., Makovicky, E., Makovicky, M., Rose-Hansen, J., and Karup-Moller, S. (1997): Partition coefficients for Ni, Cu, Pd, Pt, Rh, and Ir between monosulphide solid solution and sulphide liquid and the formation of compositionally zoned Ni-Cu bodies by fractional crystallization of sulfide liquid. Canadian Journal of Earth Science 34, 366-374.

Dietz, R., (1964): Sudbury Structure as an Astrobleme. The Journal of Geology 72, 412-434.

Davis, D., (2008): Sub-million-year age resolution of Precambrian igneous events by thermal extraction-thermal ionization mass spectrometer Pb dating of zircon: Application to crystallization of the Sudbury impact melt sheet. Geology, 36, 383-386.

Farrow, C. E. G., and Lightfoot, P.C., (2002): Sudbury PGE revisited: Toward an Integrated model, The Geology, Geochemistry, Mineralogy and Mineral Beneficiation of Platinum Group Element: Canadian Institute of Mining, Metallurgy and Petroleum 54, 13-130.

Farrow, C. E. G., Everest, J.O., King, D.M., Jolette, C., (2005): Sudbury Cu-(Ni)-PGE systems: Refining the classification using McCreedy West mine and Podolsky project case studies, Exploration for Deposits of Platinum-Group Elements: Mineralogical Association of Canada 35, 163-180.

Golightly, J. P. (2009): The Ni-Cu-PGE Deposits of the Sudbury Igneous Complex. A Field Guide to the Geology of Sudbury Ontario 6243, 223.

Keays, R. R., and Lightfoot. P. C., (2004): Formation of Ni-Cu-Platinum Group Element sulfide mineralization in the Sudbury Impact Melt Sheet. Mineralogy and Petrology 82, 217-258.

Lightfoot, P. C., Keays, R. R., and Doherty, W., (2001): Chemical evolution and origin of nickel sulfide mineralization in the Sudbury Igneous Complex, Ontario, Canada. Economic Geology 96, 1855-1875.

Lightfoot, P. C., (2017): Nickel sulfide ores and impact melts: Origin of the Sudbury Igneous Complex.

Lightfoot, P. C., and Zotov, I. A. (2005): Geology and geochemistry of the Sudbury Igneous Complex, Ontario, Canada: Origin of nickel sulfide mineralization associated with an impact generated melt sheet. Geology of Ore Deposits 47, 349-381.

Morrison, G. G., Jago, B. C., and White, T. L., (1994): Footwall mineralization of the Sudbury Igneous Complex, Proceedings of the Sudbury-Noril'sk Symposium 5, 119-132.

Murray, A., (1856): Geological Survey of Canada, 1853-1856, 180-181.

Naldrett, A. J., and Pessaran, A., (1992): Compositional variation in the Sudbury ores and prediction of the proximity of footwall copper-PGE ore bodies 159, 47-62.

Naldrett, A. J. (2009): Evolution of Ideas About the Origin of the Sudbury Igneous Complex and its Associated Ni-Cu-PGE Mineralization. A Field Guide to the Geology of Sudbury Ontario 6243, 223.

Ripley, E. M., Lightfoot, P. C., Stifter, E. C., Underwood, B., Taranovic, V., Dunlop III., M., and Donoghue, K. A. (2015): Heterogeneity of S isotope compositions recorded in the Sudbury Igneous Complex, Canada: Significance to formation of Ni-Cu sulfide ores and the host rocks. Economic Geology 110, 1125-1135.

Rousell, D. H. and Card, K. D. (2009): Geological Setting. A Field Guide to the Geology of Sudbury Ontario 6243, 223p.

Rousell, D. H., Paakki, J. J., and Gray, M. J. (2009): Mineralization in the Whitewater Group. A Field Guide to the Geology of Sudbury Ontario 6243, 223.

III Nickel Rim South mine & Onaping Depth project

Dina Klimentyeva

Nickel Rim South deposit

The Nickel Rim South deposit (Table 1) was discovered in 2001 as a result of exploration campaign that focused on small and medium-sized deposits, and is expected to operate until 2022.

Table 1: Overview over the Nickel Rim South operations.

current operator	Glencore
reserves (proven and probable)	9.6 Mt at 1.57 % Ni, 2.85 % Cu, 1.20 g/t Pt, 1.35 g/t Pd, 10.20 g/t Ag, and 0.46 g/t Au
deposit type	magmatic-hydrothermal
start of operation	2010

The deposit is located in the footwall of the Sudbury igneous complex (Figure 1), the main mineralization styles include magmatic contact ore within the base of the complex, and vein type below the base, with veins reaching several meters in thickness. Figure 2 summarises the main ore types of the Nickel Rim South. The contact between sublayer norite and the host rock granodiorite breccia contains so-called contact disseminated, vein-type and massive sulfide mineralization, with pyrrhotite and pentlandite dominating over chalcopyrite and an alteration zone with chlorite and epidote. The amount of ore minerals varies from <1% in disseminations to >65% in the massive sulfide. In the Sudbury impact breccia, transitional mineralization style is represented by massive sulfide veins and disseminations, with pentlandite + chalcopyrite and

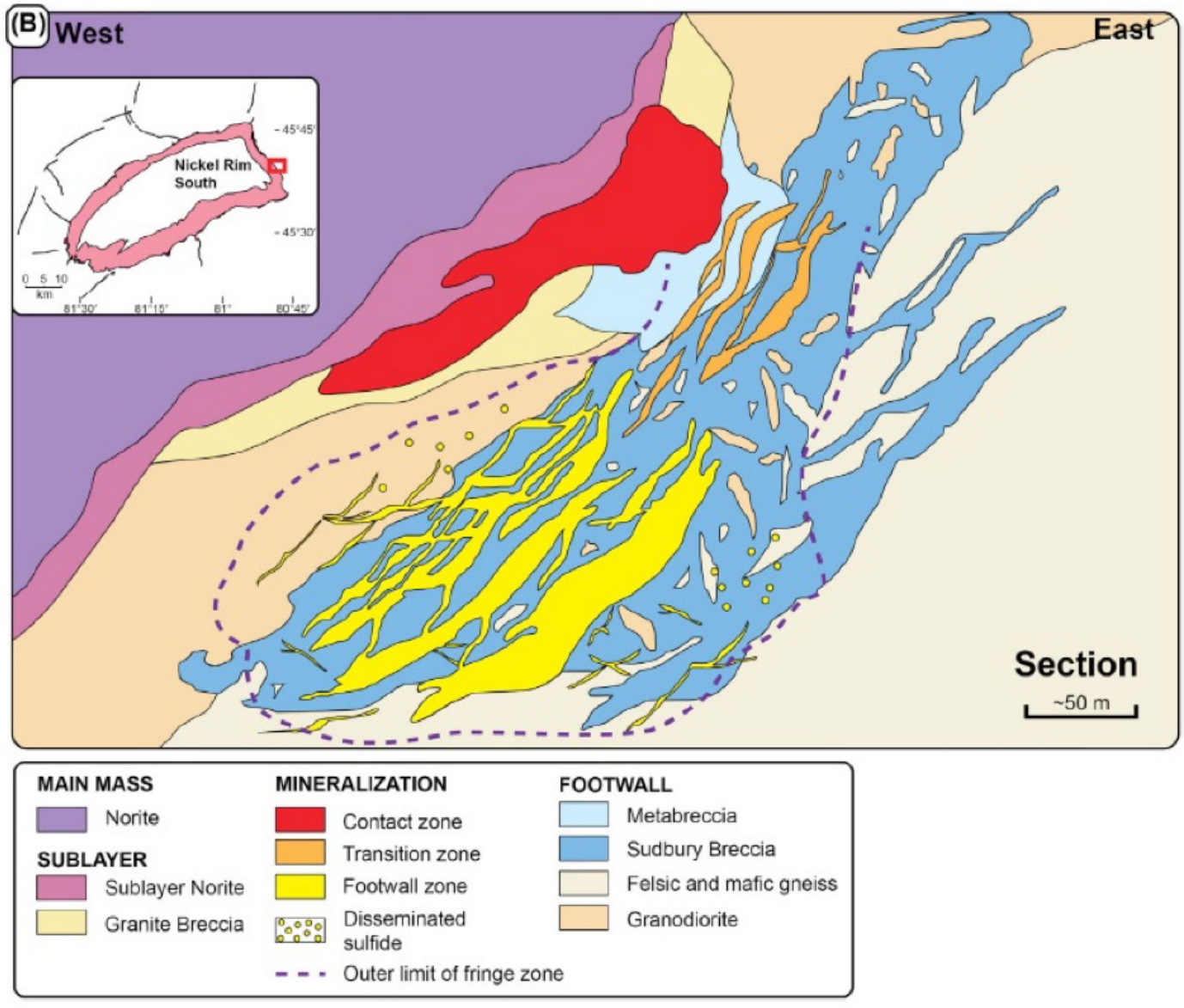

Figure 1: Geology of the Nickel Rim South deposit after Lightfoot (2017).

subordinate pyrrhotite, and epidote + chlorite + actinolite alteration haloes adjacent to the veins. In the footwall zone the ore vein assemblage changes from chalcopyrite + pentlandite ± magnetite to chalcopyrite + pentlandite + millerite, followed by chalcopyrite + millerite or bornite, and rims of native silver; this mineralization is accompanied by intense chlorite + epidote alteration (Stewart et al. 2014). Below the footwall mineralization zone, the low-sulfide, PGE-rich mineralization is present.

The overall metal content is as follows (Table 1): Ni and Cu contents increase from the contact to the transitional and upper portion of the footwall zone. PGE contents follow the same trend, but show a dramatic increase in the core of the footwall zone. These trends are reflected in the changing mineral assemblage and are explained by the fractionation of sulfides in the melts away from the contact, from high Fe-Ni at the contact to high Cu-Ni further away (McLean et al. 2005).

The Nickel Rim South mine visit included three stops:

- 1120/445 undercut, with grades of Ni 1.5% 6% Cu. Sublayer norite / dark norite
- 1355/287 sublayer norite and breccia
- 1445/250-262 late granite breccia. Clasts of norite, gneiss; chalcopyrite mineralization in the breccia matrix.
- 1535 Sudbury breccia with clasts of granodiorite and granite, footwall mineralization. Semi-massive chalcopyrite and veinlets, disseminated chalcopyrite in the granitic clasts.

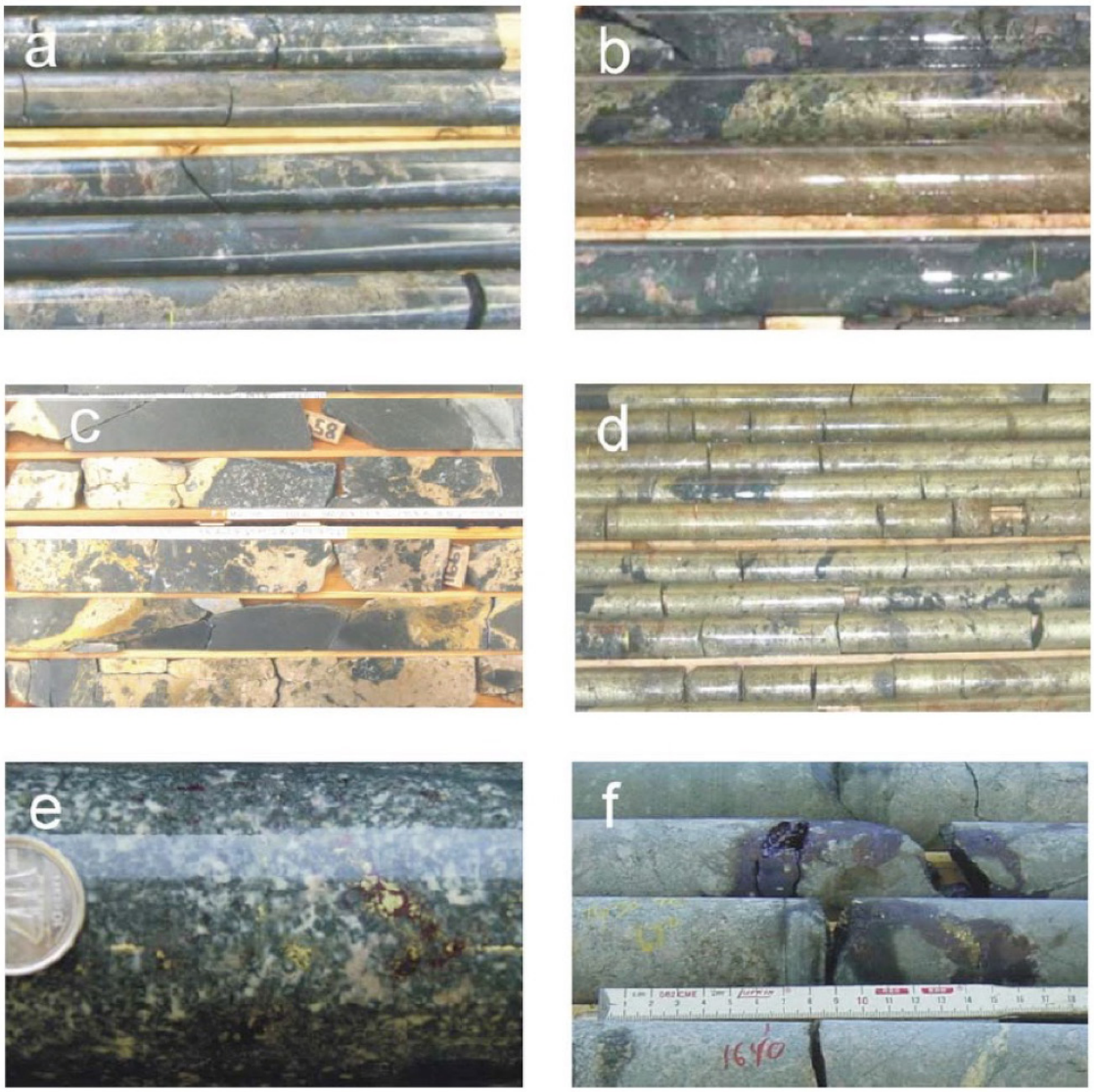

Figure 2: The Nickel South Rim mineralization styles after McLean et al. (2005). a) Contact massive sulfide mineralization; b) transitional mineralization with pyrrhotite-pentlandite-chalcopyrite; c) footwall mineralization with chalcopyrite-pentlandite veins, up to meter scale; d) footwall mineralization, chalcopyrite-pentlandite-pyrrhotite veins; e) and f) periphery of the footwall mineralization zone, with disseminations (e) and veins (f) of chalcopyrite, millerite, bornite and pentlandite.

Onaping Depth project

The Onaping depth project (Table 2) was approved in 2018, with planned production start in 2023. The discovery was made in the 1990s, but development was not possible until recently due to great depth of the deposit's location. Approved project costs amount to US$700 million. The mine will be Glencore's first all-electric mine; going all-electric will allow to reduce greenhouse gas emissions by 44%, as well as 23% reduction in shaft diameter (Hiyate, 2019). The ore at Onaping depth is represented by massive sulfide in the upper part of the ore body and sulfide stringers in the footwall zone, pentlandite + chalcopyrite are the main ore minerals. The ore is overlain by Sudbury breccia and underlain by footwall gneiss. The origin of sulfide stringers is thought to be related to the remobilization of Cu from the upper massive sulfide zone (Bamber et al., 2004)

Table 2: Overview over the Onaping Depth project.

current operator	Glencore
reserves (proven and probable)	13.8 Mt at 2.25 % Ni, 1 % Cu
deposit type	contact

Norman West exploration project

A series of deep copper deposits with mineralization similar to Onaping depth in mineralization style. Semi-massive sulfides, veinlets, pervasively mineralized breccia matrix constitute the ore at Norman West; orebodies are characterized by lens-like shape. Blocks of gabbro, on the order of 14-20 meters, as well as intermediate, mafic and felsic gneiss, represent the wallrock. Main ore minerals are pyrrhotite, cubanite, pentlandite and chalcopyrite. Figures 3-6 document the observations.

References

Bamber, A., Klein, B., Morin, M., and Scoble, M. (2004): Reducing selectivity in narrow-vein mining through the integration of underground pre-concentration. In: Proceedings of the Fourth CANMET International Symposium on Narrow Vein Mining Techniques.

Hiyate, A. (2019): GLENCORE digs deep in Sudbury. Canadian Mining Journal 140, 46-49.

Lightfoot, P. C. (2017): Nickel sulfide ores and impact melts: Origin of the Sudbury Igneous Complex. Amsterdam: Elsevier, 401-429.

McLean, S. A., Straub, K. H., and Stevens, K. M., (2005): The discovery and characteristics of the Nickel Rim South Deposit, Sudbury, Ontario. In: Exploration for Platinum-group element deposits. Mineralogical Association of Canada Short Course 35, 359-368.

Stewart, R., Kontak, D., and Sweeny, M. (2014): Characterization of hydrothermal alteration related to magmatic Ni-Cu-PGE mineralization at the Nickel Rim South deposit, Sudbury, Ontario. Geological Society of America annual meeting 46, 637.

Samples:

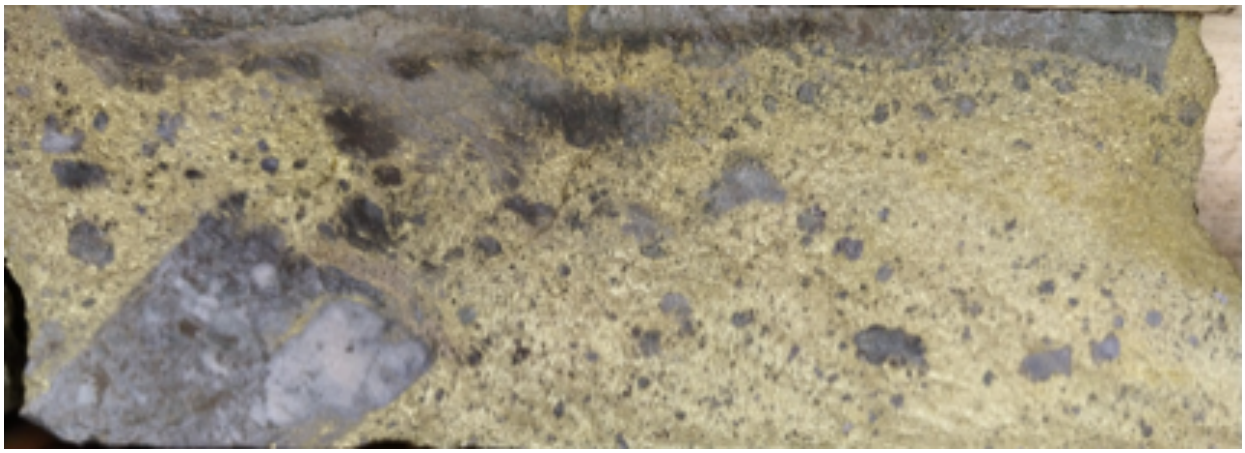

Figure 3: Mineralized breccia matrix, with pyrrhotite (bronze rim on the breccia clast, and veinlets) and dominantly chalcopyrite/cubanite. Photo: D. Klimentyeva

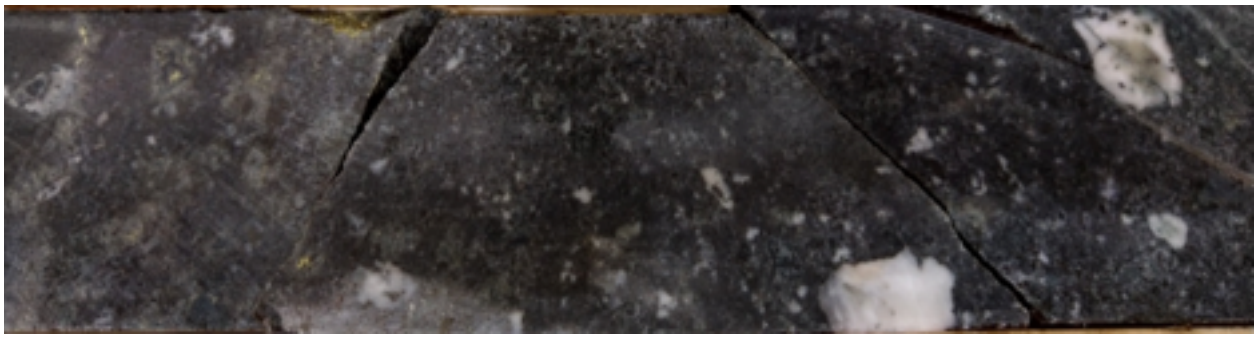

Figure 4: Dark norite breccia with disseminated pyrrhotite, chalcopyrite and probably re-melted felsic gness clasts. Width of the core: 4 cm. Photo: D. Klimentyeva

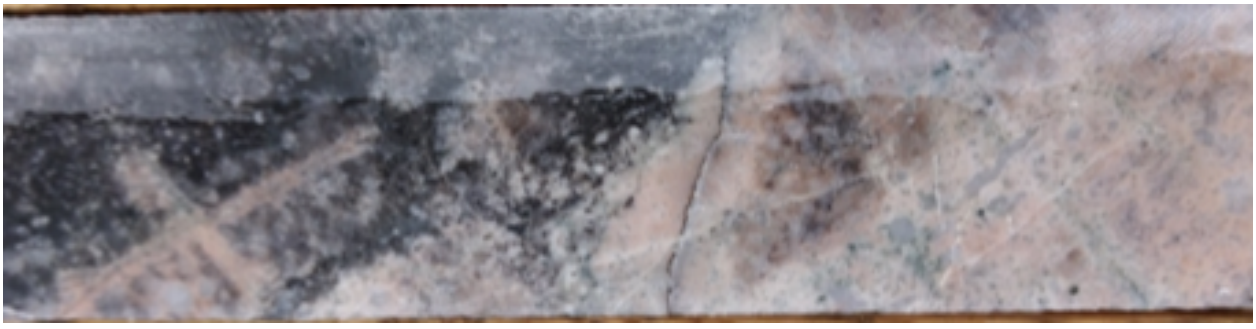

Figure 5: Clasts of veined granite in the norite breccia. Width of the core: 4 cm. Photo: D. Klimentyeva

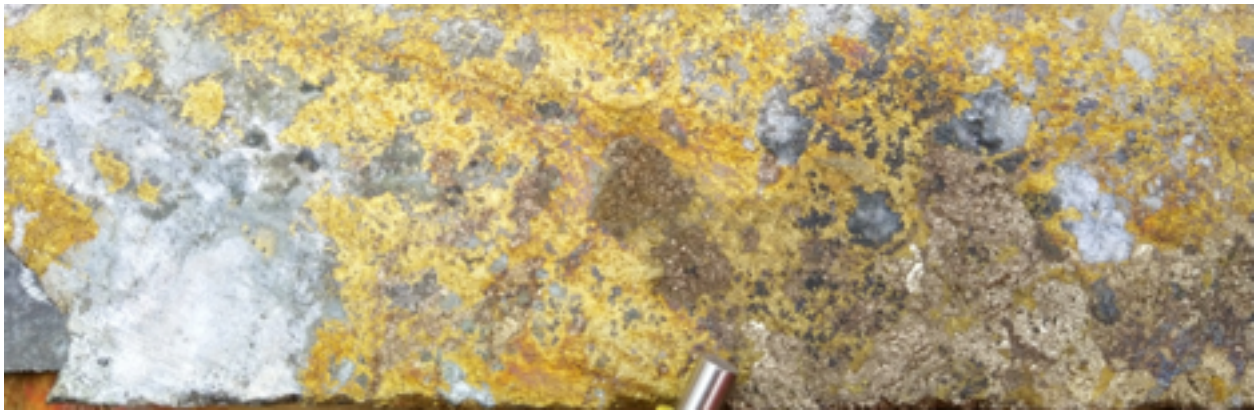

Figure 6: Pentlandite "eyes", distinguished by the brass-white color and cleavage, chalcopyrite. Mineralized Sudbury breccia. Photo: D. Klimentyeva

IV Abitibi Greenstone Belt: general geology

Jean-Marc Benz

Introduction

The Abitibi Greenstone Belt (AGB) is situated in the eastern part of the southern Superior province (Figure 1; Thurston et al., 2008). Further, the AGB is located on the Superior Craton of Canada and stretches west-east across the Ontario-Québec border. The AGB is the youngest (~2.7 Ga) and the largest (~700 x 300 km) of the existing Archean terranes in the Canadian Shield (Ludden et al., 1986; Anderson et al., 2017).

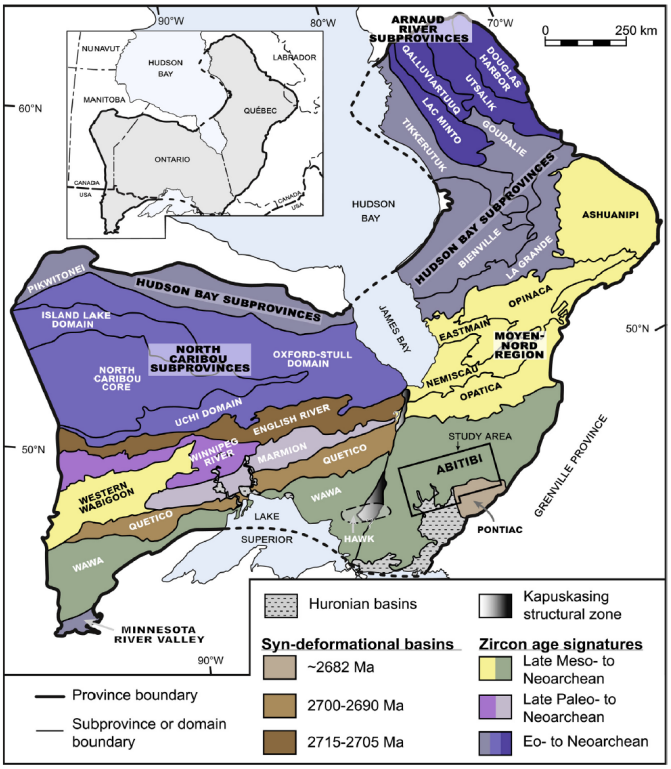

Figure 1: Subdivision of the Superior Province and location of the Abitibi Greenstone Belt; from Frieman et al. (2017), based on Stott et al. (2010).

The AGB is interpreted as a volcanic arc collage that evolved over a time span of ca. 90 Ma (Anderson et al., 2017). The division of the AGB is based on the predominance of a granite-gneiss terrane in the central portion that splits the belt along the east-west axis (Figure 2). The genetic model suggested for the evolution of the AGB is a rifted volcanic arc environment similar to Phanerozoic regions such as the Hokuroko basin of Japan, the Taupo volcanic zone and the Sumatra and Nicaragua volcanic axes.

The AGB is also one of the most studied greenstone belts of the world with respect to important Cu, Zn, Ni and Au deposits (Anderson et al., 2017). By 2005, the total mineral production value was 120 billion dollars mostly obtained from world-class volcanogenic massive sulfide (VMS) deposits (syngenetic Noranda-type deposits), gold-rich VMS deposits (e.g. Laronde-Penna) and epigenetic gold deposits (e.g. Sigma-Lamaque; Thurston et al., 2008). The former were generated in submerging volcanic zones bounded by wrench faults and the latter resulted from emergent volcanoes cored by calc-alkaline plutons in a compressional environment. In addition, porphyry type deposits are present in the AGB (Ludden et al., 1986).

Regional geology

The autochthonously formed AGB is surrounded by several structural boundaries (Ludden et al., 1986; Thurston et al., 2008). The western extent of the Archean terrane is limited by the Kapuskasing structural zone, the east and southeast extent by the Grenville front, and the Opatica subprovince represents the northern boundary (Figure 1). The Kapuskasing and Grenville front are post-Archean structures which juxtapose high-grade terrane and low-grade Archean supracrustal rocks. A transect of the AGB from east to west across the Kapuskasing structure displays decreasing metamorphic grade towards the Archean supracrustal rocks of the Wawa subprovince. The Grenville front juxtaposes Archean grey-gneisses of upper amphibolite facies with Archean metavolcanic rocks in the Chibougamau region and reworked Archean granulites with the Pontiac metasediments and migmatites in the southeastern extremities of the AGB subprovince. The Opatica granite-gneiss terrane is of Archean age (Ludden et al., 1986). The major internal structural features of the AGB are east-trending synclines containing mostly volcanic rocks and intervening domes cored by synvolcanic and/or syntectonic plutonic rocks (gabbro-diorite, tonalite and granite) intermitting with east-trending bands of turbiditic wackes. Most of the volcanic and sedimentary strata dip vertically and in most cases are separated by abrupt, east-trending faults with variable dip. Further, numerous late-tectonic plutons from syenite and gabbro to granite with lesser dikes of lamprophyre and carbonatite cut the AGB (Thurston et al., 2008).

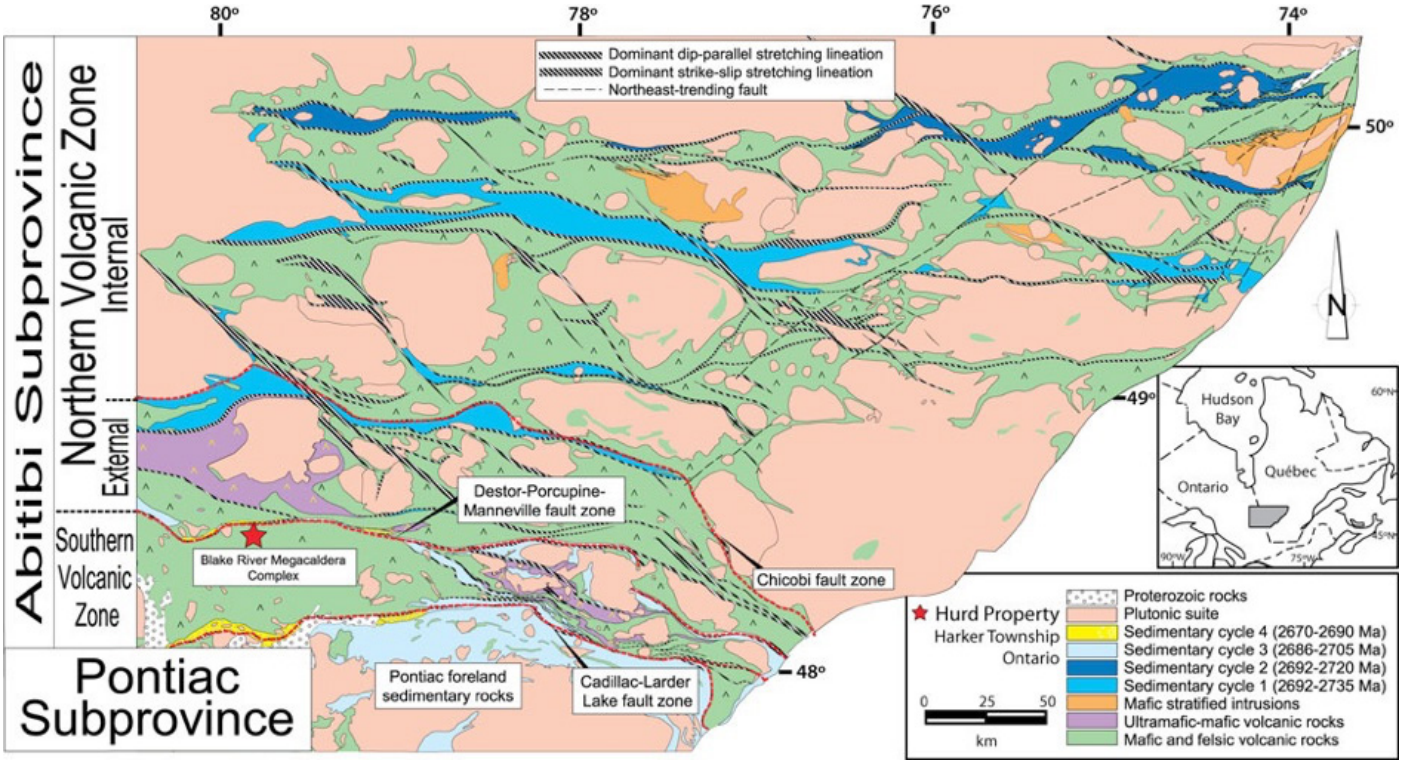

Figure 2: Map showing the Abitibi Subprovince (Anderson et al., 2017).

Volcanic evolution and stratigraphy

The AGB can be divided into two volcanic zones, the Northern Volcanic Zone (NVZ) and the Southern Volcanic Zone (SVZ) (Figures 2-4). The NVZ is made up by the volcanic complexes in the Chibougamau, Chapis and Matagami regions while the SVZ is made up by the Val d'Or, Rouyn-Noranda, Porcupine and Timmins region. Furthermore, there are two granite-gneiss zones, the central granite-gneiss zone and the southern granite-gneiss zone (Figure 3). The central granite-gneiss zone divides the NVZ and the SVZ, the southern granite-gneiss zone comprises the Pontiac metasediments, monzonitic plutons and migmatites (Ludden et al., 1986).

The NVZ is ~2720 Ma or older and consists of basaltic to andesitic and dacitic massive volcanic rocks cored by comagmatic sill complexes and layered mafic-anorthositic plutonic complexes. In contrast to SVZ, the volcanic series of the NVZ delineates a complete evolutionary spectrum from basalt to rhyodacite. The volume of felsic material is in general small in comparison with the SVZ. The associated plutons are overlain by felsic pyroclastic rocks that were comagmatic with the emplacement of the tonalitic plutons at 2717±2 Ma. The NVZ is characterized by submergent volcanism with volcanic edifices being cored by coeval plutons. The extensive REE fractionation and the K-rich nature of the comagmatic plutons indicate assimilation of felsic crustal components. The metallogenetic style is expressed by the presence of syngenetic massive sulfide deposits.

Figure 3: Summary of the distribution of major lithologies in the AGB (Ludden et al., 1986).

The SVZ dissects and superimposes the older volcanic rocks of the NVZ. The lithologies of the SVZ are dominated by komatiitic to tholeiitic volcanic plateaus of subaqueous volcanics and large bimodal (mafic-felsic tholeiite and andesite-rhyolite) volcanic centers. These volcanic rocks were erupted between ~2710 Ma and ~2700 Ma, centered on ring fractures and formed in rift basins as a result of wrench-fault tectonics and located between major shear zones. The rhyolitic eruptive episodes in the central volcanic complexes are of high volume (ca. 50 – 1000 km^3). The crustal assimilation of the magmas is dominantly mafic and similar in composition to the invading magmas. The metallogenetic style is expressed by the epigenetic formation of porphyry-type Cu (Au) deposits (Ludden et al., 1986).

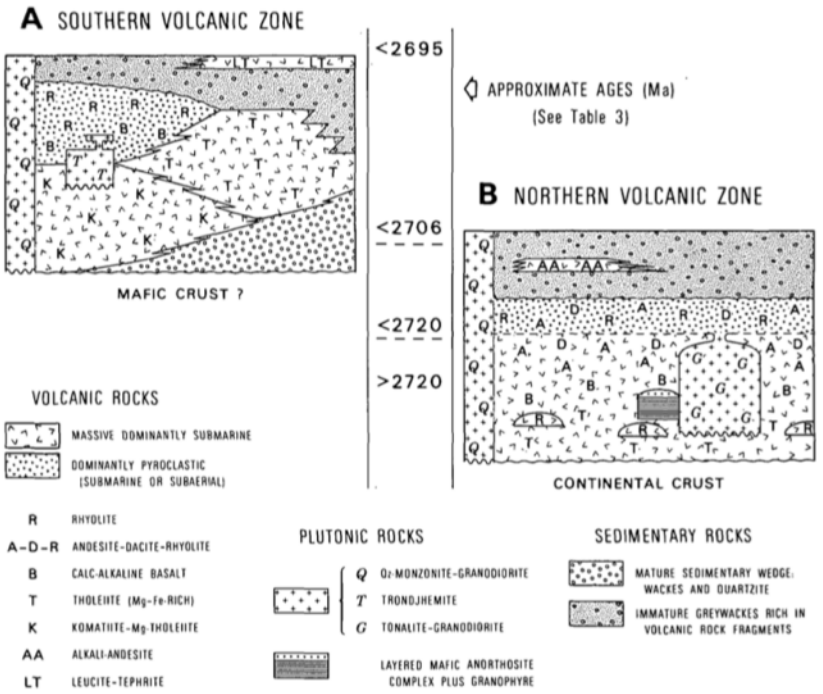

Figure 4: Schematic stratigraphic section of the southern volcanic zone (SVZ) and the northern volcanic zone (NVZ); from Ludden et al. (1986).

Age relationships

Conclusions from U-Pb and Pb-Pb measurements of zircons obtained by Ludden et al. (1986) show that the major period of mafic volcanism in the NVZ occurred prior to 2719 Ma. Further, contemporaneous eruption of felsic pyroclastic piles with the emplacement of the Chibougamau tonalite occurred at 2717 Ma. The major deformation phase of the NVZ was terminated prior to 2706 Ma. The activity of komatiitic-tholeiitic and rhyolitic volcanic centers in the SVZ lasted from 2710 to 2696 Ma. As a result, SVZ formation is 10 to 20 Ma later than NVZ formation. The underlaying Redstone River Group is 2725 Ma old (Ludden et al., 1986). More recent studies, e.g. Thurston et al. (2008), increased the detailed time resolution of the AGB. As a result the AGB was subdivided into seven discrete volcanic stratigraphic episodes on the basis of U-Pb zircon ages. Starting with pre-2750 Ma volcanic units and ending with 2696 Ma volcanic episodes (Figure 5, right column; Thurston et al., 2008). Nevertheless, the division of the AGB as used from Ludden et al. (1986) is still frequently applied in recent studies.

Tectonic evolution

Considering the different evolutionary styles of NVZ and SVZ, where the NVZ shows clear evidence of emplacement into continental crust and the SVZ displays features of rifting and submergence, the tectonic setting changed fundamentally between NVZ and SVZ genesis. During genesis of the NVZ, thin skinned tectonics resulting from rifting and subsidence were prevalent. This lead to emplacement of magmas into shallower crustal levels as needed to promote subaqueous VMS-forming hydrothermal activity. The porphyry-type deposits of the NVZ are favorably formed when mafic magmas are kept at depth. A possible tectonic evolution of the AGB would be a subduction zone in north – south orientation (relative to the present orientation of the belt) with a compressive front (corresponding to the SVZ) and an extensional setting behind the arc (corresponding to the NVZ). The present orientation of the volcanic arc would be NE-SW. The amount of shortening is still unknown (Ludden et al., 1986).

References

Anderson, L. D., Bebout, G. E., Izawa, M. R. M., Bridge, N. J., and Banerjee, N. R. (2017): Chemical alteration and preservation of sedimentary/organic nitrogen isotope signatures in a 2.7 Ga seafloor volcanic sequence. International Journal of Astrobiology, 1-16.

Frieman, B. M., Kuiper, Y. D., Kelly, N. M., Monecke, T., and Kylander-Clark, A. (2017): Constraints on the geodynamic evolution of the southern Superior Province: U-Pb LA-ICP-MS analysis of detrital zircon in successor basins of the Archean Abitibi and Pontiac subprovinces of Ontario and Quebec, Canada. Precambrian Research 292, 398-416.

Ludden, J., Hubert, C., and Gariepy, C. (1986): The tectonic evolution of the Abitibi greenstone belt of Canada. Geological Magazine 123, 153-166.

Mueller, W. U., Daigneault, R., Mortensen, J. K., and Chown, E. H. (1996): Archean terrane docking: upper crust collision tectonics, Abitibi greenstone belt, Quebec, Canada. Tectonophysics 265, 127-150.

Stott, G. M., Corkery, M. T., Percival, J. A., Simard, M., and Goutier, J. (2010): A revised terrane subdivision of the Superior Province. Ontario Geological Survey Open File Report 6260, 20–1 to 20–10.

Thurston, P. C., Ayer, J. A., Goutier, J., and Hamilton, M. A. (2008): Depositional gaps in Abitibi greenstone belt stratigraphy: A key to exploration for syngenetic mineralization. Economic Geology 103, 1097-1134.

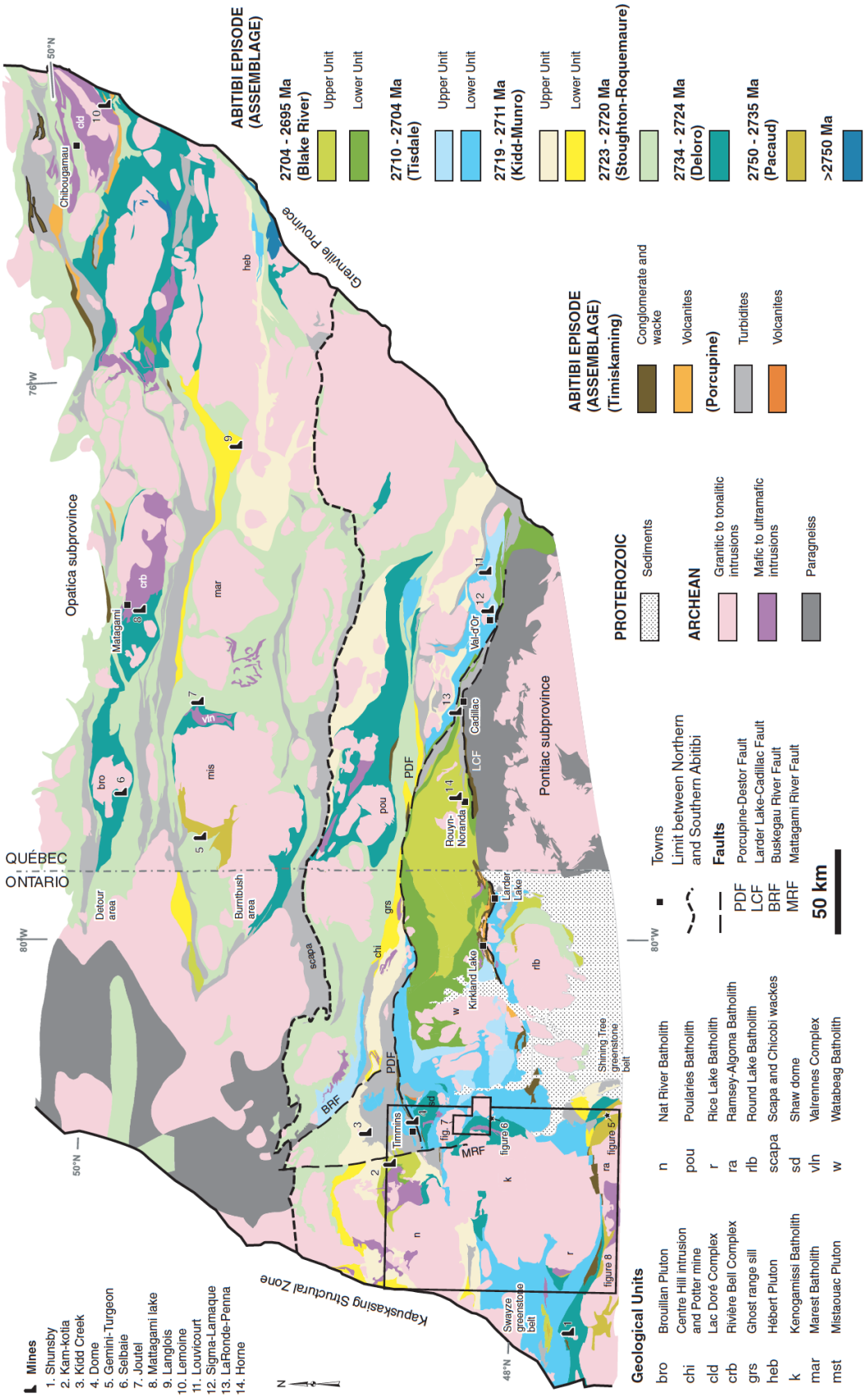

Figure 5: Stratigraphic map of the AGB (Thurston et al., 2008).

V Geology of the Porcupine Camp

Kamil Bulcewicz

Introduction

The Abitibi Greenstone Belt contains several mining camps (Porcupine, Duparquet, Matachewan, Kirkland Lake, Rouyn-Noranda, Malartic, and Val d'Or) operating on orogenic gold deposits situated along the Porcupine-Destor and Larder Lake-Cadillac fault/deformation zones (Hufford, 2015). The (Timmins-) Porcupine mining camp consists of a group of deposits dispersed over 35 km and situated on the western end of the so-called Abitibi Gold Belt (Figure 1). Over the years, the Porcupine camp has not only been the most productive camp in the area, but also the largest known Archean gold district on Earth (Bateman et al. 2008). For historical and present times, gold production and resources of the Timmins area are estimated to sum up to ca. 2150 tons of gold (Gosselin & Dubé, 2005; in Bateman et al., 2008).

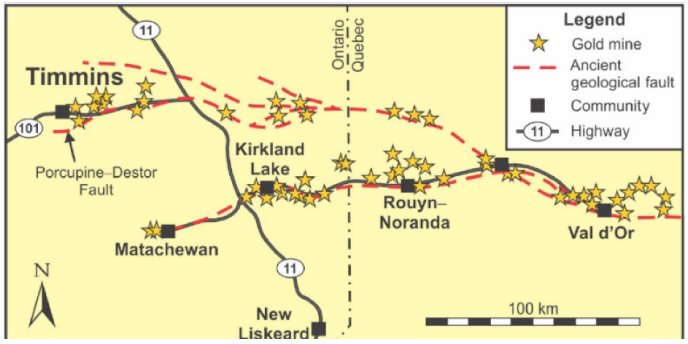

Figure 1: Map showing the distribution of gold deposits connected with Porcupine-Destor Fault Zone. The Porcupine Camp area is composed of a group of deposits nearby Timmins. From NRC & OGS (2015).

Historical view on the Porcupine Camp

Unique gold deposits of Northern Ontario have been discovered during the construction of Temiskaming and Northern Ontario Railway (T&NO), which was built to connect the city of North Bay in the south with the fertile lands of northern Clay Belt (Bleeker, 1995). Prospectors were attracted by the wealth of the first discovery (the Cobalt silver camp, 1903) and travelled, mostly by canoe, to the remote northern areas. During the ongoing exploration, the federal government negotiated Treaty No. 9, which pushed the native Mattagami First Nation people out of 2/3 of present day Northern Ontario area. Shortly after, the finding of a gold-rich quartz vein on a small island on

Figure 2: View on the Pearl Lake and shaft of McIntyre Mine (Timmins). Photo: K. Bulcewicz

Night Hawk Lake (1907) marked the first significant discovery (Doherty, 1986, in Bleeker, 1995) and the Golden City camp (now called Porcupine) was established. In 1909, a larger group of prospectors led by John S. Wilson found abundant gold mineralization in a dome-shaped outcrop. This discovery led to the establishment of the Dome Mine, which was the first mine built during the Porcupine Gold Rush. Further prospecting led to the foundation of other mines, with McIntyre Mine (Figure 2) and Holinger Mine closing the famous "Big Three". In 1911, when the gold rush was at its heights, the disastrous Great Porcupine Fire destroyed the miners' camps and took toll of 73 casualties. After the fire, restoring mining companies motivated the development of the town, named after one of the founding fathers of Canadian mining industry, Noah Timmins. After many financial ups and downs, the Porcupine camp companies suffered a large economic breakdown in the early 60's, when increasing labour costs and fixed prices forced many gold mines to close. In the middle of a market slump, the Kidd Creek base metal deposit was discovered 25 km north of Timmins (Bleeker, 1995). Determined to keep their finding a secret, the exploring company made a decoy drilling to misguide the competitors before announcing the industry-boosting discovery in 1964 (Hester, 1991, in Bleeker, 1995).

The Kidd Creek deposit, which appeared to have gigantic resources of base metals estimated at ~135 Mt,

became the largest source of zinc and silver in the world during the production peak (Bleeker, 1995). Other resources like nickel sulphides, talc, asbestos (associated with komatiites), chalcopyrite (porphyry-hosted Cu-Au deposit), and scheelite (in quartz veins) were also mined in the area during historical times (Bleeker, 1995). Nevertheless, gold was always of primary interest, as the Porcupine camp is thought to be the preeminent gold district in the world with over 40 gold mines spawned in the area over the years.

Present-day mining activity in the Timmins area

According to the Ontario Mining Association (OMA), there are 18 active gold mines in Ontario, and 7 of them are operating nearby Timmins. The Dome Mine, the first mine in the area, was closed in 2017 after 107 years of activity. The Kidd Creek Mine (Glencore) is still operating. The Porcupine Camp area is presently a subject of prospecting for gold (Goldcorp, Gowest Gold) and magnesite/talc (Globex Mining) deposits.

Lithostratigraphy of the Porcupine Camp

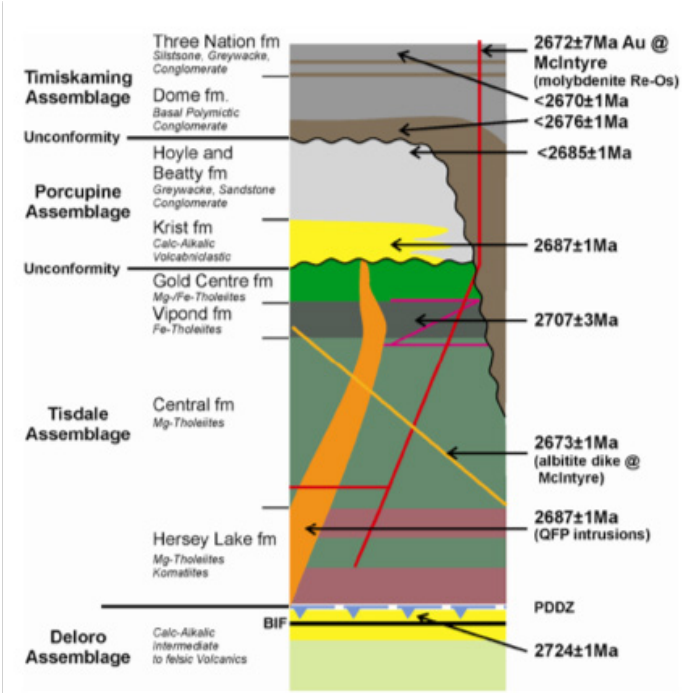

Figure 3: Lithostratigraphic chart of the Porcupine camp area; from Houlé et al. (2008).

The lithostratigraphic record of the Porcupine camp area is dominated by four of Abitibi supercrustal assemblages (Deloro, Tisdale, Porcupine, Timiskaming) and intrusive rocks (Figures 3, 5; Bateman et al., 2008). The two lowermost units are dominated by mafic volcanic rocks, while the stratigraphically higher Porcupine and Timiskaming units are of sedimentary origin. All units were metamorphosed under greenschist facies conditions at ca. 2677-2643 Ma.

The Deloro assemblage (2730-2724 Ma) is observed in the southeast of the camp area. It is built of calc-alkaline mafic lavas with minor iron formation and felsic volcanic rock occurrences (Houlé et al., 2008). The Tisdale assemblage (2710-2704 Ma) is composed of 600 m-thick komatiites and basaltic komatiites (Figure 4) covered by tholeiitic lavas with carbonaceous shale and ultramafic lavas also present. The Deloro and Tisdale units are separated by an unconformity (ca. 15 Ma stratigraphic hiatus) and by the Porcupine-Destor fault zone (Bateman et al., 2008). The Tisdale assemblage is intruded by stocks and dike swarms of quartz-feldspar porphyries (ca. 2690 Ma) not observed in the upper units. A discontinuous horizon of discordantly lying carbonaceous shale separates the Porcupine unit (2690-2685 Ma) from underlying assemblages. The basal part of the unit is composed of poorly-sorted pyroclastic deposits (Krist Formation), geochemically identical with aforementioned quartz-feldspar porphyries (Bateman et al., 2008). Fine- to medium-grained turbidite deposits (Beatty-Hoyle Formation) are derived from all older assemblages and overlie the Krist Formation in the Porcupine syncline (Bateman et al. 2008). Separated by an angular unconformity lie the Timiskaming assemblage rocks (2676-2670 Ma). Basal conglomerate and turbiditic fan-derived rocks (mainly graywackes) of the Dome Formation mark the opening of the Timiskaming basin. Overlying quartz-lithic sandstones and conglomerates of the Three Nations Formation are interpreted as deltaic-fluvial deposits (Bateman et al., 2008). The youngest lithostratigraphic units of the Porcupine Camp are intrusive rocks: Pamour porphyries, common albitite dikes and diabase dikes.

Figure 4: Dacite pillow lava with varioles filled with albite and chlorite-rich halo (metamorphosed volcanic glass); Tisdale assamblage (Timmins). Photo: K. Bulcewicz

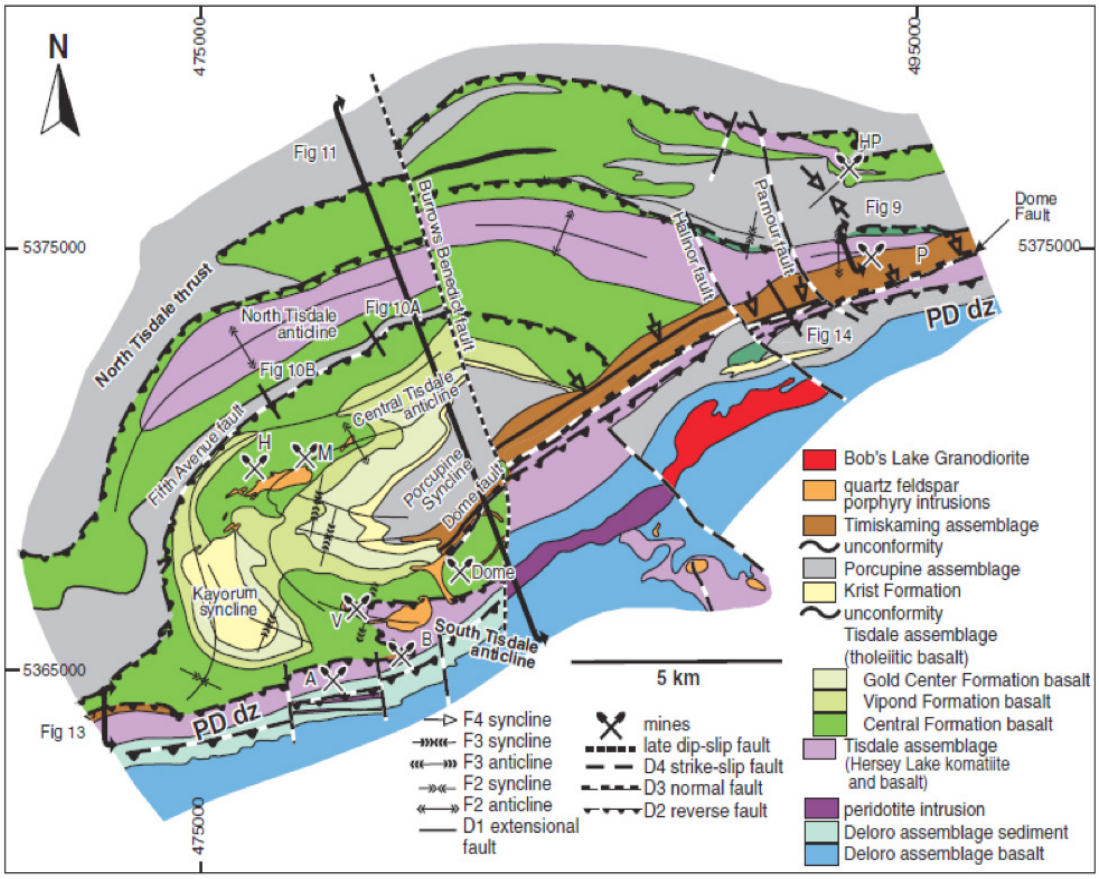

Figure 5: Geological map of the Porcupine camp area; from Houlé et al. (2008). PDdz = Porcupine Destor deformation zone; mines: A = Aunor Delnite, B = Buffalo Ankerite, D =Dome, H = Hollinger, HP = Hoyle Pond, M = McIntyre, P = Pamour, V = Vedron.

Structural evolution of the Porcupine Camp

Seven deformation episodes were identified in the area involving mainly the Tisdale, Porcupine and Timiskaming assemblages (Figure 6; Bateman et al., 2008). D1 is connected with uplift and extension of the Tisdale assemblage, which resulted in development of the Tisdale-Krist unconformity. Next phases (D2-D5) developed in an overall thrusting-strike-slip transpressional regime. D2 involved both Tisdale and Porcupine assemblages, resulting in imbrication of south-over-north folds and thrust sheets, which marked the first activity in the Porcupine Destor deformation zone (PDdz). D3 deformation was the episode of left-lateral strike-slip movement, which produced en echelon folds in older units and formed transtensional syn-D3 half-graben along the northern flank of the PDdz hosting sediments of the Timiskaming basin. The Dome fault probably forms the southern edge of that basin (Bateman et al., 2008). D4 structures formed during right-lateral strike-slip movement, while subsequent D5 compression resulted in deformation of earlier lineations. D6 produced very minor structures (e.g. local crenulation folds), while D7 structures associated with orogen-parallel shortening comprise kink folds and chevron folds. North-trending strike-slip faults (Burrows-Benedict, Hallnor, and Pamour faults) are the latest structures. They consist of both left- and right-lateral displacements typically up to 50 m, except two right-lateral faults with 500 m displacements (Bateman et al. 2008).

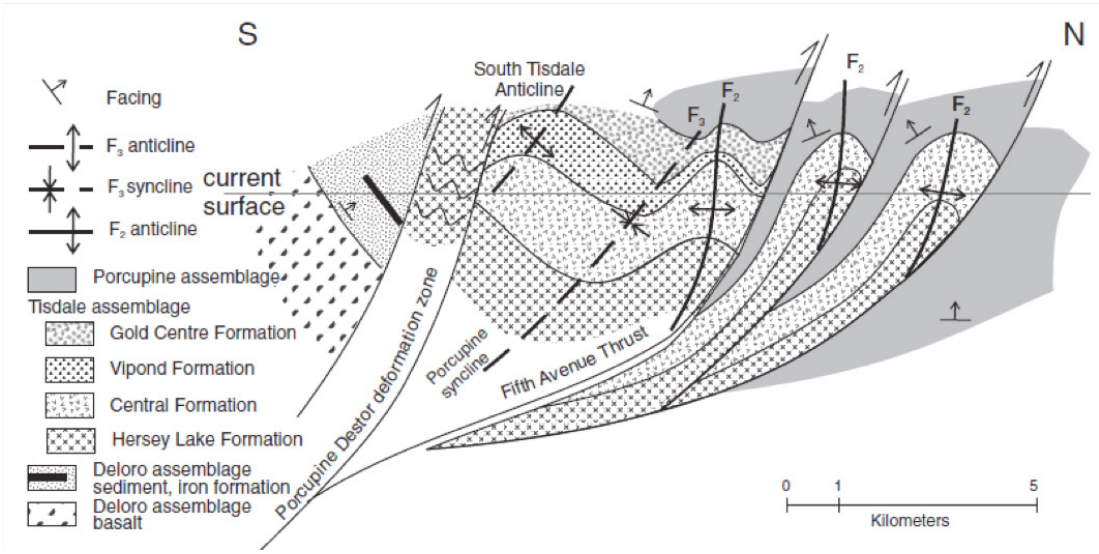

Figure 6: Geological cross-section perpendicular to Porcupine-Destor deformation zone; from Bateman et al. (2008).

Gold mineralization

There were many phases of gold mineralization in the Porcupine camp connected with different deformation episodes. The majority of gold deposits in the area lie in close proximity to the PDdz in the hanging wall of the D2 thrusts, which placed the Tisdale assemblage lavas onto Porcupine assemblage sediments (Bateman et al., 2005; Bateman et al., 2008; Stromberg et al., 2018). It is quite a unique feature, as most Archean gold deposits lie in the footwall of fault zones (Goldfarb et al., 2001). Thus, it appears that early thrusting was unusually well developed in this area (Bateman et al. 2008). Mineralization predating D3 is associated mainly with relatively low-grade, syn-D2 ankerite veins, clasts of which are found in the Timiskaming conglomerate (Bateman et al., 2005). The highest grade ore in the camp area, a quartz-fuchsite vein in the Dome mine emplaced into intensely carbonatized komatiites, probably also predates the D3 episode (Moritz & Crocket, 1991, in Bateman et al., 2008). However, syn-D3 development of the Timiskaming unconformity in strike-slip regime is key to bulk gold distribution in the camp area. Post-Timiskaming period of mineralization is composed of at least two major events: (1) development of Cu-Au-Ag-Mo mineralization (ca. 2672 Ma) hosted in the Pearl Lake Porphyry and (2) development of mostly quartz-carbonate vein-hosted mineralization related to D3-D4 deformation events (Bateman et al., 2005; Bateman et al., 2008; Stromberg et al., 2018). Generally, there are several types of quartz gold veins (Figure 7) which occur in both sedimentary rocks, volcanic rocks and porphyries, mostly in shear-related positions but their timing relationships are not always clear. In the Hollinger-McIntyre deposit (the largest gold deposit in Canada), Cu-Au-Ag-Mo sulfide mineralization is crosscut by ankerite-quartz veins that are in turn crosscut by rich, syn-D3 fault-filling quartz–ankerite–albite–scheelite–tourmaline–sulfides–tellurides-gold veins (Bateman et al., 2008). En echelon arrays of quartz veins are also present, indicating both left- and right-lateral movement on host structures (Moritz & Crocket, 1990, in Bateman et al., 2008). In other cases, randomly oriented and locally folded swarms of quartz-gold veins appear both in Timiskaming assemblage ("sedimentary trough ore") and Tisdale assemblage rocks ("greenstone ore"). In turn, "dacite ore" quartz-ankerite-gold veins show spatial relationship with conglomerate-filled ravines in the Timiskaming unconformity (Bateman et al. 2008). Late, syn-D5 ladder-arrayed veins also occur, but they host minor mineralization (Bateman et al., 2008).

Bateman et al. (2008) conclude, that only a long-lived or recurrently active auriferous hydrothermal fluid source and plumbing system stable enough to focus fluids into a relatively small volume of rock could have resulted in such a complex evolution of the Porcupine camp gold deposits. The duration of the hydrothermal activity cannot be pin-pointed, but most probably exceeds 7-25 Ma (Stromberg et al., 2018). The gold-bearing fluids may have derived from buried and metamorphosed pyrite-rich accretionary prism sediments of the Pontiac subprovince, which were probably thrusted underneath the Abitibi Belt (Calvert & Luden, 1999, in Leventis, 2017).

Figure 7: Metaconglomerate (Timinskaming assamblage) with gold-bearing veins (native gold inclusions in pyrite); Timmins. Photo: K. Bulcewicz

Base metal mineralization

On the northern fringe of the Porcupine camp in the Munro township area lie resourceful VHMS deposits (Kidd Creek, Potter, Potterdoal, Chance deposits; Barrie, 1999). They are hosted in the Kidd-Munro assemblage, dominated by mafic to ultramafic with minor felsic volcanic rocks (Barrie, 1999). At the Kidd Creek mine, the massive sulfide deposit lies within a steeply dipping volcanic sequence filling a syn-volcanic graben or half-graben (Walker et al., 1975) bordered by structural basins to the west ("Kidd west basin") and north of the mine ("Kidd 66 basin"; Barrie, 1999). The Porcupine assemblage rocks are thrusted onto the volcanic rocks in the southern part of the mine. The komatiites and minor barren rhyolite occurrences dominate the lowermost part of the volcanic sequence. The upper part consists mainly of basalt, gabbro sills and rhyolite with lesser graphitic argillite (Barrie, 1999). The rhyolites hosting the ore have a broad range of structures from massive (locally flow-banded),

coarse breccia (even meter-big blocks) to tuff-size clastic structure (Walker et al., 1975). They have undergone significant alteration (silicification, sericitization, chloritization etc.) in near proximity of the orebodies. The ore is concentrated in three elongated lenses plunging steeply to the north-northeast (Bleeker, 1999, in Barrie, 1999) and has developed in three major petrological types: (a) stringer ore, characterized by irregular chalcopyrite and minor sphalerite stringers within volcaniclastic rhyolite; (b) massive ore, composed mainly of pyrite, sphalerite, chalcopyrite, galena and pyrrhotite, occasionally banded or bedded within carbonaceous horizon; (c) breccia ore, heterogeneous type characterized by fragments of pyrite/sphalerite variably mixed with the barren-rocks, usually found nearby the graphitic argillite horizon (Walker et al., 1975). As Walker et al. (1975) suggest, the massive ores may have been deposited directly above a fumarole which brought mineralizing fluids to the sea floor, while the breccia ores indicate that accumulation of sedimentary sulfides (including bedded ore) and carbonaceous sediments was interrupted by explosive activity. From the structural features of the Kidd Creek deposit one may conclude that they represent the interplay between near-surface epigenetic and syn-sedimentary processes, which acted in the vicinity of a subaqueous rhyolitic volcano (Walker et al. 1975).

References

Barrie, C. T. (1999). The giant Kidd Creek volcanic-associated massive sulfide deposit, Abitibi Subprovince, Ontario. In: Volcanic-associated massive sulfide deposits: Processes and examples in modern and ancient settings. Society of Economic Geologists, 247-260.

Bateman, R., Ayer, J. A., and Dubé, B. (2008): The Timmins-Porcupine Gold Camp, Ontario: Anatomy of an Archean Greenstone Belt and Ontogeny of Gold Mineralization. Economic Geology 103, 1285-1308.

Bateman, R., Ayer, J. A., Dubé, B., and Hamilton, M. A. (2005): The Timmins–Porcupinegold camp, northern Ontario: the anatomy of an Archaean greenstone belt and itsgold mineralization: Discover Abitibi Initiative; Ontario Geological Survey, Open File Report 6158, 90p.

Bleeker, W. (1995): Surface geology of the Porcupine Camp. Geological Survey of Canada Open File 3141, 13-37.

Goldfarb, R., Groves, D., and Gardoll, S. (2001): Orogenic gold and geologic time: A global synthesis. Ore Geology Reviews 18, 1-75.

Houlé, M. G., Ayer, J. A., Baldwin, G., Berger, B. R., Dinel, E., Fowler, A. D., Moulton, B., Saumur, B.-M. and Thurston, P. C. (2008): Field trip guidebook to the stratigraphy and volcanology of supracrustal assemblages hosting base metal and gold mineralization in the Abitibi Greenstone Belt, Timmins, Ontario; Ontario Geological Survey, Open File Report 6225, 84p.

Hufford, G. (2015): Tectono-hydrothermal evolution of the Neoarchean Abitibi Greenstone Belt, Canada. MS Thesis, Colorado School of Mines.

Leventis, N.-G., (2017): Exploring the source of metals in Archean orogenic gold deposits in the Abitibi Greenstone Belt, Canada. MS Thesis, Stockholm University.

Natural Resources Canada [NRC] and Ontario Geological Survey [OGS] (2015): Timmins: Canada's greatest goldfields!. GeoTours Northern Ontario series.

Stromberg, J., Barr, E., and Banerjee, N. (2018): Early Carbonate Veining and Gold Mineralization in the Timmins Camp: Depositional Context of the Dome Mine Ankerite Veins. Ore Geology Reviews 97, 55-73.

Walker, R. R., Matulich, A., Amos, A. C., Watkins, J. J., Mannard, and G. W. (1975): The geology of the Kidd Creek Mine. Economic Geology 70, 80–89.

VI Komatiites

Kamil Bulcewicz

Introduction

Komatiites are Mg-rich (>18 wt% MgO) ultramafic volcanic rocks with distinct spinifex textures or rocks related to lavas containing such textures (Arndt and Fowler, 2004). Estimates of their eruption temperature usually yield ca. 1550-1600 °C (Herzberg, 2016). The occurrence of large, skeletal or dendritic crystals of olivine or pyroxene mark the diagnostic texture, which is believed to form during relatively rapid crystallisation from strongly supercooled melt. Well differentiated komatiite flows are usually composed of an upper, spinifex-textured part ("A" zone) and a lower, cumulus-textured part ("B" zone) dominated by isotropic olivine phenocrysts (Pyke et al., 1973). Figure 1 shows a summary of komatiite flow types (Houlé et al., 2008). Usually, the thicker the flow, the thicker the cumulate zone, as the overall cooling rate of the flow decreases (Houlé et al., 2008). Due to their low viscosity komatiites develop a handful of volcanic facies including vent (dikes, necks, volcanic breccias etc.), sheet-flow, channelized flow, lava pond and lava lobe facies among others (Sproule et al., 2003). They constitute less than 5% of the Abitibi Greenstone Belt rocks and typically occur in volcanic successions as (a) bimodal komatiite-komatiitic basalt sequences, (b) bimodal komatiite-basalt sequences, or (c) bimodal komatiite-rhyolite-dacite-andesite sequences (Houlé and Lesher, 2011).

Physical volcanology of the Munro sequence komatiites

Munro township area hosts the most significant outcrops of Abitibi komatiites. At Pyke Hill, the classic internal subdivision of komatiite lava flows has been established based on observations of at least 60 flows identified over a 125 m-width exposure (Pyke et al., 1973). The flow thickness in the Munro area varies from 0.75 m to 13.5 m with 3 m being the average. West from the Pyke Hill lie very well exposed massive olivine adcumulate rocks. Previously, they were interpreted to represent an approximately 120 m thick "Lava Lake", but recent studies showed that most of the sequence is rather composed of a series of thick flows (Arndt, 1986; Houlé et al., 2008). In the middle section of the adcumulate series unusual spinifex-textured zones (Figures 2, 3) occur, primarily thought to be the result of new magma influx to the "Lava Lake". Therefore, as Houlé et al. (2008) suggest, such zones may be related to partial melting and recrystallization due to residual heat from rapidly accumulated flows. In the upper part of the series well-developed columnar jointing also occurs.

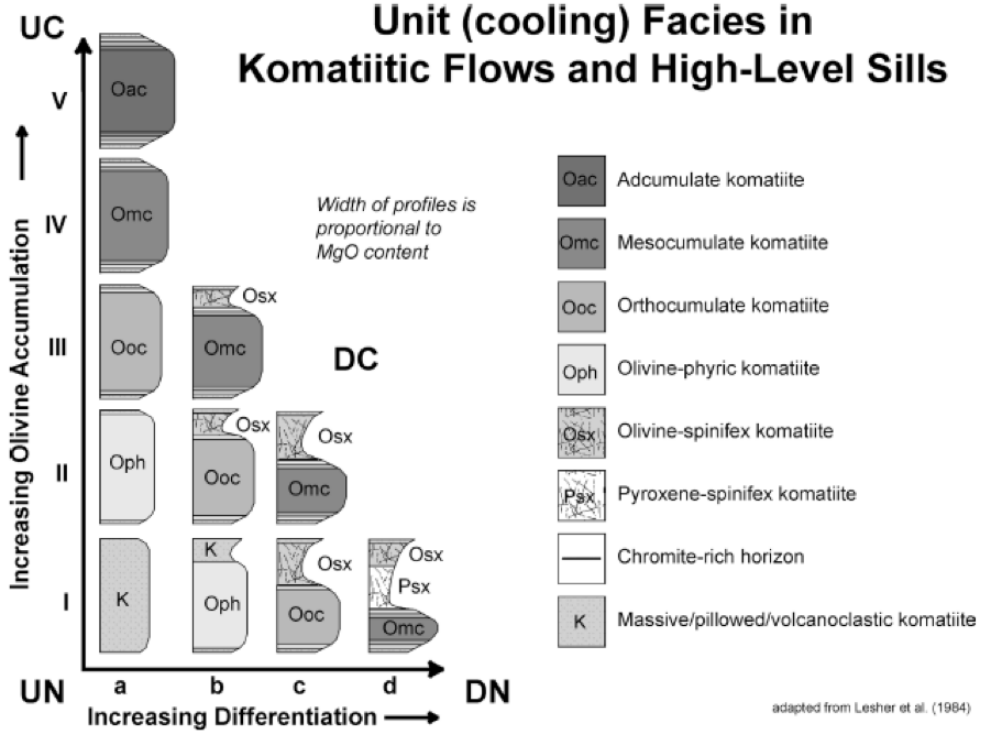

Figure 1: Chart showing relationship between level of differenctiation and developed komatiite flow lithotype; from Houlé et al. (2008). UC = undifferentiated cumulate; UN = undifferentiated non-cumulate; DC = differentiated cumulate; DN = differentiated non-cumulate.

Figure 2: Spinifex-textured sill in komatiite sequence of Deloro Assamblage (Timmins area). Photo: K. Bulcewicz

Figure 3: Fully developed komatiite lava flow with well-developed A-zone (upper, spinifex-textured) and B-zone (lower, cumulate-zone); outcrop on the road between Rouyn-Noranda and Rivière-Héva. Photo: K. Bulcewicz

The complex pattern of (sub)concordant thin spinifex-textured sills intrude the Pyke Hill and Serpentine Hill lava flows. They probably represent multiple injections of a new magma into a cooler, semi-consolidated pile of lava flows (Figure 4; Houlé et al., 2009). Most sills were emplaced in the channel near the spinifex/cumulate boundary of consolidated host flows. Zones of random spinifex textures and relatively coarse olivine crystals (several cm long, 1 cm wide) occur in thicker sills. In the host flows adjacent to the sills a coarse olivine zone can also be observed, due to heat-induced recrystallization (Houlé et al., 2008).

Ni-Cu-PGE mineralization

Most of komatiite-associated Ni-Cu-(PGE) mineralization occurring in the Kidd-Munro and Tisdale assemblages is thought to be mainly controlled by two factors. (1) Presence of Mg-rich lava channels (heat and metal sources) and (2) sulfide-facies iron formations, sulfidic slates, or exhalative sulfide lenses (sulfur sources) (Sproule et al., 2003). In the Dundonald area, situated 45 km NE of Timmins, both sedimentary rock-hosted sills and upper lying lava flows with Ni-Cu-(PGE) mineralization were identified (Houlé et al., 2009). As Houlé et al. (2009) suggest, sulfur saturation may have occurred during high-level sill emplacement and allowed the development of ore mineralization in both subvolcanic and volcanic rocks by influencing the migrating channelized magma.

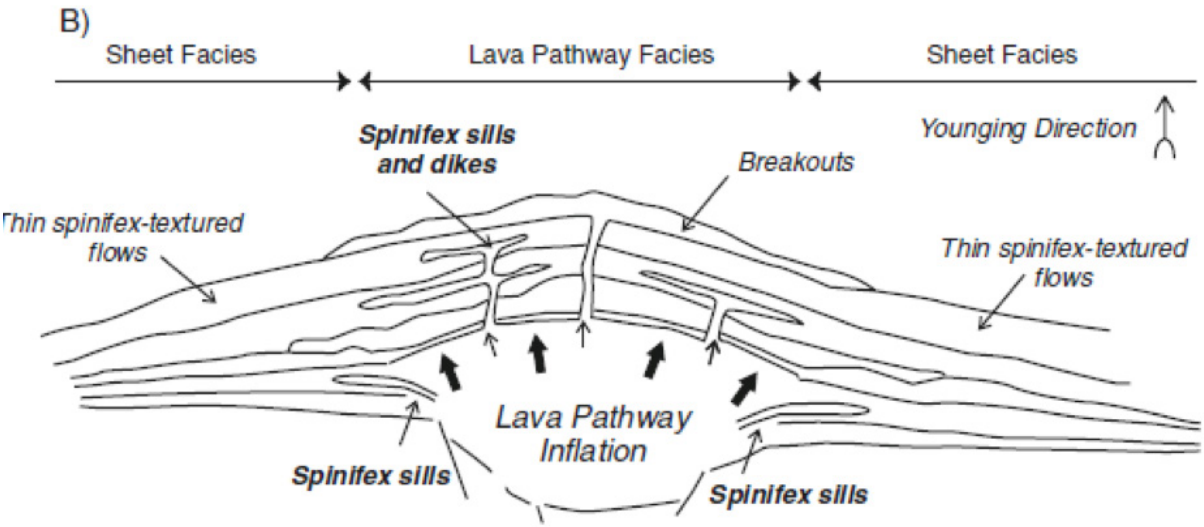

Figure 4: Interpretative model of spinifex-textured sills emplacement within the pile of komatiitic lava flows observed in the Pyke Hill and Serpentine Hill area; from Houlé et al. (2009).

References

Arndt, N., and Fowler A, (2004): Textures in komatiites and variolitic basalts. In: The Precambrian Earth: tempos and events. Elsevier, 298-311.

Herzberg, C. (2016): Petrological Evidence from Komatiites for an Early Earth Carbon and Water Cycle. Journal of Petrology 57, 2271–2288.

Houlé, M. G., and Lesher, C. M. (2011): Komatiite-Associated Ni-Cu-(PGE) Deposits, Abitibi Greenstone Belt, Superior Province, Canada. In: Magmatic Ni-Cu and PGE Deposits: Geology, Geochemistry, and Genesis.

Houlé, M. G., Préfontaine S., Fowler, A. D., and Gibson, H. L. (2009): Endogenous growth in channelized komatiite lava flows: Evidence from spinifex-textured sills at Pyke Hill and Serpentine Mountain, Western Abitibi Greenstone Belt, Northeastern Ontario, Canada. Bulletin of Volcanology 71, 881-901.

Houlé, M. G., Ayer, J. A., Baldwin, G., Berger, B. R., Dinel, E., Fowler, A. D., Moulton, B., Saumur, B.-M. and Thurston, P. C. (2008): Field trip guidebook to the stratigraphy and volcanology of supracrustal assemblages hosting base metal and gold mineralization in the Abitibi Greenstone Belt, Timmins, Ontario; Ontario Geological Survey, Open File Report 6225, 84p.

Pyke, D.R., Naldrett, A.J., and Eckstrand, O.R. (1973): Archean Ultramafic Flows in Munro Township, Ontario. Geological Society of America Bulletin, 955-978.

Sproule, R. A., Lesher, C. M., Ayer, J. A., and Thurston, P. C. (2003): Geochemistry and metallogenesis of komatiitic rocks in the Abitibi greenstone belt, Ontario; Ontario Geological Survey, Open File Report 6073, 119p.

VII Kidd Creek Mine

Andreas Etter

Overview

The Kidd Creek mine (VMS deposit type) is located 25 km north of Timmins, Ontario (Abitibi subprovince). It currently belongs to Glencore and is run by the subsidiary company Kidd Operations. The deposit was discovered in 1963 by drill-testing and electromagnetic survey. The economic deposits locally were covered by only 6 m of glacial till deposits, which are easy to remove. Open pit mining was started in 1966 and production from underground began in 1972. Mining at the Kidd Creek mine is being enlarged with an annual exploitation rate of approximately 3 Mt. This is achieved by a large open pit mine and underground mining to a depth of almost 3200 m (Figure 1; Barrie et al., 1999). The mine's exploitable rock material amounts to ca. 138.7 Mt. The average grades of the economic elements exploited at the Kidd Creek mine are listed in the Appendix. Other economic elements, which are exploited at Kidd Creek mine are S, Se, Cd, Sn, Ge and In. Special about the Kidd Creek mine is its coherent ore body (not patched together, but rather one single ore body), its large extent and the chemistry of its footwalls (Barrie et al., 1999).

Geologic setting

The Kidd Creek volcanogenic massive sulfide (VMS) deposit belongs to the Kidd-Munro assemblage, which extends 30 km west and north and 165 km east to the Quebec border (from Kidd Creek mine). Several other nearby deposits belong to this complex: The Chance deposit (0.2 Mt), the Potter mine (1 Mt) and the Potterdoal mine (minor Cu-Zn-Ag production; Barrie et al. 1999). Several other minor deposits can be found eastward.

The lithologies found within the assemblage are: plagioclase-phyric dacite, tholeiitic basalt, picrite, minor argillite, minor high silica rhyolite, and numerous high-level mafic to ultramafic sills (or decapitated flows; Barrie et al. 1999).

The Kidd-Munro assemblage has been exposed to at least three marking deformation events between 2.65 to 2.70 Ga (correlated to the Kenoan orogeny). There were three tectonic events, causing regional folding, influencing the area close to the Kidd Creek mine: a first phase of high-amplitude, upright regional folds;

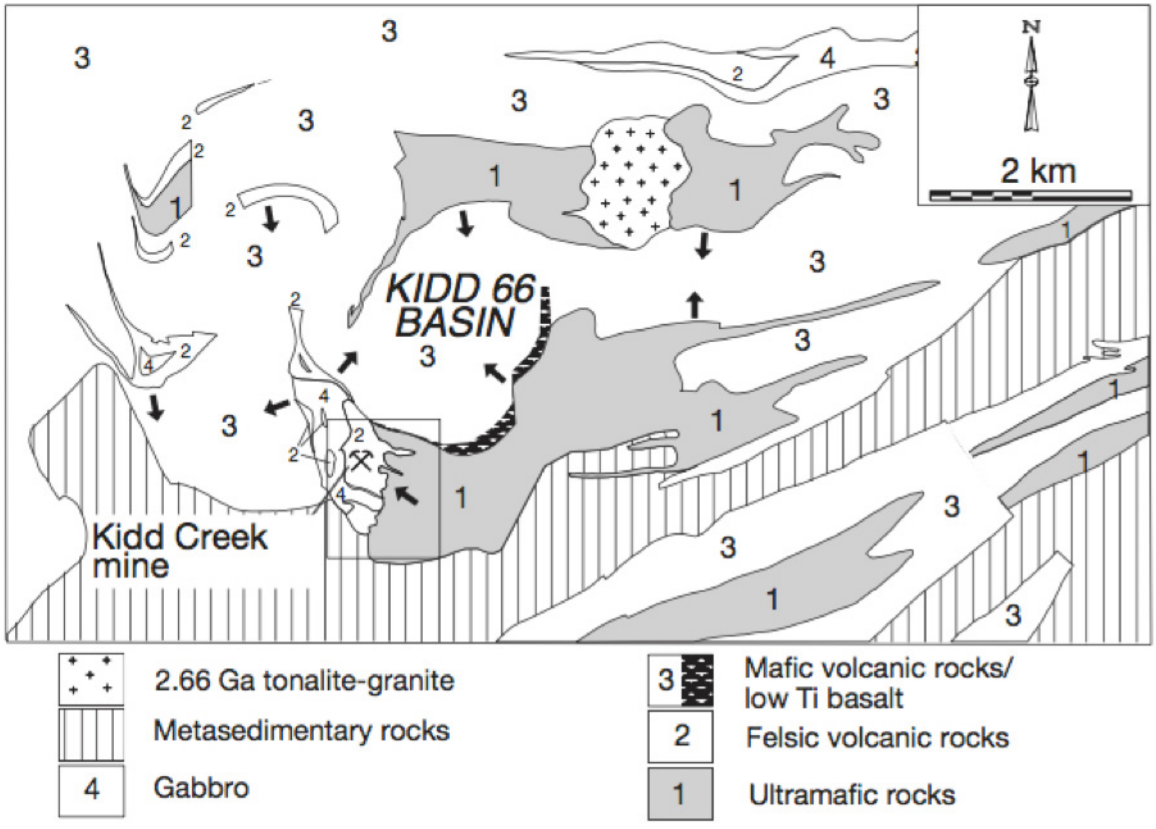

Figure 1: Geological map of the area surrounding the Kidd Creek mine; from Barrie et al. (1999).

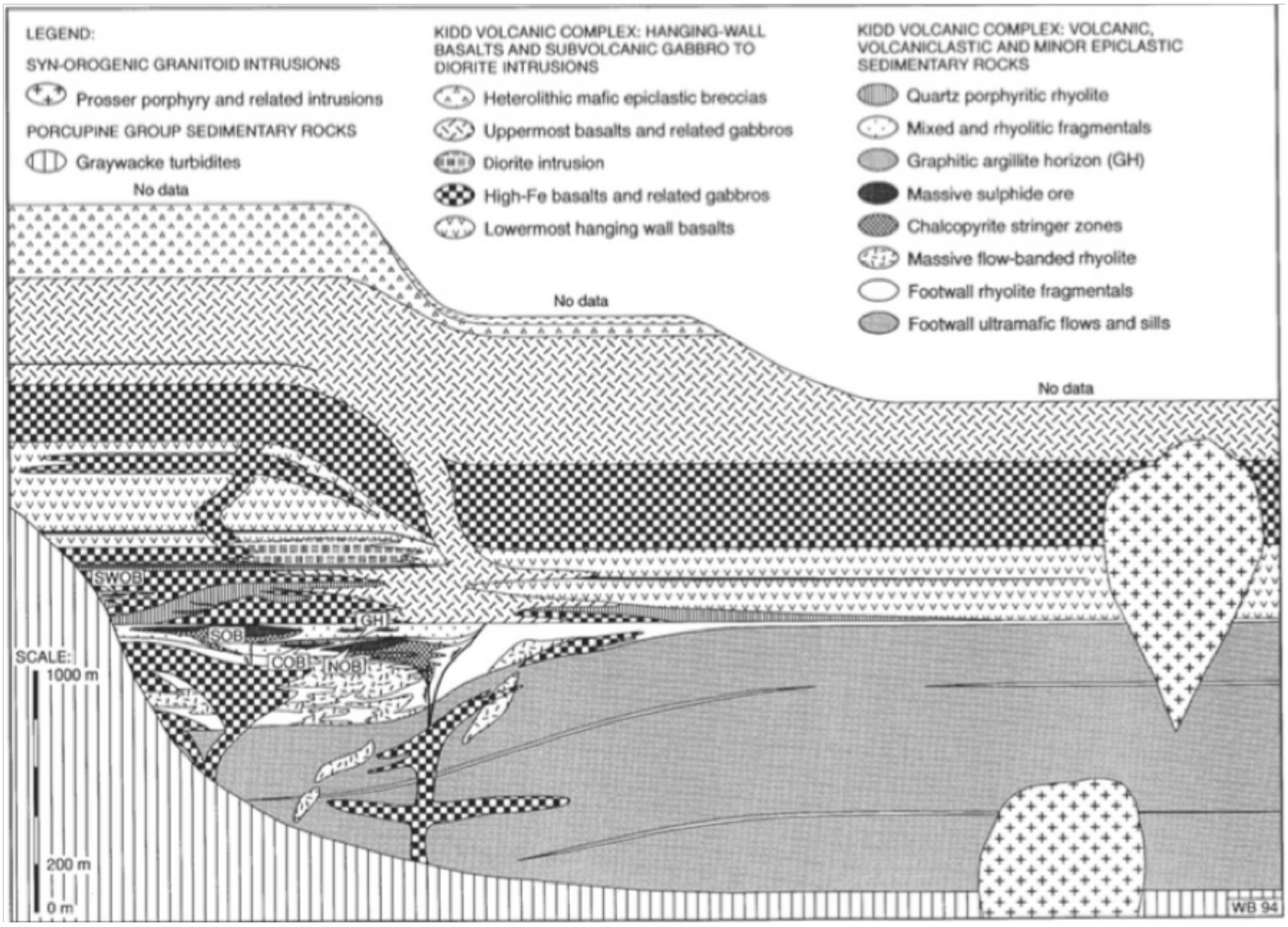

Figure 2: Stratigraphic cross section of the Kidd Creek mining area; from Barrie et al. (1999).

a second phase of east-northeast-oriented compression, resulting in steeply northeast-ward dipping folds; and a later northwest-oriented shortening giving rise to folds that are oriented perpendicular to the second-generation folds (resulting in a dome-and-basin to mushroom pattern). Two basins were formed nearby the mine: the Kidd 66 Basin in the north and the Kidd West Basin in the west. Those basins were formed by the combination of the two shortening axes (interference pattern). Later on, brittle deformation occurred due to the complicated folding pattern, creating several steep faults, which are oriented preferably north-westward (Barrie et al., 1999).

The ore body

The Kidd Creek deposit is located inside a pre-existing depression, which may represent a syn-volcanic graben or half-graben (Walker et al., 1975), surrounded by rhyolitic fragments and chalcopyrite stringer zones. It is bordered by structural basins to the west ("Kidd west basin") and north of the mine ("Kidd 66 basin"; Barrie et al., 1999). The Porcupine assemblage rocks are thrusted onto the volcanic rocks in the southern part of the mine.

The stratigraphic succession in the immediate surrounding of the ore body is composed of seven main units: (1) ultramafic flows (500-1000 m true thickness); (2) high-silica rhyolite flows and epiclastic/autoclastic breccias (100-400 m); (3) sulfide-rich ore horizons (0.1-50 m); (4) a locally graphitic, fine-grained siliciclastic unit (2-20 m); (5) gabbro sills (300-1000 m); (6) predominantly epiclastic high silica rhyolite rocks (100-300 m) in the hanging wall; and (7) basalt flows, hyaloclastite, and breccias (1000-2000 m; Barrie et al., 1999). The rhyolites hosting the ore have a broad range of structures from massive (locally flow-banded), coarse breccia (even meter-big blocks) to tuff-size clastic structure (Walker et al., 1975). They have undergone significant alteration (silicification, sericitization, chloritization etc.) in near proximity of the ore bodies.

The orebody consists of three main bodies plunging steeply to the north-northeast (Barrie et al., 1999): the northern ore body, the central ore body and the southern ore body. All three are located in an area of less than one square kilometer (surface and deeper as well). The ore bodies extend from almost the surface to a depth greater than 3 km, with an almost vertical

inclination.

The three ore bodies can be divided into an upper and a lower part. The upper one is sphalerite-rich and the lower one is chalcopyrite-rich. The upper part contains pyrite, sphalerite, pyrrhotite, minor chalcopyrite, tetrahedrite and galena. The lower part contains pyrite, chalcopyrite, small amounts of pyrrhotite, sphalerite and traces of native silver. The gangue minerals are typically quartz, sericite, carbonate and chlorite (Barrie et al., 1999).

Three major petrological types can be observed: (a) stringer ore, characterized by irregular chalcopyrite and minor sphalerite stringers within volcaniclastic rhyolite; (b) massive ore, composed mainly of pyrite, sphalerite, chalcopyrite, galena and pyrrhotite, occasionally banded or bedded within carbonaceous horizon; (c) breccia ore, heterogeneous type characterized by fragments of pyrite/sphalerite variably mixed with the barren rocks, usually found near the graphitic argillite horizon (Walker et al., 1975).

As Walker et al. (1975) suggest, the massive ores may have been deposited directly above a fumarole which brought mineralizing fluids to the sea floor, while the breccia ores indicate that accumulation of sedimentary sulfides (including bedded ore) and carbonaceous sediments was interrupted by explosive activity. From the structural features of the Kidd Creek deposit one may conclude that they represent the interplay between near-surface epigenetic and syn-sedimentary processes which acted in the vicinity of a subaqueous rhyolitic volcano (Walker et al. 1975).

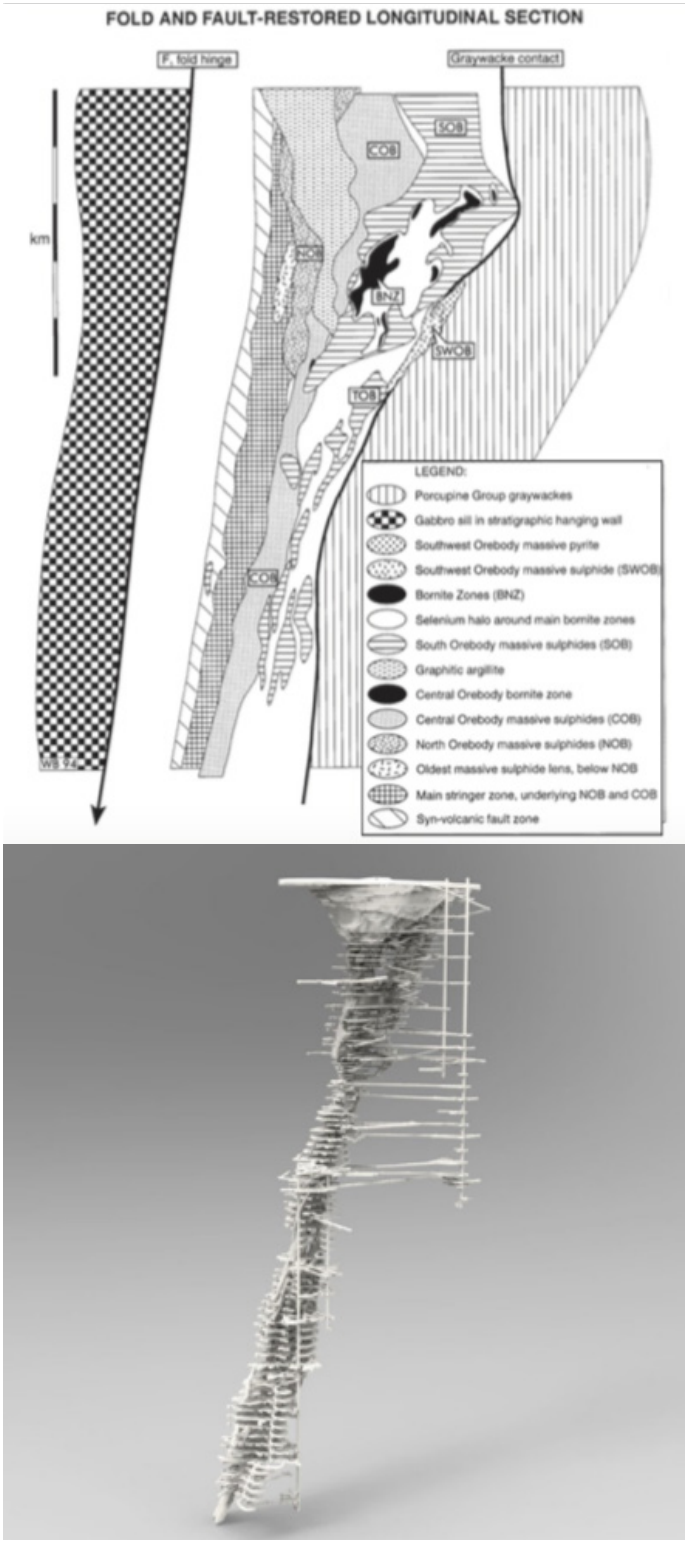

Figure 3: Longitudinal cross section through the Kidd Creek mining area (upper; Barrie et al., 1999) and a scheme of the mine itself (lower; https://3druck.com).

References

Barrie, C. T., Hannington, M. D., and Bleeker, M. D. (1999): The Giant Kidd Creek Volcanic-Associated Massive Sulfide Deposit, Abitibi Subprovince, Canada. Reviews in Economic Geology 8, 247-259.

Gibson, H., Richardson, D., Hannington, M., Gibbins, S., DeWolfe, M., and Duff, D. (2003): The Kidd Creek Volcanogenic Massive Sulfide Deposit: A Growing Giant, After Forty Years of mining, Exploration, and Research. The Gangue G.A.C. - Mineral Deposits Division 78, 1-18.

https://3druck.com/pressemeldungen/weltweit-tiefste-mine-fuer-kupfer-zinkgewinnung-im-massstab-15000-4338136/#jp-carousel-38133; accessed: 14.07.2019

Ross, P. S., and Mercier-Langevin, P. (2014): Igneous Rock Associations 14. The Volcanic Setting of VMS and SMS Deposits: A Review. Geoscience Canada 41, 365-377.

Walker, R. R., Matulich, A., Amos, A. C., Watkins, J. J., and Mannard, G. W. (1975): The geology of the Kidd Creek mine. Economic Geology, 70(1), 80-89.

Appendix

Table A.1: Main elements exploited at the Kidd Creek mine, 0-2400 m depth; total mass is at least 138.7 Mt (values from Barrie et al. 1999).

Element	Average Ore Grade (%)	Absolute Mass (Whole Section; in Mt)
Cu	2.35	3.26
Zn	6.5	9.02
Pb	0.23	0.32
Ag	0.009	0.01

Table A.2: Main elements exploited at the Kidd Creek mine, 2400-3000 m depth; total mass is 17 Mt (values from Barrie et al. 1999).

Element	Average Ore Grade (%)	Absolute Mass (Whole Section; in Mt)
Cu	1.85	0.31
Zn	8.43	1.43

VIII Horne Smelter, Strathcona Mill, and Sudbury Smelter

Andrei Dmitrovskii

Horne Smelter - Introduction

Copper is an extremely useful metal today because of its corrosion properties and high thermal and electical conductivity. Typical copper sulfide ores contain 0.5 – 2 % Cu (Larouche, 2001). Minerals containing Cu in these ores include chalcopyrite ($CuFeS_2$), bornite (Cu_5FeS_4) and chalcocite (Cu_2S; Larouche, 2001).

The Horne smetler works as a factory of e-scarp processing (Lennartsson, 2013). Main metallic elements, which are contained in the feedstock beside Cu and Fe usually are Sb, Bi, As, Au, and Ag, so the chemical complexity of the e-scarp feedstock needs to be taken into account (Lennartsson, 2013).

Table 1: Key facts of the Horne Smelter (Glencore).

Production:	Copper anodes (Cu 99.1%), precious metals
Feedstock:	e-scarp
Location:	Rouyn-Noranda, Quebec
Name:	Named after the prospector Edmund Horne who found the Cu-Au site of the Horne mine in 1927. The mine was closed in 1976.
Activity:	The smelter was commissioned in 1973. It is the largest processor of electronic scrap (Cu and precious metals) in North America.
Capacity:	840 kt Cu and precious metal bearing materials per year

Horne Smelter - Technology

The workflow of pyrometallurgical Cu production includes the following steps: flotation, matte smelting, converting, fire-refining and electorefining (Figure 1). 99.9% of the Cu cathodes are produced as a result of this sequence (Larouche, 2001). At the Horne smelter, three of these steps are performed: matte smelting or so-called Noranda smelting (producing molten matte with 72-74 % Cu), Pierce-Smith converting and fire-refining. Copper concentration in the feedstock is 20-45% (Larouche, 2001).

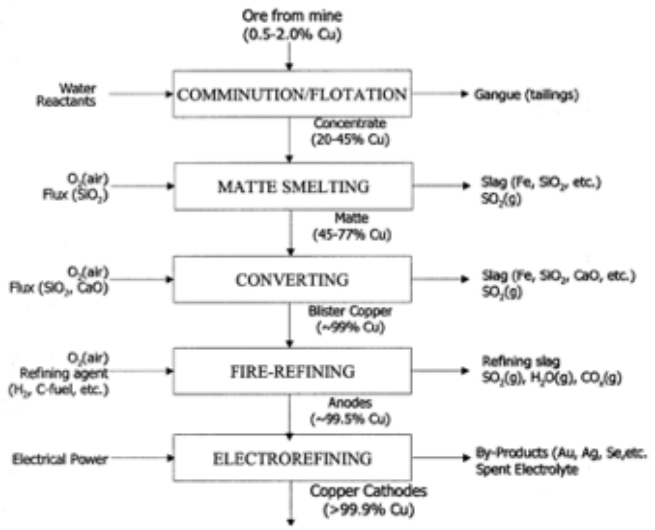

Figure 1: General flowsheet of conventional copper production process; from Larouche (2001).

Matte smelting: In this stage, the Cu concentrate is melted and part of the S and Fe is remover by oxidation (Larouche, 2001). Smelting is carried out at temperatures around 1200 °C, under oxidizing conditions (Larouche, 2001). To achieve such temperatures coal burning is used.

Reaction 1 describes this process for chalcopyrite concentrate feedstock. The Noranda furnace, which is used for smelting, is a 0.1 m thick horizontal molybdenium barrel. It is 21.3 m x 5.1 m in size and has 54 tuyeres with 5.4 cm in diameter. Tuyeres are used for oxygen pumping (Schlesinger et al., 2011). Slag is either discarded directly if the Cu content is low (< 1 %) or re-processed. The off-gas is cleaned from dust and is used in sulfuric acid production (Lennartsson, 2013).

Reaction 1:
4 $CuFeS_2$ (concentrate) + O_2 (blast) + SiO_2 (flux). → 2 (Cu_2S-Fe-S) (matte) + (2 FeO SiO_2) (slag) + 4 SO_2 (off-gas) + heat

Pierce-Smith converting: The objective of the stage is to transfer the remaining Fe in the matte into slag and S into SO_2 gas. There are two substages of this process: Firstly, Fe is eliminated in the slag-forming stage. The result is accumulation of Cu_2S (Larouche, 2001), according to Reaction 2. Secondly, white metal is oxidi-

zed with air (Larouche, 2001), according to Reaction 3. Resulting matte contains 71-72 % Cu and 3-5 % Fe.

Reaction 2:
2 FeS (in matte) + 3 O_2 (blast) + SiO_2 (flux) = 2 FeO SiO_2 (slag) + 2 SO_2 (off-gas)

Reaction 3:
Cu_2S (in matte) + O_2 (blast) = 2 Cu (blister) + SO_2 (off-gas)

For high-grade scrap (> 90 % Cu), e.g. Cu granules made from cables, a fire refining process in an anode furnace is suitable. The main part of fire refining process is oxidization of impurities. This process is based on oxidation of molten matte, as described by Reaction 4, where Me is some impurity (Lisienko et al., 2018). After the fire refining process the anodes contain an average of 99.2-99.3 % Cu (Forsen et al., 2017). Cu recovery is ca. 90-95 % (Schlesinger et al., 2011).

Reaction 4:
(a) 4 Cu + O_2 = 2 Cu_2O
(b) Cu_2O = 2 Cu + O
(c) Me + O = MeO
(d) Me + Cu_2O = MeO + 2 Cu

Strathcona Mill and Sudbury Smelter - Introduction

Strathcona Mill and Sudbury Smelter are parts of Glencore's Sudbury Integrated Nickel Operations (INO) that perform Cu and Ni as well as precious metal and Co production (Glencore).

Table 2a: Key facts of the Strathcona Mill (Glencore).

Location:	Onaping, Ontario, Canada
Type:	rod mill and ball mill
Feedstock:	Ni and Cu concentrates

Table 2b: Key facts of the Sudbury Smelter (Glencore).

Location:	Falconbridge, Ontario, Canada
Operation:	since 1930
Feedstock:	Ni-Cu concentrate from Raglan, Sudbury and XNA (Australia) lines
Capacity:	95000 t of Ni, Co and Cu per year

Strathcona Mill - Technology

Strathcona Mill receives ore from the two Sudbury mines (Nickel Rim South Mine and Fraser Mine) and third-party ores (Glencore). 30-35% of Ni ore consist of sulphide minerals (Levesque, 2015). Pyrrhotite ($Fe_{(1-x)}S$) constitutes 75-80 % of sulfides exhibiting ferromagnetic properties (Levesque, 2015). Nickel ores are characterised by pyrrhotite/pentlandite ratio between 4.5 and 6 (Kelebek et al., 1996). The main mineral of Cu ore is chalcopyrite ($CuFeS_2$). This ore type has a small percentage of pentlandite $(Fe,Ni)_9S_8$ and pyrrhotite (Kelebek et al., 1996). Grades of pentlandite nickel feed and chalcopyrite are about 4% while grade of pyrrhotite varies from year to year: it was 19 % in 2016 and 30 % in 2017 (Qi et al., 2019).

Froth flotation (Figure 2) is used in the Strathcona Mill to produce ore concentrates. Froth flotation is a process based on wetting of substances (Schelinger et al., 2011). Usually, sulfide minerals are wetted by water (they are hydrophilic) but using some reagents one can make them hydrophobic. Selectively made hydrophobic minerals can be floated to the slurry surface by the air bubbles while hydrophilic minerals stay in the slurry (Schelinger et al., 2011). As a result metal concentrate is produced after removal of water. A simplified flowsheet of the Strathcona Mill is shown in Figure 3.

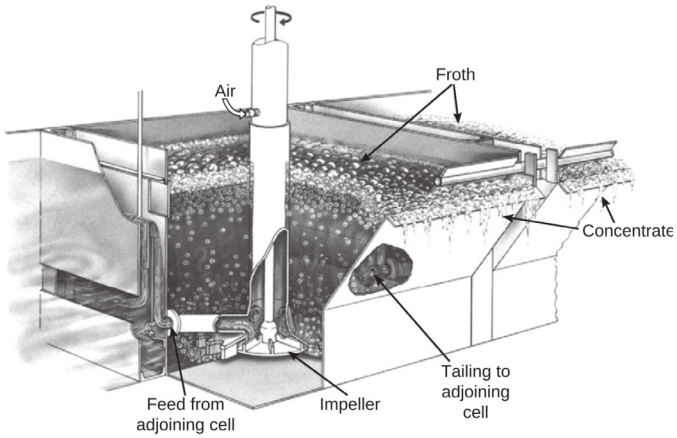

Figure 2: Cutaway view of cubic flotation cell; from Schelinger et al. (2011).

Ore processing in the Strathcona Mill consists of three circuits. Two of them are nickel circuits that process about 180 t per hour of Ni ore (feeds A and B in Figure 3) each and the third circuit processes up to 75 t per hour of Cu-rich ore (feed C).

The first step in all circuits is rougher-scavenger flotation (Figure 4). Rougher flotation is carried out in saturated pulp with a pH values of 9-9.5, which is ad-

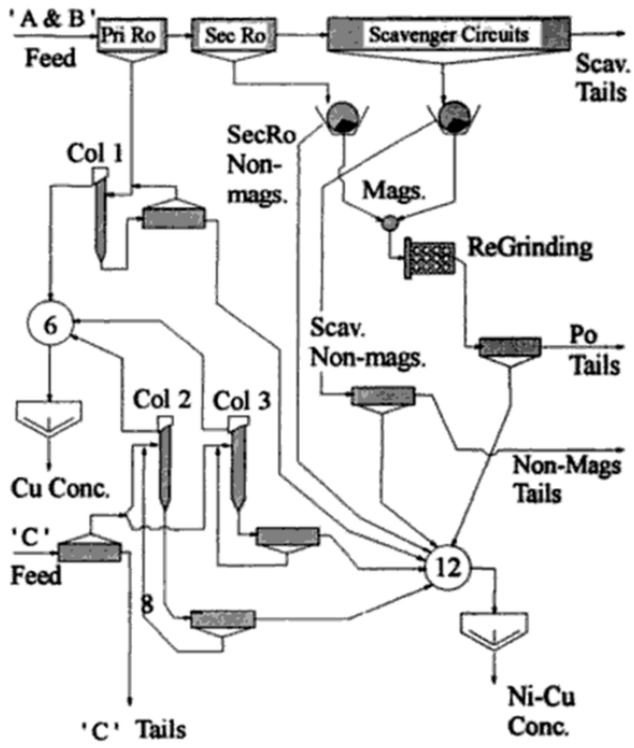

Figure 3: Strathcona Mill process flowsheet (from Kelebek et al., 1996)

justed with lime. This stage consists of two rougher substages. Subsequent scavenger flotation is applied to rougher tailings. An objective of this stage is to recover target metals that were not recovered during the rougher stage. All non-magnetics from the secondary rougher substage tailings go directly to combined Cu-Ni concentrate while non-magnetics from the scavenger are additionally upgraded (Kelebek et al., 1996). Magnetic tailings are transferred to the magnetic separation stage for pyrrhotite-pentlandite division. After pyrrhotite rejection this substance goes to regrinding (Kelebek et al., 1996).

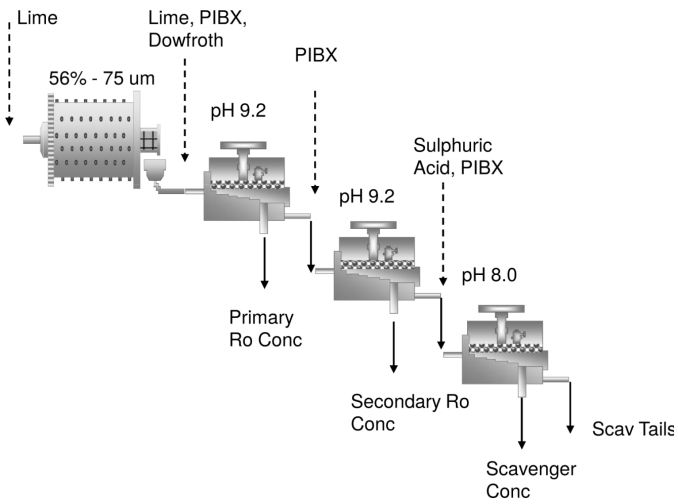

Figure 4: Rougher and scavenger stages; from Muinonen et al. (2014).

In all circuits chalcopyrite-pentlandite separation is done in column cells using cyanide chemistry with pH >12 (Kelebek et al., 1996), as chalcopyrite becomes hydrophobic with the addition of basic reagents (Schelinger et al., 2011).

Pyrrhotite recovery may reach 70-80% after the scavenger stage (Kelebek et al., 1996). Results of the Mill activity are two concentrate streams: Ni-Cu concentrate for smelting and Cu concentrate for smelting and refining (Glencore).

Sudbury Smelter - Technology

Essentially, the steps of Ni production are the same as the ones shown in Figure 1, but again only roasting and smelting are performed here. The key processing steps are: feed receiving and preparing, fluid bed roasting and off-gas cleaning, electric furnace smelting and converter aisle.
The feed received at the smelter is a slurry containing 70% solids and 30% water. Feedstock of the Sudbury smelter is Ni concentrate containing 5-9 % Ni and a Cu concentrate containing 30 % Cu and 1 % nickel (Sara group) from Copper Cliff and Levack mills. These concentrates are produced from ores that contain 1-2.5 % Ni.

Roasting is a process of heating of sulfide ores in presense of air for sulfur removal from the concentrate to increase the concentration of Ni. For instance, roasting of pentlandite and pyrrhotite ores is described by reaction 5 (Crundwell, 2011).

Reaction 5:

(a) at 700 °C:
$Ni_{4.5}Fe_{4.5}S_8(s) + 12.5\ O_2(g) \rightarrow 4.5\ NiO(s) + 4.5\ FeO(s) + 8\ SO_2(g)$

(b) at 700 °C;
$Fe_8S_9(s) + 13\ O_2(g) \rightarrow 8\ FeO(s) + 9\ SO_2(g)$

Sulfur dioxide emission is one of the main environmental issues linked to the sulfide ore smelting process (Crundwell, 2011). This off-gas is transferred into sulfuric acid in an acid plant, according to Reaction 6.

Reaction 6:

(a) $2\ SO_2 + O_2 \rightarrow 2\ SO_3$

(b) $SO_3 + H_2O \rightarrow H_2SO_4\ (g)$

The next step is electric furnace smelting. The furnace in Falconbridge has dimensions of 9 m x 30 m x 3 m (Crundwell, 2011). During this process warm (~300

°C) calcine goes into the hot (~1300 °C) electrically heated furnace with a silica flux. Molten material separates into 2 immiscible liquids: sulfide Ni-rich matte and Fe-saturated and Ni-poor slag (Crundwell, 2011). Molten matte (specific gravity 4.8-5.3) is in the bottom of the furnace in steady-state, molten slag is in the middle (specific gravity 2.7-3.3) and solid calcine at the top (Crundwell, 2011). Produced matte composition is 36 % Ni, 11 % Cu, 1 % Co, 33 % Fe and 7 % S.

To recapitulate, the recovery of a certain metal for a certain ore is a percentage of this metal that was extracted from the total ore‘s metal content during ore processing excluding metal that went into the slag. The recovery of Cu and Ni in the electric furnace is about 98% for both metals. The recovery of cobalt is between 50 and 80% (Crundwell, 2011).

References

Crundwell, F. K., Moats, M. S., Ramachandran, V., Robinson, T. G., and Davenport, W. G. (2011): Smelting of Nickel Sulfide Concentrates by Roasting and Electric Furnace Smelting. In: Extractive Metallurgy of Nickel, Cobalt and Platinum-Group Metals, 199-214.

Forsen, O., Aromaa, J., and Lundstrom, M. (2017): Primary Copper Smelter and Refinery as a Recycling Plant—A System Integrated Approach to Estimate Secondary Raw Material Tolerance. Recycling 2, 19.

Glencore: Horne smelter, http://www.glencorerecycling.com/en/RecyclingServices/recycling-operations/Pages/Horne-Smelter.aspx (accessed on June 28th 2019).

Glencore Nickel: http://www.glencore.ca/en/What-we-do/Metals-and-minerals/Nickel (accessed on June 30th 2019).

Kelebek, S., Wells, P. F., and Heinrich, G. W. (1996): Metal ion characterization of monoclinic pyrrhotite from nickel-copper ores using EDTA extraction. Changing Scopes in Mineral Processing, 295-300.

Larouche, P. (2001): Minor elements on copper smelting and electrorefining, Master Thesis, McGill Univesity. Retrieved from: http://digitool.library.mcgill.ca/webclient/StreamGate?folder_id=0&dvs=1563136791279~726

Lennartsson, A. (2013): Development of a process model for a Peirce-Smith converter. Licentiate Thesis, Luleå University of Technology. Retrieved from: https://www.diva-portal.org/smash/get/diva2:998911/FULLTEXT01.pdf

Levesque, M. Y., and Millar, D. L. (2015): The link between operational practices and specific energy consumptionin metal ore milling plants – Ontario experiences. Minerals Engineering 71, 146–158.

Lisienko, V. G., Holod, S. I, and Zhukov, V. P. (2018): Modeling of Metallurgical Process of Copper Fire Refining. KnE Engineering / VII All-Russian Scientific and Practical Conference of Students, Graduate Students and Young Scientists.

Lotter, N. O., Kormos, L. J., Oliviera, J., Fragomeni, D., and Whiteman, E. (2011): Modern Process Mineralogy: Two case studies. Minerals Engineering 24, 638–665.

Qi, C., Liu, J., Malainey, J., Kormos, L. J., Coffin, J., Deredin, C., Liu, Q., and Fragomeni, D. (2019): The role of Cu ion activation and surface oxidation for polymorphicpyrrhotiteflotation performance in Strathcona Mill. Mineral Engineering 134, 87-96.

SARA Group (2008): Sudbery Area Risk Assesment, Historical Review of Air Emissions from the Smelting Operations. Link: http://www.sudburysoilsstudy.com/EN/media/Volume_I/SSS_Vol_I_Chapter_3_HistoricalReviewofAirEmissions_FINAL%20_Jan2008.pdf (accessed on June 30th 2019)

Schlesinger, M. E., King, M. J., Sole, K. C., and Davenport, W. G. (2011): Production of Cu Concentrate from Finely Ground Cu Ore. In: Extractive Metallurgy of Copper (5th ed.), 51-71.

Schlesinger, M. E., King, M. J., Sole, K. C., and Davenport, W.G. (2011): Submerged Tuyere Smelting: Noranda, Teniente, and Vanyukov. In: Extractive Metallurgy of Copper (5th ed.), 111-125.

IX Blake River Group megacaldera complex

Julian Reyes

Geology of the Blake River Group

The Blake River Group (BRG) is located in the Abitibi Suprovince, western Quebec, and it is the youngest volcanic sequence in the Abitibi Greenstone Belt (2704–2695 Ma; McNicoll et al., 2014; Figure 1; Chapter IV). The sequence consists of tholeiitic, transitional and calc-alkaline submarine volcanics, with an east-west trend. Evidence of the submarine environment are pillow lavas and pillow breccias with turbidite and argillite interbeds (Leverington & Schindler, 2018). Different volcanic centers have been identified by rapid facies changes, variations in the thickness and increased proportion of felsic volcanics of individual units combined with structural and crosscutting relationships (McNicoll et al., 2014).

The most extensive sequence of the BRG is overlying the Tisdale Group between the Porcupine–Destor and Larder Lake–Cadillac fault systems (Houlé et al., 2008). The BRG is conformably overlying volcanics of the Tisdale group (2710-2704 Ma) in the western part. The BRG is overlain by younger (<2687 Ma) turbiditic deposits of the Cadillac Group and the Kewagama Group (McNicoll et al., 2014) and unconformably overlain by the alkalic volcano-sedimentary (polymictic conglomerates) sequence of the Timiskaming Group (2680–2669 Ma) and Proterozoic conglomerates of the Cobalt Group (McNicoll et al., 2014). Archean gabbroic, dioritic, tonalitic synvolcanic and syenitic, dioritic, granodioritic, granitic syntectonic intrusions cross-cut the BRG, as well as Proterozoic gabbroic dykes of the Nipissing Diabase (Ontario Geological Survey, 2016; Figure 2-3).

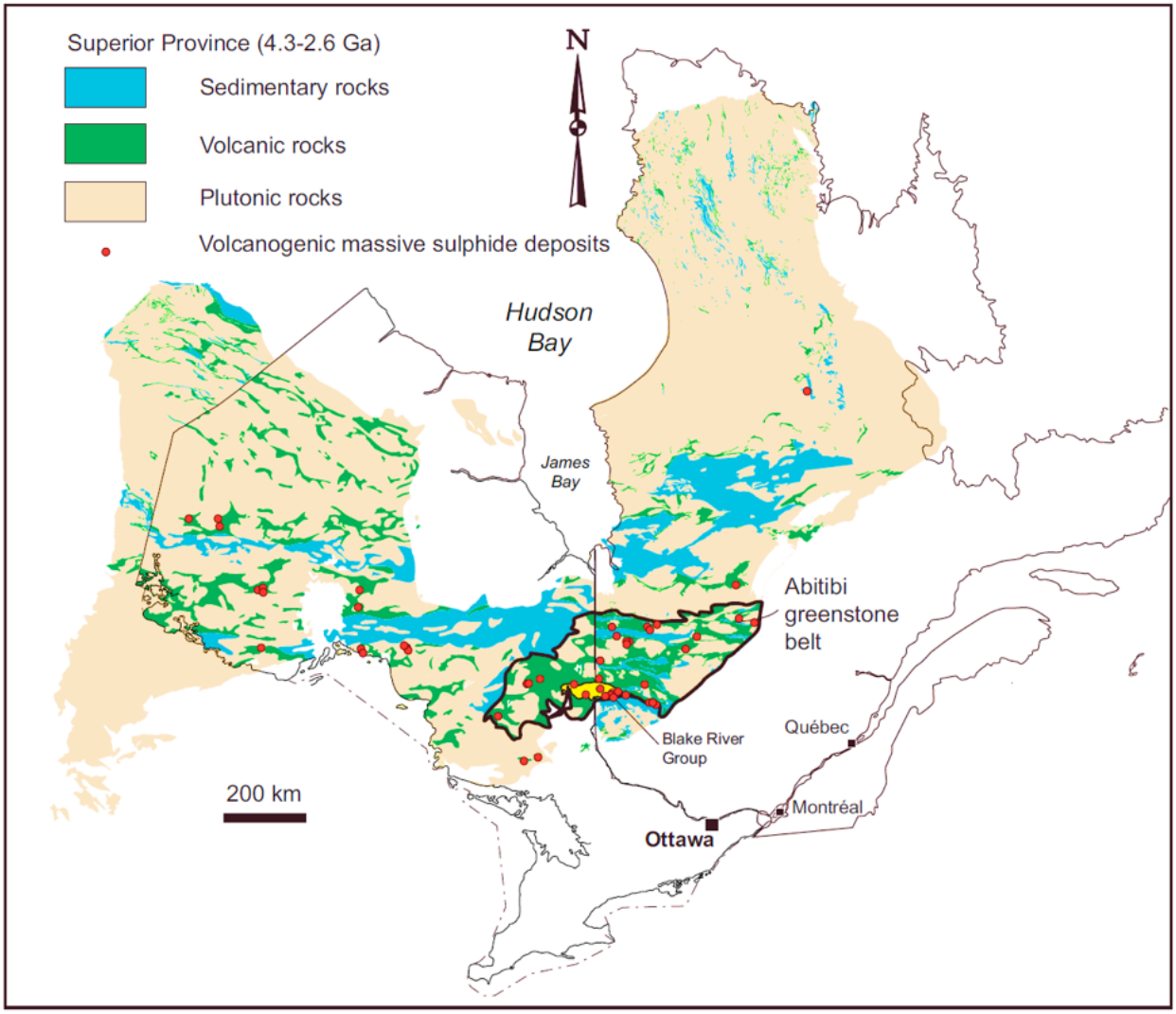

Figure 1: Map of the Superior Province showing the location of the Abitibi greenstone belt and of the Blake River Group (in yellow). The principal VMS deposits of the Superior Province are also shown. Figure from Mercier-Langevin et al. (2011).

The BRG has been subjected to major north-south shortening with subsequent sub-greenschist (north) to lower amphibolite (south) facies metamorphism with weak deformation. The central section is dominated by major folds in a tilting strata (Ontario Geological Survey, 2016). Additionally, the formation is bounded by the Larder Lake-Cadillac fault system to the south and the Porcupine-Destor fault system to the north, where it is characterized by laterally extensive shears and tight folds. Locally, alteration and deformation have overprinted primary textures in the sequence (McNicoll et al., 2014).

The BRG is stratigraphically subdivided in a lower (2704–2702 Ma) and upper part (2701–2696 Ma; Figure 4). The lower unit is formed by tholeiitic basalts and Fe- and Mg-rich basalts with minor turbiditic sediments and felsic volcanic units (rhyolite flows and pyroclastics; Houlé et al., 2008). The lower BRG crops out in the south and north margins of the Blake River synclinorium. The lower group also crops out in the Kamiskotia area, along the west flank of the Nat River

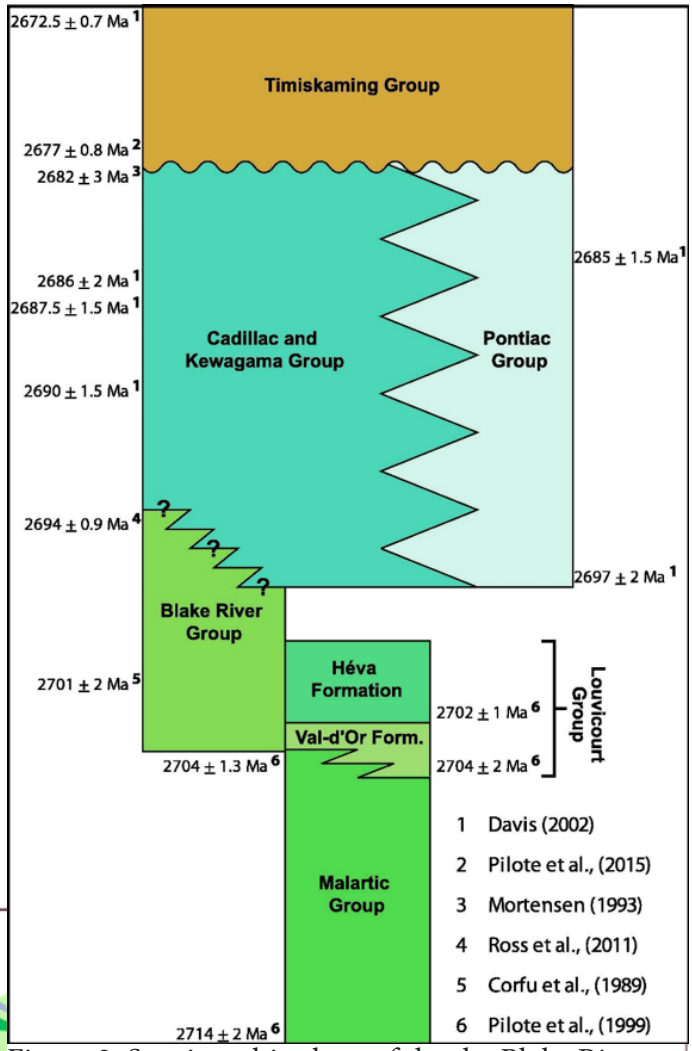

Figure 3: Stratigraphic chart of the the Blake River Group with relevant istopic ages. Figure from Bedeaux et al. (2017).

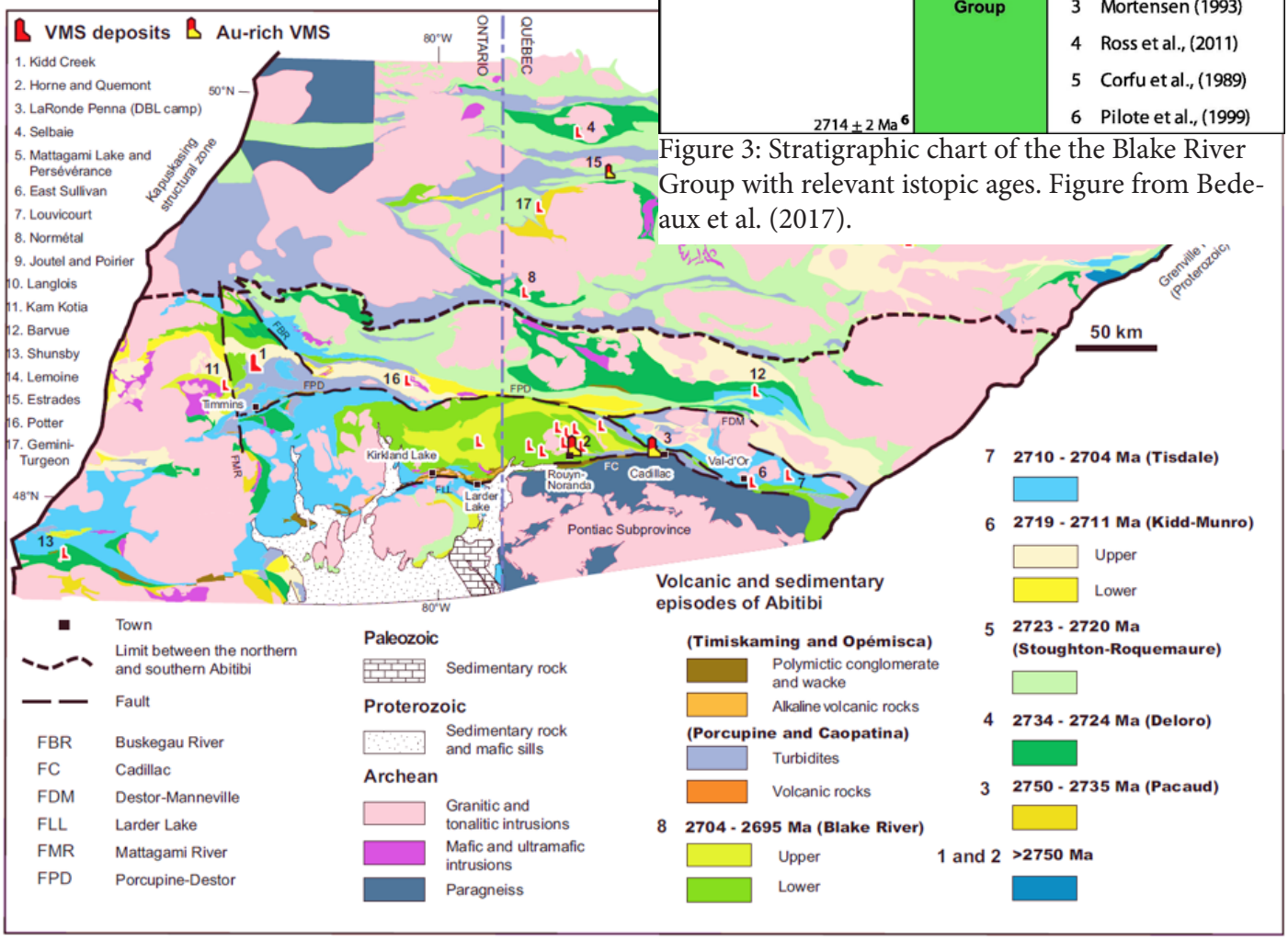

Figure 2: Map of the Abitibi greenstone belt, with location of the VMS and Au-rich VMS deposits. With the Blake River Group highlighted. Figure from Mercier-Langevin et al. (2011).

batholith, underlain by the Kidd–Munro assemblage (Houlé et al., 2008; Figure 2).

On the other hand, the upper unit is formed by andesite and calc-alkalic basalt flows with local bimodal tholeiitic basalt and rhyolite. It crops out in four different areas: (1) in the center of the Blake River synclinorium; (2) in the Kamiskotia area, along the east flank of the Nat River batholith; (3) in the center of the Swayze greenstone belt, Swayze Group, overlying the Tisdale Group; (4) formed by felsic to calc-alkalic intermediate volcanic rocks (2701 Ma) in southeast the Kirkland Lake area, Skead Formation, in the southern and eastern flanks of the Round Lake batholith, overlying the Stoughton–Roquemaure Group (Houlé et al., 2008).

Several volcanogenic massive sulfide (VMS) deposits are hosted in the BRG, including five of the largest Au-rich VMS deposits recognized in the world (McNicoll et al., 2014). The deposits are hosted in two VMS districts: Doyon-Bousquet-LaRonde and Noranda districts, distinguished by their alteration assemblages, deformation overprinting and metallogeny (Huston et al., 2011; Figure 6). Furthermore, there are gold deposits spatially related to mafic intrusions in the BRG. For example, diorite is found in the hanging wall of the Francoeur deposit and the diorite intrusion hosts a mineralized shear zone, the El Coco deposit (Ontario Geological Survey, 2016).

The BRG is subdivided in three different events / complexes (Figure 4-5). The most important of those, the Noranda complex, is a 35-km-diameter, 7-9 km thick, volcanic center formed by basalt to rhyolite units cross-cut by gabbroic and dioritic dikes (Leverington & Schindler, 2018). The complex is interpreted as a large shield volcano and it has been divided into five

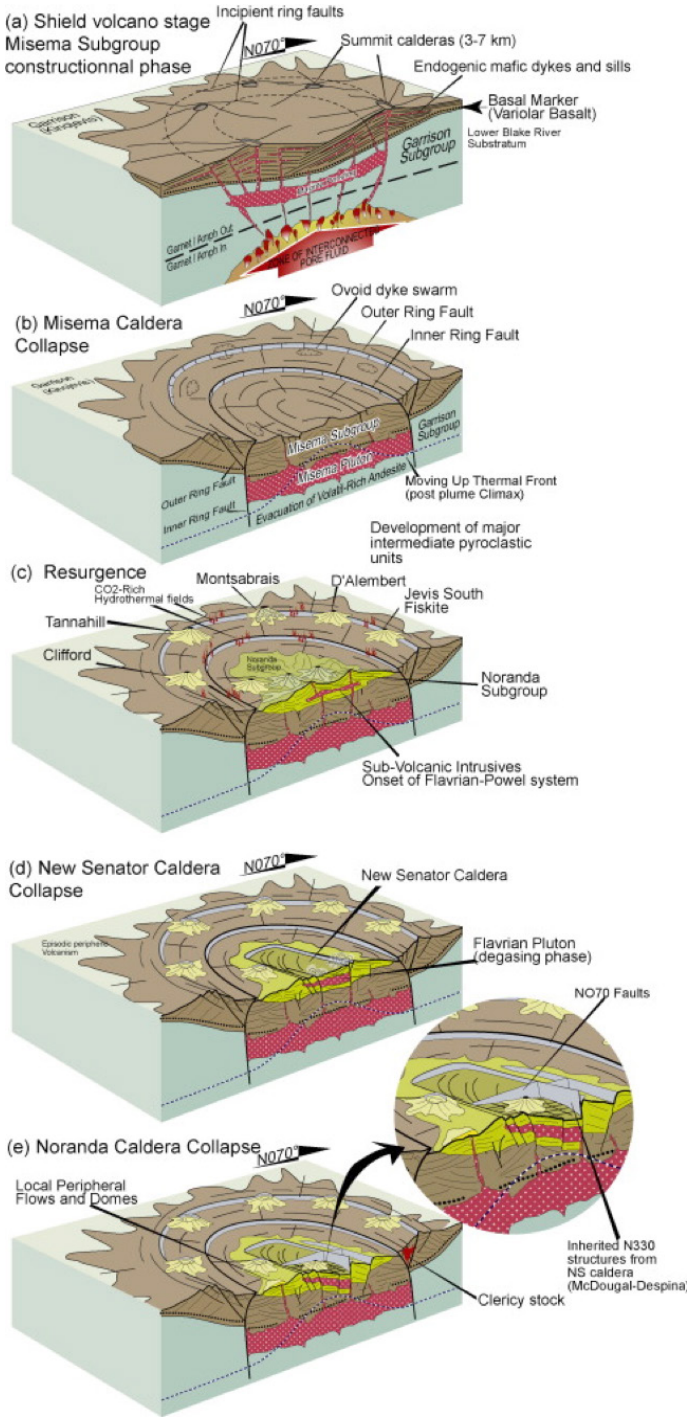

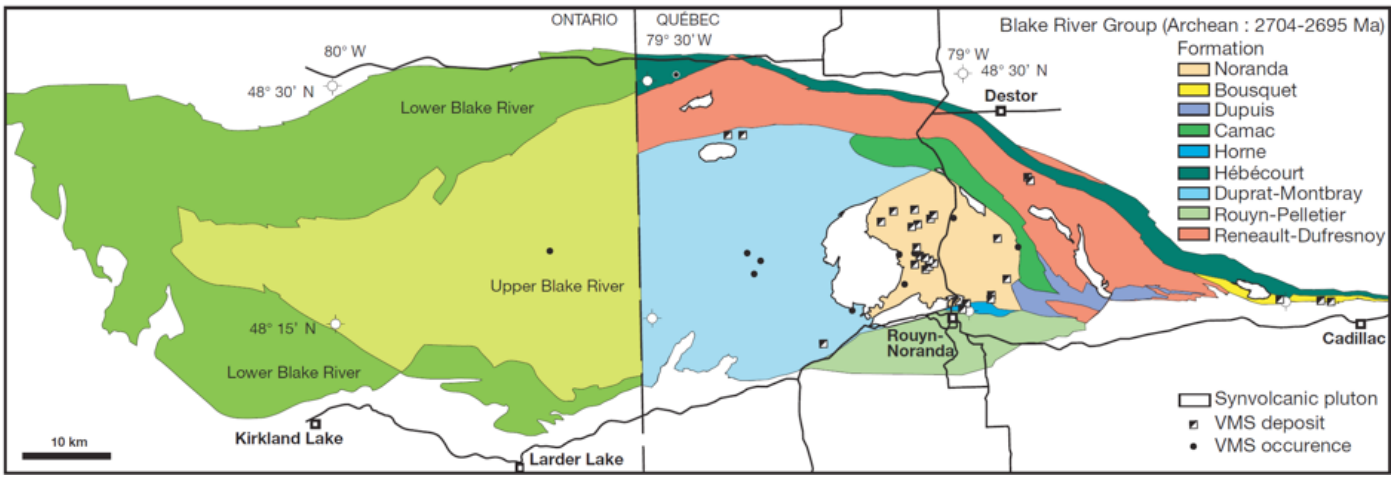

Figure 4: Map of the BRG with the stratigraphic subdivision and nomenclature in Quebec and Ontario (McNicoll et al., 2014).

sequences which young to the east. Each of them is composed of a mafic-intermediate basal unit (up to 65-90% of the cycles) and a bimodal (andesite-basalt and rhyolite) upper unit (Ontario Geological Survey, 2016).

Noranda district deposits

The Noranda district deposits are related to chloritization and sericitization in a pipe-like structure. Moreover, there is evidence of regional fluid flow as silica-, chlorite-, epidote/quartz-bearing alterations. The mineralization (Horne mines) is pyrite + pyrrhotite + chalcopyrite + galena + sphalerite + magnetite + native gold + silver (Leverington & Schindler, 2018). There are two types of deposits in the district: small-medium deposits and Horne deposits (Figure 6 inset b; Table 1).

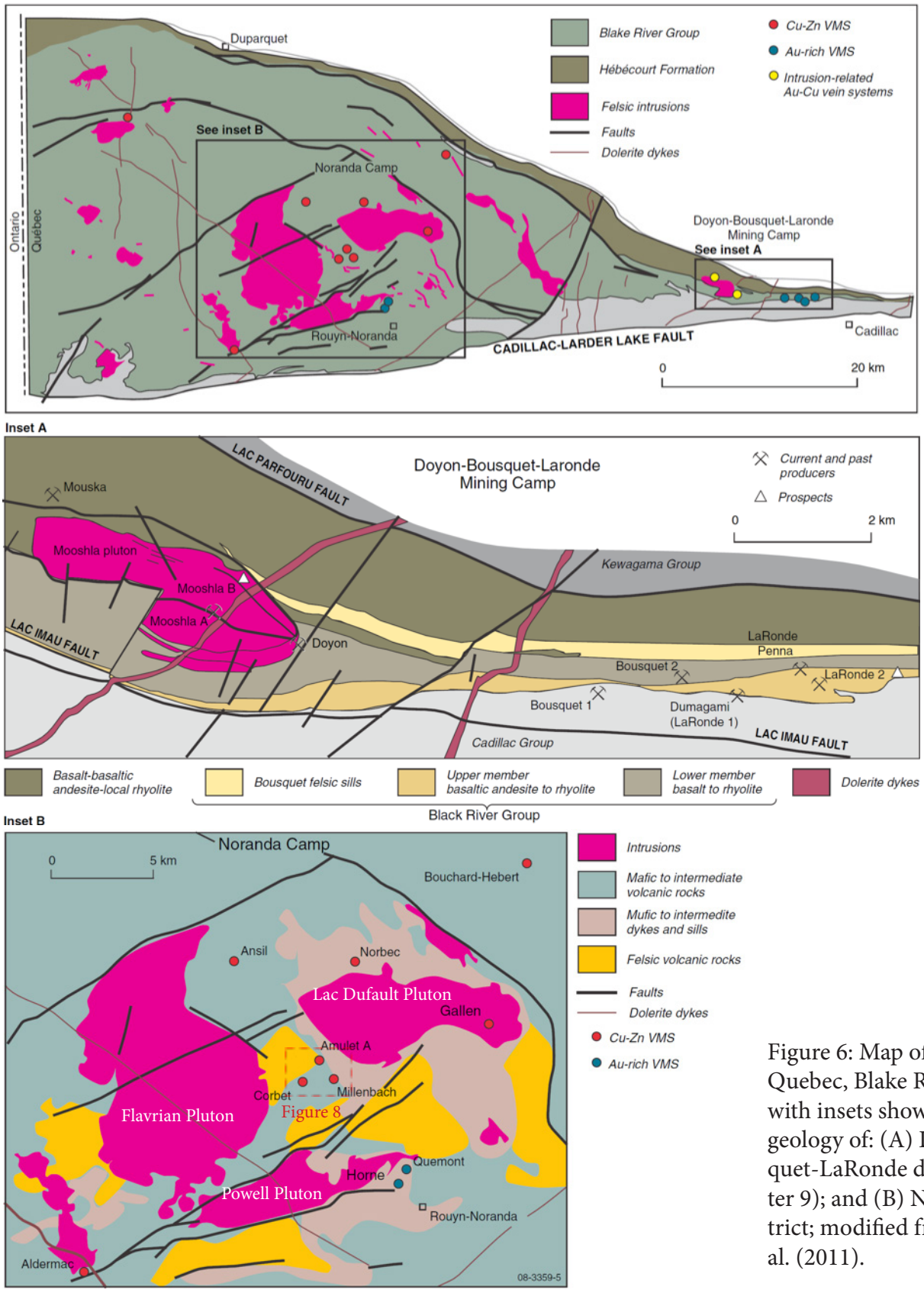

Figure 6: Map of western Quebec, Blake River Group, with insets showing detailed geology of: (A) Doyon-Bousquet-LaRonde district (Chapter 9); and (B) Noranda district; modified from Huston et al. (2011).

Most of the small-medium deposits are linked with andesitic and rhyolitic flows associated to volcanic subsidence during partial emptying of the magma chamber known as "the Noranda Cauldron" (Ontario Geological Survey, 2016; Figure 8). The Noranda district (2702 Ma) has 18 small-medium VMS deposits hosted in greenschist metamorphosed bimodal

flow dominated basaltic-andesitic and high-silica rhyolitic with pyroclastic rocks upper sequence of the Noranda cauldron (Huston et al., 2011; Ontario Geological Survey, 2016; Figure 7). The deposits are <5 Mt, Cu-Zn rich, concordant mounds linked to vent dome areas, which provided fluids in interflow horizons with coherent lavas (Ontario Geological Survey, 2016).

On the other hand, the Noranda district also host the large Horne deposits that are related with rhyolite flows and fragmental rocks in a sequence with few mafic volcanics. The host rock shows a marked depletion in incompatible elements, high field strength elements and rare earth elements indicating a differentiated parental magma compared to the host rocks of the small-medium deposits (Ontario Geological Survey, 2016). The Horne deposits are formed by extensive sub-seafloor sulfide precipitation (Ontario Geological Survey, 2016; Figure 9). They have 20-150 Mt, with high concentration of Au-Cu and low Zn. The big deposits are in a fault bounded, sediment filled, graben related to the flank of a rhyolitic vent complex (Ontario Geological Survey, 2016).

The Noranda Cauldron is linked to two poly-phase, tonalite bearing plutons: the Powell and the Flavrian plutons that were emplaced during and after the cauldron (Huston et al., 2011). Up to six phases have been identified in the intrusive complex, with VMS deposits related to the earliest quartz diorite phase. Cu-Mo deposits (porphyry and breccia-hosted) are linked to the emplacement of the most extensive trondhjemitic phase post-dating VMS formation (Huston et al., 2011).

Doyon-Bousquet-LaRonde district deposits

The Doyon-Bousquet-LaRonde district (2698 Ma) has bigger but fewer (4) VMS deposits, located in an area that has experienced a higher grade metamorphic overprint (upper greenschist to lower amphiboli-

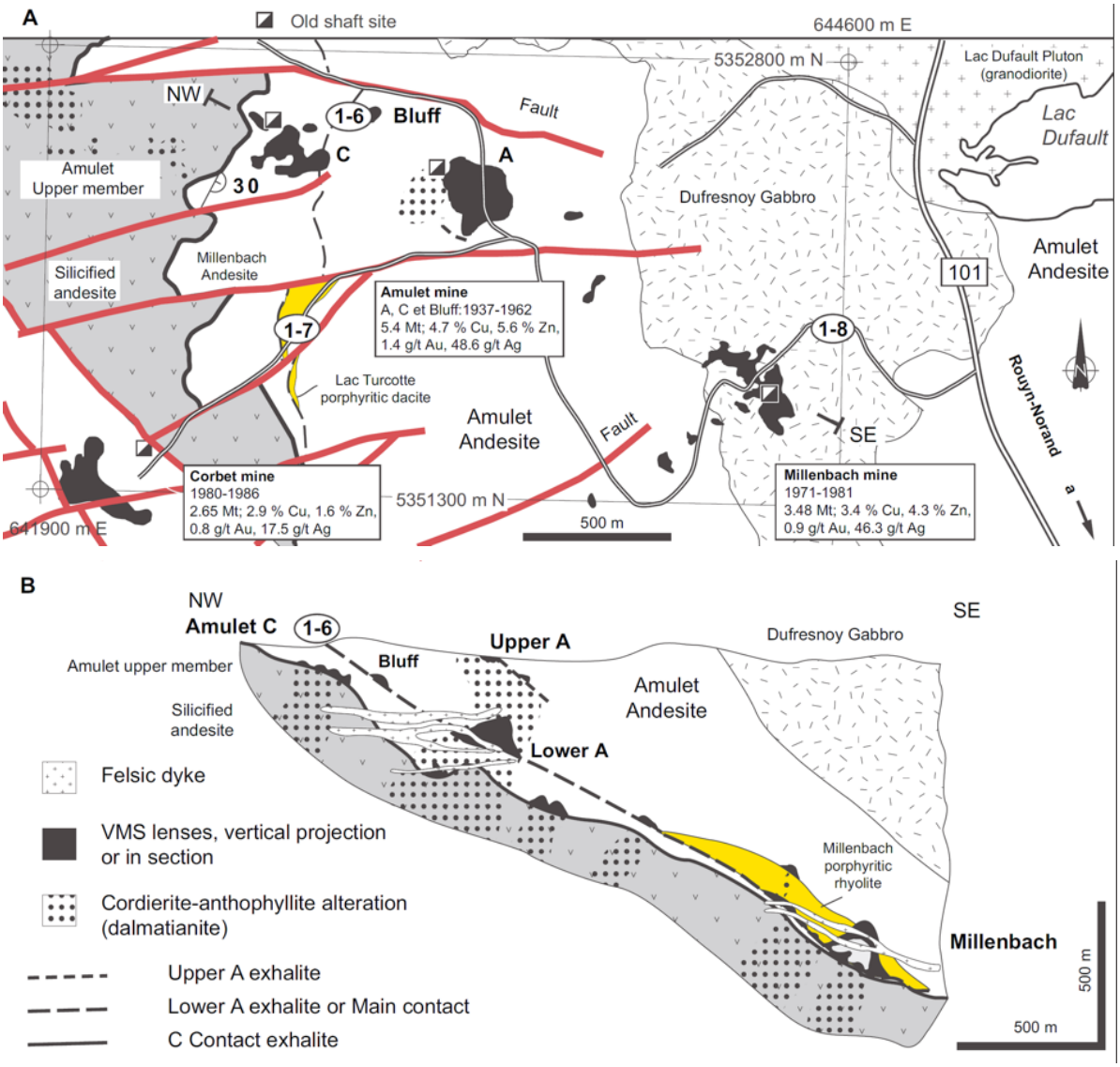

Figure 7: (a) Geological map of the former Amulet, Millenbach and Corbet mines, location in Figure 6, inset b. (b) Geological section showing the location of the Amulet-Millenbach VMS deposits. Most of the hydrothermal alteration is found in the footwall sequence. These alteration zones consist of porphyroblastic chlorite, anthophyllite and cordierite („dalmatianite“) due to contact metamorphism around the Lac Dufault pluton (Mercier-Langevin et al., 2011).

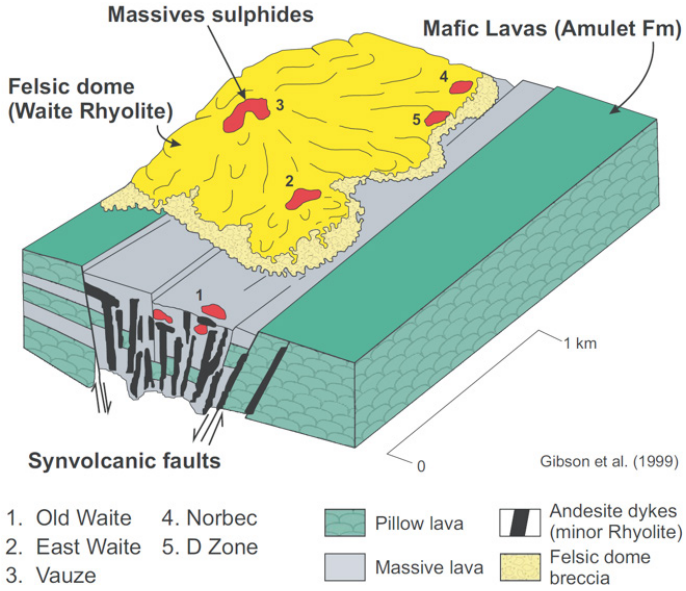

Figure 8: Schematic reconstruction of the Old Waite paleofissure in Noranda complex. Mafic and felsic volcanics, fluid flow and VMS deposits are controlled by synvolcanic faults. Figure from Mercier-Langevin et al. (2011).

te facies; Huston et al., 2011). The deposits are hosted in basalts to rhyolites of the Upper BRG, as well as in the andesitic-rhyolitic upper member of the Bousquet Formation, overlying the mafic volcanics of the Hébécourt Formation (Figure 6 inset a; Table 1).

The Doyon deposit is an intrusion-related stockwork Au-rich chalcopyrite–pyrrhotite–quartz vein deposit linked to a late phase of the Mooshla intrusive complex (gabbro to tonalite). The deposit is cross-cut by the latest stage of chloritic dikes. These late phases are related to volatile-rich magmas that created miarolitc cavities partially filled with euhedral pyrite and chalcopyrite. The deposits are related to aluminous advanced argillic alteration (now quartz–kyanite–andalusite assemblages, grading outward into quartz-muscovite±garnet-bearing assemblages; Huston et al., 2011).

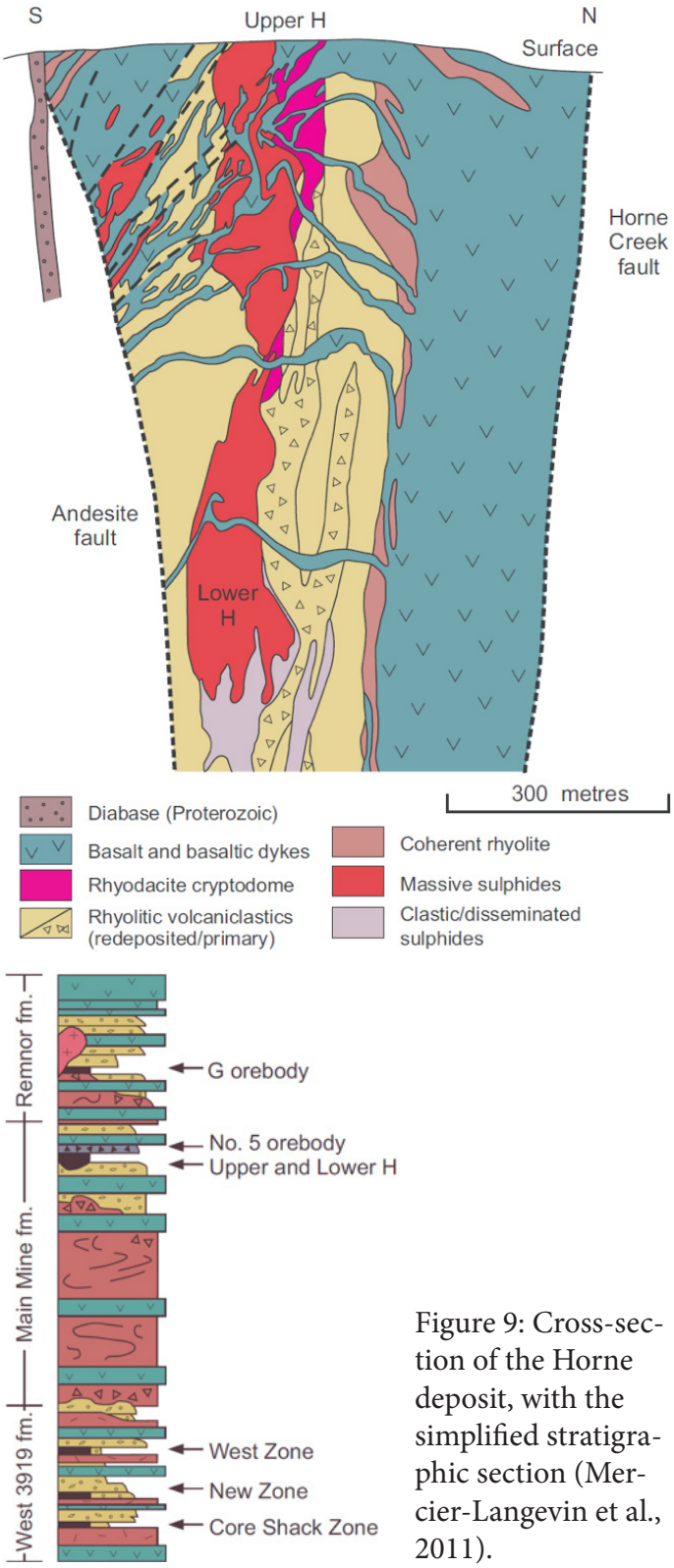

Figure 9: Cross-section of the Horne deposit, with the simplified stratigraphic section (Mercier-Langevin et al., 2011).

District	Doyon-Bousquet-LaRonde district	Noranda district
# VMS deposits	19	4
Deposits size	Small-medium	Large
Metamorphism	Greenschist	Upper greenschist – lower anfibolite
Base metal	0.3–0.6 wt.% Cu	0.8–5.0 wt.% Cu
	0.4–2.2 wt.% Zn	0.8–8.6 wt.% Zn
Gold	4.3–8.1 g/t	0.03–6.9 g/t
Host rock	Basalts to rhyolite	Basalts to rhyolite
Alteration	Argilic	Chloritization and sericitization
Contribution	Magmatic–hydrothermal	Hydrothermal

Table 1: Characteristics of the Doyon-Bousquet-LaRonde and Noranda districts. After Huston et al. (2011).

References

Bedeaux, P., Pilote, P., Daigneault, R., and Rafini, S. (2017): Synthesis of the structural evolution and associated gold mineralization of the Cadillac Fault, Abitibi, Canada. Ore Geology Reviews 82, 49-69.

Houlé, M. G., Ayer, J. A., Baldwin, G., Berger, B. R., Dinel, E., Fowler, A. D., Moulton, B., Saumur, B.-M., and Thurston, P.C. (2008): Field trip guidebook to the stratigraphy and volcanology of supracrustal assemblages hosting base metal and gold mineralization in the Abitibi greenstone belt, Timmins, Ontario. Ontario Geological Survey, Open File Report 6225, 84p.

Huston, D. L., Relvas, J. M., Gemmell, J. B., and Drieberg, S. (2011): The role of granites in volcanic-hosted massive sulphide ore-forming systems: an assessment of magmatic–hydrothermal contributions. Mineralium Deposita 46, 473-507.

Leverington, D. W., and Schindler, M. (2018): Delineating areas of past environmental degradation near smelters using rock coatings: A case study at Rouyn-Noranda, Quebec. Scientific Reports 8, 17364.

Mercier-Langevin, P., Goutier, J., Ross, P. S., McNicoll, V., Monecke, T., Dion, C., and Hannington, M. (2011): The Blake River Group of the Abitibi greenstone belt and its unique VMS and gold-rich VMS endowment. Geological Survey of Canada, Open File, 6869, 61.

McNicoll, V., Goutier, J., Dubé, B., Mercier-Langevin, P., Ross, P. S., Dion, C., and Gibson, H. (2014): U-Pb geochronology of the Blake River Group, Abitibi greenstone belt, Quebec, and implications for base metal exploration. Economic Geology 109, 27-59.

Ontario Geological Survey (2016): Technical Report 2.56810: Larder Lake Mining Division - Dokis Township - District of Cochrane. Sudbury: Ontario Geological Survey.

Pearson, V., and Daigneault, R. (2009): An Archean megacaldera complex: the Blake River Group, Abitibi greenstone belt. Precambrian Research 168, 66-82.

X LaRonde Mine: a metamorphosed VMS deposit

William Halter

Introduction

Agnico Eagle's LaRonde mine is a gold mine situated in the SE of the Abitibi Greenstone Belt. It consists of different gold-rich volcanogenic massive sulphide (VMS) deposits only a couple kilometres away from each other (Figure 1). They include the LaRonde-Penna deposit, which is one of the largest Au deposits currently mined in Canada (Mercier-Langevin et al., 2007; Thomas, 2019), and the recently opened LaRonde Zone 5 deposit, which started operations in June 2018. The older LaRonde 1 and Bousquet 2 deposits are already mined-out (Agnico Eagle, 2019). There are neighbouring deposits in the region belonging to other operators (e.g. Lafrance et al., 2003; Figure 2).

The LaRonde gold mine is the flagship mine of Agnico Eagle. With an annual production of over 360'000 ounces of gold (2018) and 3.7 million ounces of gold in proven and probable reserves, LaRonde is one of the biggest gold mines in Canada (Dubé et al., 2007b; Agnico Eagle, 2019). Since it opened in 1988, the LaRonde mine has produced almost 6 million ounces of gold. Although being mainly a gold mine, LaRonde produces also valuable by-products, such as silver, zinc and copper (Agnico Eagle, 2019).

With a total depth of over 3 km below surface the LaRonde mine is the deepest mine in America and the

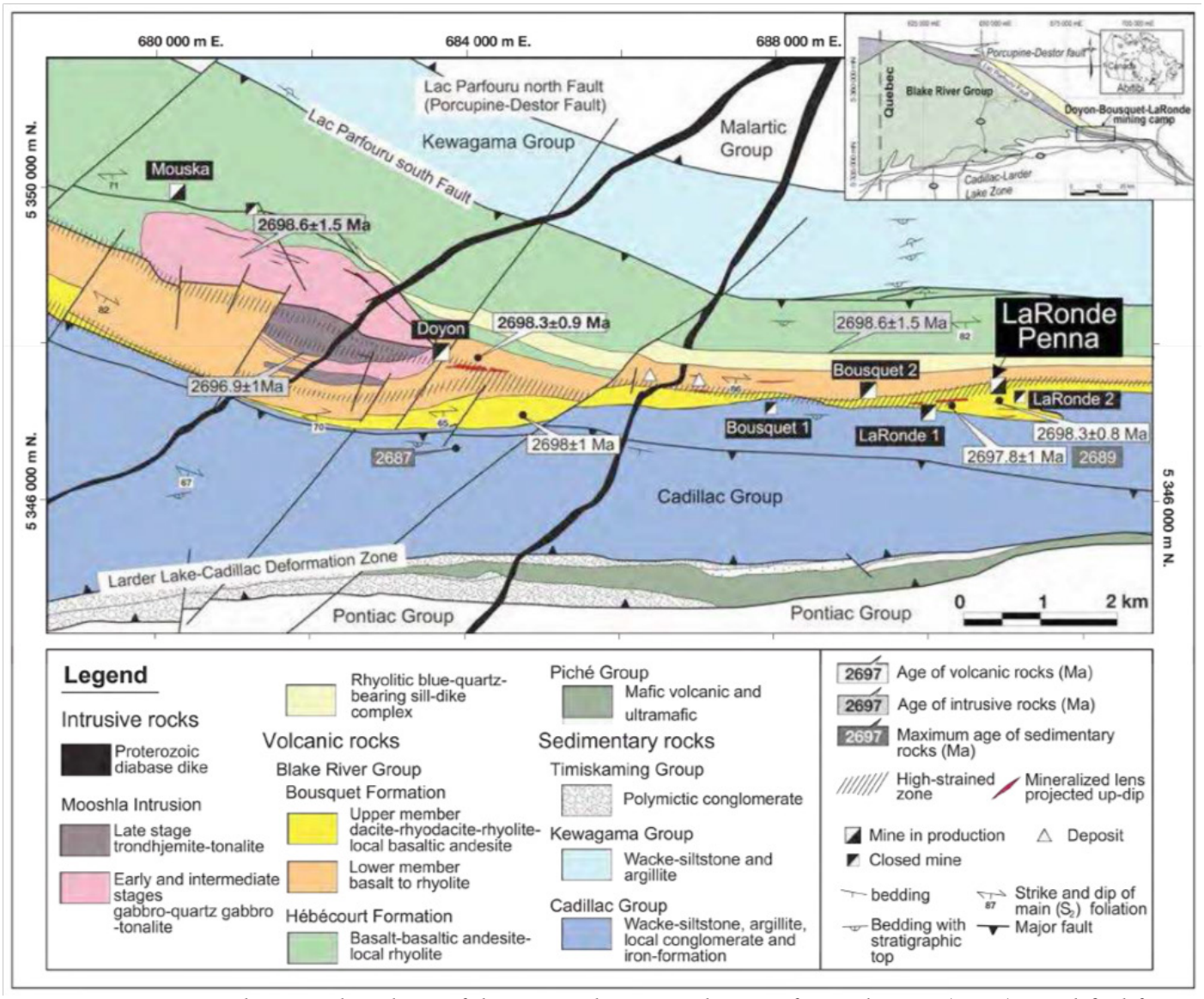

Figure 2: Location and regional geology of the LaRonde-Penna deposit; from Thomas (2019), modified from Lafrance et al., 2003).

2.2 km deep Penna Shaft, which grants access to the LaRonde-Penna deposit is the deepest single-lift shaft in the Western hemisphere (Agnico Eagle, 2019).

Table 1: Key facts about the mining operations at LaRonde-Penna

Operator	Agnico Eagle Mines Ltd., Toronto, Canada
Mine type	Underground mine
Deposit type	Gold-rich VMS deposit
Ore metals	Au, Ag, Zn, Cu
Ore grades/tonnage	(see tables 1 and 2)
Start of operation	1988 (opening LaRonde 1)
	2011 (Penna)
	2018 (Zone 5)
Au production 2018	362‘306 oz (Penna+Zone 5)
Au reserves 2018	3‘762‘000 oz (Penna+Zone 5)
Mine life	7 years (through 2025, Penna)
	8 years (through 2026, Zone 5)

Geological background

The LaRonde-Penna deposit is classified as a gold-rich VMS (Au-VMS) deposit, as the gold content (in g/t) exceeds the combined sum of all base metal contents (Zn+Cu+Pb in weight %; Dubé et al., 2007a). The mineralization is mainly localized in four massive and semi-massive lenses (Zone 7, Zone 6, 20 North lens, 20 South lens, in stratigraphically upward order, Figure 3), which vary in size, ore composition and grade. The 20 North lens is the most voluminous orebody of the LaRonde-Penna deposit with about 85% of its total gold content. The 20 South lens contains the highest gold grade with up to 38 g/t locally (Dubé et al., 2007b).

The mineralized VMS lenses sit within volcanic rocks of the Blake River Group (Chapter IX), which originated during different episodes of submarine volcanism from 2703 to 2694 Ma (Figure 4). They later experienced a north-south compression, which deformed

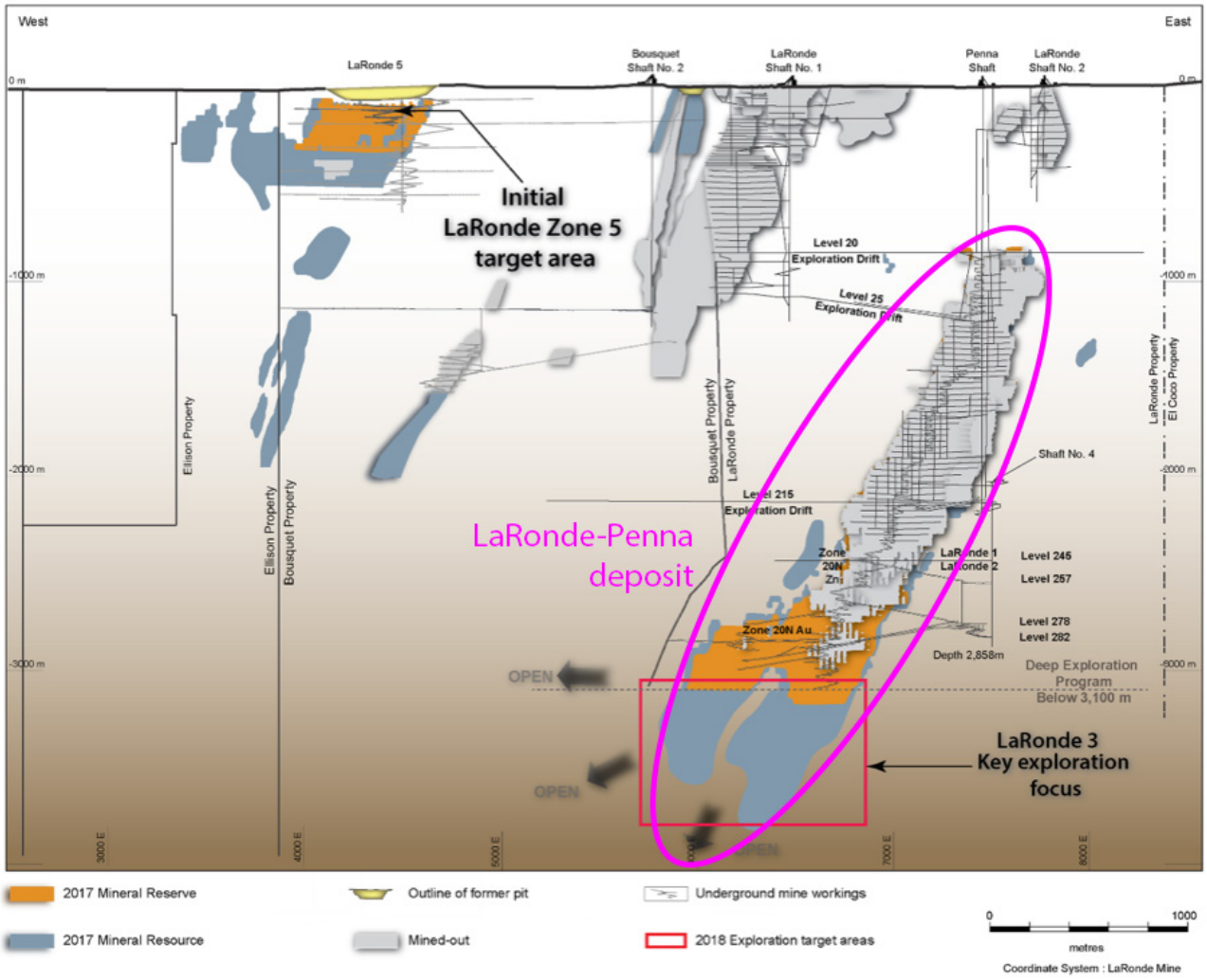

Figure 2: Location and shape of the LaRonde mine ore deposits. Currently exploited are the LaRonde-Penna and the LaRonde Zone 5 deposits. Other deposits include the mined-out LaRonde 1 and Bousquet 2 deposits. Also visible is the location of the 2.2 km deep Penna Shaft. About two third of the LaRonde-Penna deposit is already mined-out. Modified from Agnico Eagle (2019).

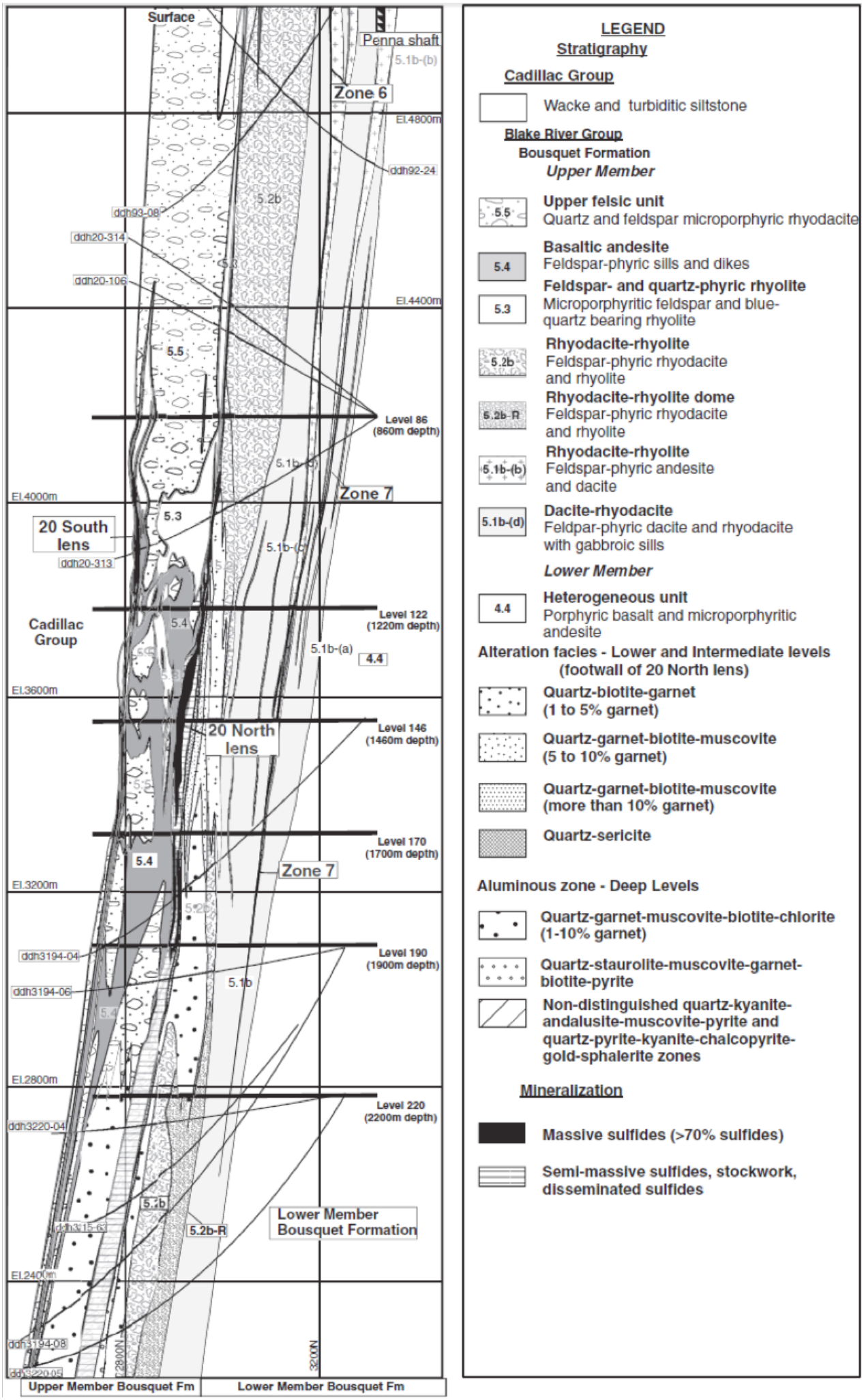

Figure 3: North-south cross-section through the LaRonde-Penna deposit, showing the stratigraphic succession from north to south and the position of the four mineralized lenses (20S lens, 20N lens, Zone 6, and Zone 7); from Dubé et al. (2007b).

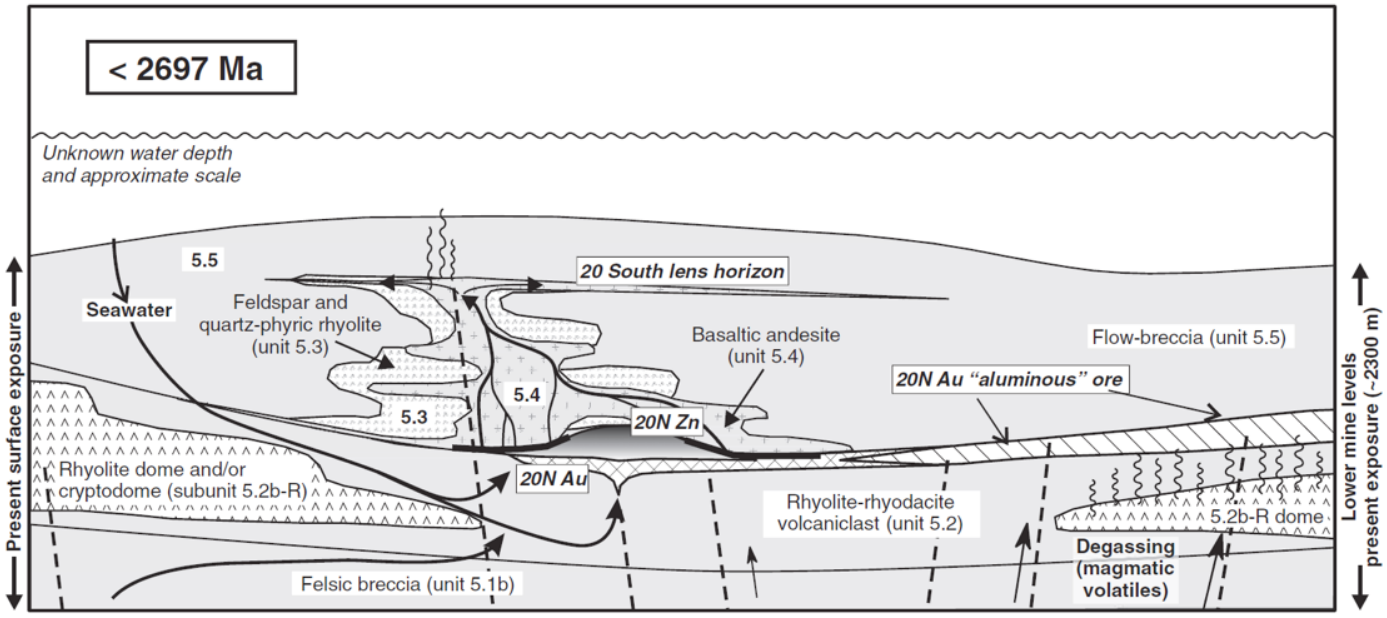

Figure 4: Schematic distribution of the two largest mineralized zones (20N lens, 20S lens) and their host rocks (same legend as in Figure 3) before metamorphic overprint (Mercier-Langevin et al., 2007).

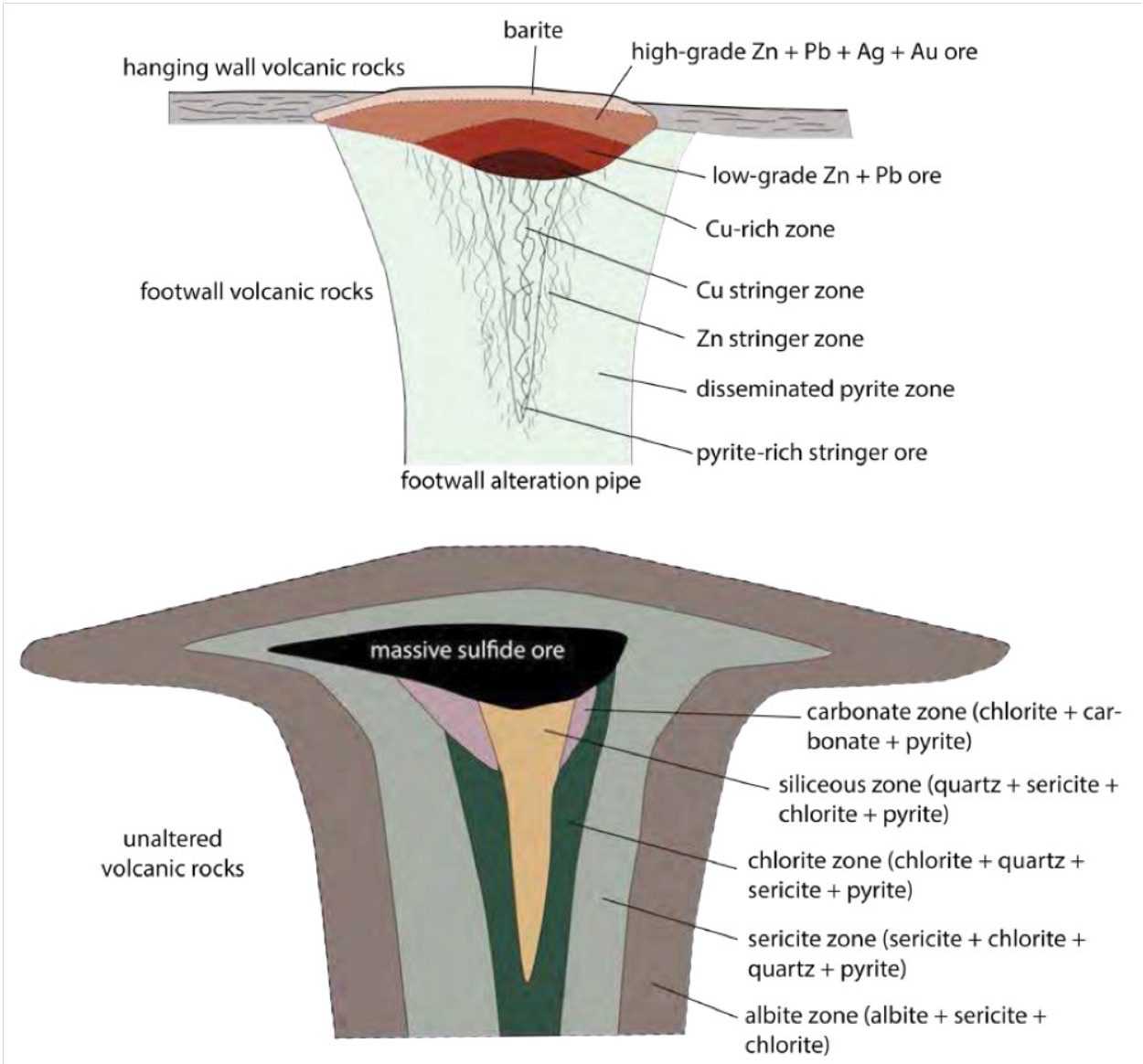

Figure 5: Schematic cross-section through a typical, idealized VMS deposit. Top: distribution of sulfide mineral zones. Bottom: distribution of hydrothermal alteration zones (Thomas, 2019; Gifkins et al., 2005).

and folded the deposit to an almost vertical position, with the footwall being to the north. During this deformation event, the deposit was metamorphically overprinted at upper greenschist to lower amphibolite-facies conditions (Dubé et al., 2007b; Thomas, 2019). However, the reactions are thought to be mostly isochemical, as only volatiles (water, CO_2) are lost in sub-solidus regional metamorphism (Hammerli et al., 2016). Thus, by measuring the elemental composition throughout the deposit one can reconstruct the corresponding hydrothermal alteration assemblages that were present before metamorphism (Thomas, 2019).

VMS and gold-rich VMS deposits

Volcanogenic massive sulphide deposits are major sources of Zn, Cu, Pb, Ag, and Au. They typically consist of a stratiform massive sulphide lens deposited at or near the ocean floor. They can also have a mineralized a stringer/stockwork zone underneath the massive sulphide lens (Figure 5; Gifkins et al., 2005; Galley et al., 2007). Over 800 VMS deposits are known worldwide with about 350 located in Canada. Various classification models of VMS deposits exist with one defining a type called gold-rich VMS (Au-VMS) deposits (Galley et al., 2007).

An Au-VMS deposit is defined as a VMS deposit containing a gold concentration (in g/t Au) which exceeds the associated combined Zn, Cu, and Pb grades (in wt%). The origin of the high gold content (up to more than 40 g/t) can vary for different deposits. As many Au-VMS deposits experienced a metamorphic overprint after the original deposition process, the origin of the gold can be either synvolcanic or syntectonic, which is not well-understood for all deposits (Dubé et al., 2007a).

The gold enrichment of the LaRonde deposits was long debated but synvolcanic origin is favored. Sub-seafloor volcanic activity released gold-rich hydrothermal fluids, which met favourable chemical conditions at lithological boundaries where the lenses are situated. However, the later tectonic processes have remobilized part of the mineralization and helped to further accumulate and localize the orebodies. In contrast to the other lenses, the 20 South lens crosscuts two stratigraphic units, which suggests a partially syntectonic origin for this ore body (Thomas, 2019, Dubé et al., 2007b).

The LaRonde-Penna deposit is an Au-VMS deposit characterized by metamorphosed advanced argillitic alteration (Dubé et al., 2007b; Thomas, 2019). This is thought to be indicative of an oxidized low-pH hydrothermal fluid, which differs significantly from the mainly reduced, near neutral to weakly acidic fluids typical of most VMS deposits. These alteration assemblages indicate high-sulphidation conditions similar to those encountered in some epithermal environments. Such Au-VMS deposits, like the LaRonde-Penna, can be interpreted as shallow-water submarine equivalents to the sub-aerial epithermal deposits (Hannington et al., 1999; Dubé et al., 2007a).

References

Agnico Eagle (2019): Agnico Eagle (online). Available at: https://www.agnicoeagle.com/. Last accessed: 28 June 2019.

Dubé, B., Gosselin, P., Mercier-Langevin, P., Hannington, M., and Galley, A. (2007a): Gold-rich volcanogenic massive sulphide deposits. In Mineral deposits of Canada: A Synthesis of Major Deposit Types, District Metallogeny, the Evolution of Geological Provinces, and Exploration Methods. (Ed.) W.D. Goodfellow. Geological Association of Canada, Mineral Deposits division, Special Publication No. 5, 75-94.

Dubé, B., Mercier-Langevin, P., Hannington, M.D., Lafrance, B., Gosselin, P., and Gosselin, G. (2007b): The LaRonde Penna world-class Au-rich volcanogenic massive sulfide deposit, Abitibi, Québec: Mineralogy and geochemistry of alteration and implications for genesis and exploration. Economic Geology 102, 633-666.

Dubé, B., Mercier-Langevin, P., Kjarsgaard, I., Hannington, M., Bécu, V., Côté, J., Moorhead., J., Legault, M., and Bédard, N. (2014): The Bousquet 2-Dumagami world-class Archean Au-rich volcanogenic massive sulfide deposit, Abitibi, Quebec: Metamorphosed submarine advanced argilitic alteration footprint and genesis. Economic geology 109, 121-166.

Galley, A. G., Hannington, M. D., and Jonasson, I. (2007): Volcanogenic massive sulphide deposits. In Mineral deposits of Canada: A Synthesis of Major Deposit Types, District Metallogeny, the Evolution of Geological Provinces, and Exploration Methods. (Ed.) W.D. Goodfellow. Geological Association of Canada, Mineral Deposits division, Special Publication No. 5, 141-161.

Gifkins, C. C., Herrmann, W., and Large, R. R., (2005): Altered volcanic rocks – a guide to description and interpretation. Centre for Ore Deposit Research, University of Tasmania, Hobart.

Hannington, M. D., Poulsen, K. H., Thompson, J. F. H., and Sillitoe, R. H. (1999): Volcanogenic gold in

massi ve sulfide environment. Reviews in Economic Geology 8, 325-356.

Lafrance, B., Moorhead, J., and Davis, D. (2003): Cadre géologique du camp minier de Doyon-Bousquet-Laronde. Ministère des Ressources naturelles, Québec, ET 2002-07, 45.

Mercier-Langevin, P., Dubé, B., Hannington, M. D., Davis, D. W., Lafrance, B., and Gosselin, G. (2007): The LaRonde Penna Au-rich volcanogenic massive sulfide deposit, Abitibi greenstone belt, Quebec: Part I. Geology and geochronology. Economic Geology 102, 585-609.

Thomas, H. (2019): Bulk compositional controls on mineral assemblages in metamorphosed ore deposits: An example from the LaRonde-Penna gold-rich VHMS deposit, Quebec, Canada. Colorado School of Mines.

Appendix

Table A.1: List of the mineral reserves and resources of the LaRonde-Penna deposit as of December 31, 2018. This deposits‘ ore contains Au, Ag, Zn, and Cu (Agnico Eagle, 2019).

LaRonde-Penna deposit									
Mineral Reserves	**Tonnes**	**Au**	**Au oz**	**Ag**	**Ag oz**	**Zn**	**Zn t**	**Cu**	**Cu t**
	(x1000)	**(g/t)**	**(x1000)**	**(g/t)**	**(x1000)**	**(%)**	**(x1000)**	**(%)**	**(x1000)**
Proven	4‘817	4.87	754	14.63	2‘265	0.54	25‘797	0.2	9‘874
Probable	11‘561	6.26	2‘327	19.72	7‘331	0.99	114‘430	0.28	32‘877
Proven & Probable	16‘378	5.85	3‘081	18.22	9‘597	0.86	140‘226	0.26	42‘751
Mineral Resources	**Tonnes**	**Au**	**Au oz**	**Ag**	**Ag oz**	**Zn**	**Zn t**	**Cu**	**Cu t**
	(x1000)	**(g/t)**	**(x1000)**	**(g/t)**	**(x1000)**	**(%)**	**(x1000)**	**(%)**	**(x1000)**
Measured	-	-	-	-	-	-	-	-	-
Indicated	4‘872	3.25	509	25.34	3‘969	0.97	47‘051	0.16	7‘582
Measured & Indicated	4‘872	3.25	509	25.34	3‘969	0.97	47‘051	0.16	7‘582
Inferred Resources	5‘494	4.95	874	14.31	2‘528	0.63	34‘523	0.24	13‘248

Table A.2: List of the mineral reserves and resources of the LaRonde Zone 5 deposit as of December 31, 2018. LaRonde Zone 5 is exclusively an Au deposit (Agnico Eagle, 2019).

LaRonde Zone 5 deposit			
Mineral Reserves	**Tonnes**	**Au**	**Au oz**
	(x1000)	**(g/t)**	**(x1000)**
Proven	4‘053	2.03	264
Probable	5‘377	2.41	417
Proven & Probable	9‘430	2.25	681
Mineral Resources	**Tonnes**	**Au**	**Au oz**
	(x1000)	**(g/t)**	**(x1000)**
Measured	-	-	-
Indicated	6‘796	2.34	510
Measured & Indicated	6‘796	2.34	510
Inferred Resources	2‘985	5.19	498

XI Polymetallic veins at the Cobalt Camp

Alina Fiedrich

Overview

In the Cobalt camp, polymetallic veins occur in Archean and Proterozoic rocks of the Cobalt Embayment. The veins were formed by hydrothermal fluids and are related to the emplacement of the Nipissing Diabase, but the source of the main product, Ag, is still debated. The camp was active from first Ag discoveries in 1903 until the 1980s.

Mining history

According to Cobalt Historical Society (2019), silver veins were discovered during the construction of the railway in 1903. Soon after, the silver rush of Cobalt began and a town of ca. 12000 people formed. Production peaked in 1922 and then declined except for two mining revivals (after World War 2 when Co was needed for steel production and around 1961, when Ag prices were exceptionally high). The last mines (Silverfields and Agnico Eagle) closed in the 1980s. The total Ag production of the Cobalt camp is estimated to amount to ca. 445 Moz (Marshall & Watkinson, 2000).

Initially, the silver veins could be mined directly at the surface, using only hand tools and dynamite. The early profits were invested into the development of the camp: mining infrastructure (e.g. mills) was built, and better equipment and power supply were needed as mining continued at deeper levels. Concentration of the ore was first performed by simple hand sorting, later cyanide and mercury were employed, and in 1915 the flotation method was introduced (Cobalt Historical Society, 2019). The Silver Heritage Trail, maintained by the Historical Society of Cobalt, preserves part of the historical mining and processing sites (Figure 1).

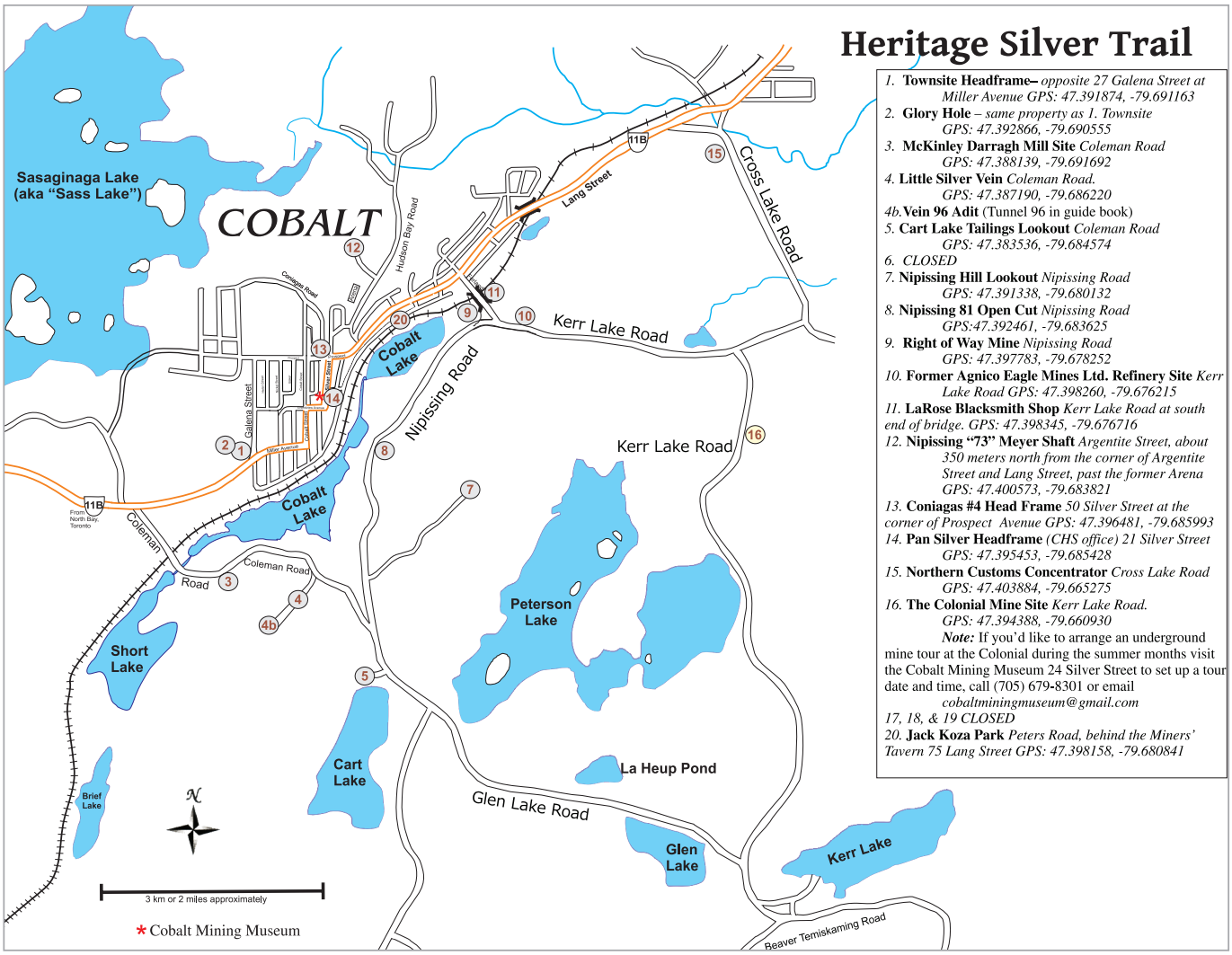

Figure 1: Map of the Heritage Silver Trail; from Cobalt Historical Society (2019).

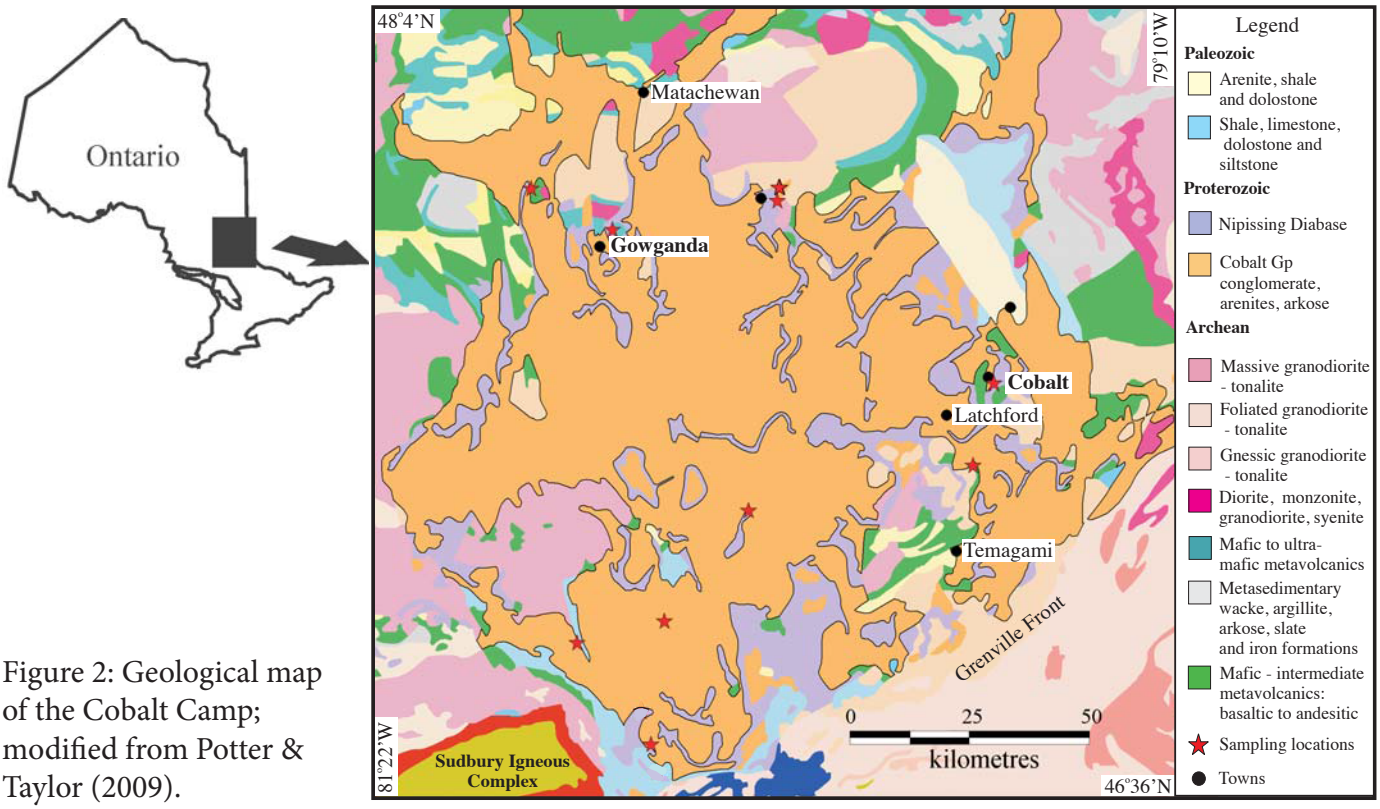

Figure 2: Geological map of the Cobalt Camp; modified from Potter & Taylor (2009).

Geological background

The Cobalt Camp (Cobalt-Gowganda mining area; Figure 2) is located in the Cobalt Embayment of the Canadian Shield. The Cobalt Embayment features Archean volcanic and sedimentary rocks of the Superior and Southern Provinces with greenschist facies metamorphic overprint and Early Proterozoic sedimentary rocks of the Huronian Supergroup (e.g. Hattori & Hodgson, 1991). Both units were intruded by the ca. 2220 Ma Nipissing Diabase (Andrews et al., 1986).

In the Cobalt area, the Nipissing Diabase consists of a series of sills, dikes, and plugs of olivine tholeiite. On a more regional scale, the Nipissing Diabase varies in composition between dominantly tholeiitic and sub-alkaline (Lightfoot & Naldrett, 1996), with petrologic variations resulting from post-emplacement fractionation and assimilation (Jobin-Bevans, 2009, and references therein). Based on its geochemical signature, it is interpreted as the intrusive part of eroded continental flood basalts (Jobin-Bevans, 2009, and references therein). Different types of mineralization are associated with the Nipissing Diabase, from polymetallic (Ag) veins near Cobalt to contact-related and intrusion-hosted Ni-Cu-PGE-dominated sulfide deposits toward the southwest (Figure 4). Around the Nipissing Diabase, a wide alteration halo of spotted chlorite developed in the Cobalt area (e.g. Joyce, 2011).

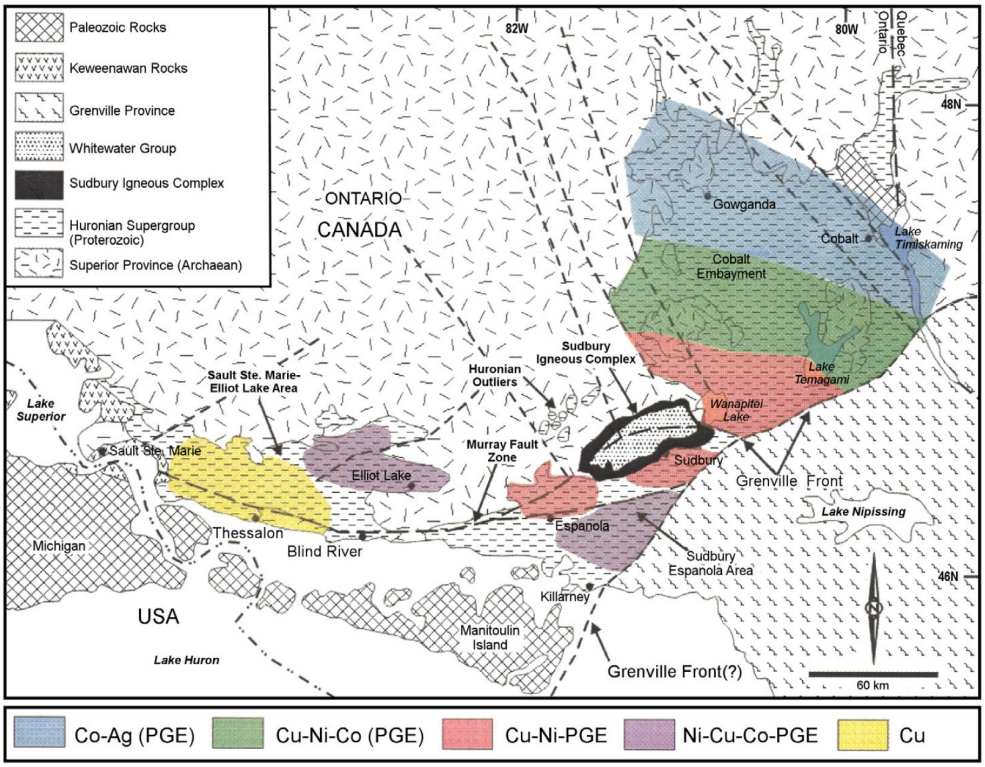

Figure 3: Regional distribution of mineralization related to the Nipissing Diabase between Lake Temagami and Sault Ste. Marie; from Jobin-Bevans (2009), after Card & Pattison (1973).

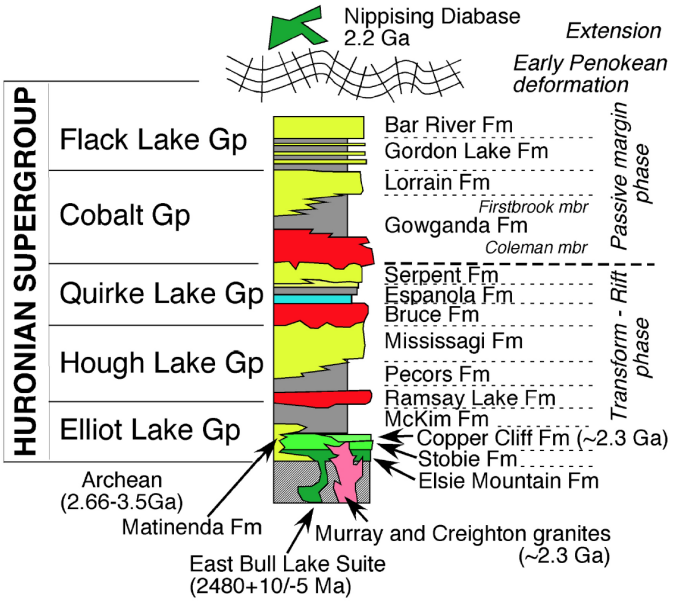

Figure 4: Lithostratigraphy and tectonic history of the Huronian Supergroup; from Long (2009), based on Long (2004). gray = mudsteone, blue = limestone, greenish-yellow = sandstone, red = conglomerate. Other colours indicate intrusive and extrusive rocks.

The Huronian Supergroup (Figure 4) consists of ca. 2.45-2.22 Ga, predominantly sedimentary lithologies. It represents the development of a continental margin upon formation of a Paleoproterozoic ocean (Long, 2009, and references therein). The Huronian was regionally metamorphosed at greenschist-facies and locally to amphibolite-facies conditions (Long, 2009, and references therein). In the Huronian of the Cobalt area, polymetallic veins occur mainly in the Coleman member (Figure 4), which consists of conglomerate, siltstone, and sandstone deposited under a continental ice sheet (Joyce, 2011; Long, 2009, and references therein).

Polymetallic veins

Polymetallic veins (also 5-element veins; Ag-Bi-Co-Ni-As) formed in the Huronian sedimentary rocks, Archean gneisses, and in the Nipissing diabase. They are up to ca. 30 cm in diameter and can be dilatant, sheared, or brecciated. Mineralization along the veins is discontinuous. The most common ore minerals comprise: arsenides/sulfarsenides of Co, Ni, and Fe, native Ag and Bi, antimonides, and sulfides of Pb, Sn, and Cu. The gangue mineralogy comprises carbonates (mostly calcite, some dolomite), quartz, chlorite, amphibole, epidote, alkali feldspar, and albite (Petruk, 1971). The veins are typically zones with silicate minerals forming a selvage in contact to the host rocks, followed by a zone of early, pyrite-dominated sulfide

Major Vein Minerals	Early	Main Stage	Late
Alkali feldspar			
Chlorite			
Quartz			
Calcite			
Hematite			
Pyrite			
Precious-Metals			
Chalcopyrite			
Cobaltite			
Cu-Bi-Pb-sulfides			
Galena			

Figure 5: Paragenetic sequence of vein minerals; from Potter & Taylor (2009).

Figure 6: Polymetallic vein with remobilized Ag veinlets in Huronian sedimentary rock; ca. 15 cm across. Sample from Temiskaming mine. Photo from Joyce (2011).

mineralization and silicate gangue, the main-stage mineralization at the transition from silicate to carbonate gangue, and late-stage massive calcite and galena in the center (Figures 3, 4; e.g. Potter & Taylor, 2009). The polymetallic veins are commonly structurally bound to faults and fold hinges (e.g. Smyk & Watkinson, 1990) and exhibit a carbonate and sodic alteration halo of less than 10 cm (Potter & Taylor, 2009).

Pb-Pb dating of vein minerals revealed two distinct ages, indicating two separate hydrothermal events (Potter & Taylor, 1990): An age of 2236 ± 180 Ma overlaps with the emplacement of the Nipissing diabase; an age of ca. 1160 Ma coincides with basin-wide K-Na-metasomatism related to the waning stages of the Penokean orogeny.

The Nipissing diabase likely contributed to the formation of polymetallic veins by providing heat to give rise to a long-lived hydrothermal system and may

have also generated fluid pathways. The presence of (a) a high-salinity Ca-dominated fluid (brine) throughout vein formation and (b) a low-salinity liquid-like fluid during main-stage ore formation suggests that ore mineral precipitation was triggered by fluid mixing, which destabilized the Ag chloride complexes in the high-salinity fluid (Marshall et al., 1993). Fluid inclusions further indicate conditions of vein formation of ca. 300-340 °C and 80-130 MPa (Marshall et al., 1993). The Archean sedimentary rocks are rich in sulfides, and may represent a source of metals that were leached by the hydrothermal fluid or may have facilitated metal dissolution by sulfide remobilization (Smyk & Watkinson, 1990). However, the source of Ag remains debated, as an unexposed, deep-seated magma source or the Nipissing diabase were also invoked.

References

Andrews, A. J., Masliwec, A., Morris, W. A., Owsiacki, L., and York, D. (1986): The silver deposits at Cobalt and Gowganda, Ontario. II: An experiment in age determinations employing radiometric and paleomagnetic measurements. Canadian Journal of Earth Sciences 23, 1507-1518.

Card, K. D., and Pattinson, E. F. (1973): Nipissing diabase of the Southern Province, Ontario. In: Huronian Stratigraphy and Sedimentation, Geological Association of Canada, Special Paper 12, 7-30.

Cobalt Historical Society (2019): Heritage Silver Trail. Available at: http://heritagesilvertrail.ca/10-map.html (accessed on June 29, 2019).

Hattori, K., and Hodgson, C. J. (1991): Gold-related geology in the Kirkland Lake and Timmins camps, Ontario (Field Trip 5). Geological Survey of Canada, Open Field 2160, 64p.

Jobin-Bevans (2009): Nipissing Gabbro. In: A Field Guide to the Geology of Sudbury, Ontario; Ontario Geological Survey, Open File Report 6243, 31-37.

Joyce, D. K. (2011): The Cobalt-Gowganda Silver Mining Area. https://www.davidkjoyceminerals.com/pagefiles/articles_cobaltgowganda.asp (accessed on June 29, 2019).

Lightfoot, P. C. and Naldrett, A. J. (1996): Petrology and geochemistry of the Nipissing Gabbro: exploration strategies for nickel, copper, and platinum group elements in a large igneous province. Ontario Geological Survey, Study 58, 80p.

Long, D. G. F. (2004): The tectonostratigraphic evolution of the Huronian basement and the subsequent basin fill: geological constraints on impact models of the Sudbury event. Precambrian Research 129, 203-223.

Long, D. G. F. (2009): The Huronian Supergroup. In: A Field Guide to the Geology of Sudbury, Ontario; Ontario Geological Survey, Open File Report 6243, 14-30.

Marshall, D. D., Diamond, L. W., and Skippen, G. B. (1993): Silver Transport and Deposition at Cobalt, Ontario, Canada: Fluid Inclusion Evidence. Economic Geology 88, 837-854.

Marshall, D., and Watkinson, D. H. (2000): The Cobalt mining district: Silver sources, transport and deposition. Exploration and Mining Geology 9, 81-90.

Petruk, W. (1971): Mineralogical characteristics of the deposits and textures of the ore minerals. The Canadian Mineralogist 11, 108-139.

Potter, E. G. and Taylor, R. P. (2009): The lead isotope composition of ore minerals from precious metal-bearing, polymetallic vein systems in the Cobalt Embayment, northern Ontario: metallogenic implications. Economic Geology 104, 869–879.

Smyk, M. C., and Watkinson, D. H. (1990): Sulphide remobilization in Archean volcano-sedimentary rocks and its significance in Proterozoic silver vein genesis, Cobalt, Ontario. Canadian Journal of Earth Sciences 27, 1170-1181.

XII Banded Iron Formations and Early Earth

Dean Khan

Introduction

A banded iron formation (BIF) is a chemically precipitated sedimentary deposit containing at least 15% iron. Thin layers of iron oxides are interbedded with Fe-poor shales or silicates on a millimetre to centimetre scale. These deposits currently make up more than 60% of global iron ore reserves (Zhu et al., 2014). BIFs are abundant in the Pre-Cambrian, some of the oldest associated with the Isua Greenstone belt in Greenland forming 3.7-3.8 Gya. Peak production of BIFs occurred 2.4 Gya, about the time of the great oxygenation event (GOE), stopping around 1.8 Gya. The GOE saw the saturation of shallow water with respect to O_2 resulting in the precipitation of magnetite as dissolved Fe and Fe^{2+} reacted with the free oxygen (Holland, 2006). There is subsequently a billion-year hiatus in BIF deposits as all dissolved oceanic iron had already oxidised. The last set of BIF deposits form from 750 Mya concurrent with global glaciation events during the late Tonian and Cryogenian. BIF deposits are distributed in Pre-Cambrian craton and shield regions of all continents, except Antarctica where only one BIF deposit has been found (Trendall, 2013).

Types of BIFs

BIFs are categorised into three groups – Superior, Rapitan and Algoma. Superior type deposits, named after Lake Superior on the US/Canada border, are characterised by the significant continuity of individual layers sometimes for 10's to 100's of kilometres (Trendall, 2013). These deposits formed 2.7-1.8 Gya, around the time of the GOE in marine shelf environments. High phytoplankton productivity produces an oxygenated layer which reacts with upwelling dissolved Fe2+ to form the BIF (Frei et al., 2013).

Rapitan type deposits are associated with late Pre-Cambrian global glaciation. Global anoxia during snowball Earth events and a build-up of dissolved ferrous iron in sea water primed the oceans for Rapitan type deposits (Martin, 1965). As glaciers retreated ocean water became oxidised once more precipitating iron oxides (Baldwin et al., 2012).

Algoma type deposits are generally smaller than the Superior type deposits and form throughout the Pre-Cambrian. These BIFs are associated with rift settings and lack large scale lateral continuity. Sequences with this type of BIF contain significant amounts of submarine volcanic material and many lie in the same stratigraphic horizon as volcanogenic massive sulphide deposits (Sial, 2015).

Numerous BIF sites in North America are capped with a breccia deposited sometime between 1.875 and 1.83 Gya (Figure 3). This breccia contains fragments of impact ejecta hypothesised to have come from the Sudbury impact event 1.85 Gya. Some breccia deposits contain deformed masses of chert, suggesting no unconformity between BIF deposition and the impact event. Above the breccia lies organic rich mudstones with little to no iron formation subsequently occurring. The Sudbury impact likely had a significant effect on ocean water chemistry resulting in a hiatus in BIF formation until the Rapitan type deposits a billion years later. This has been suggested to be due to the mixing of the previously stratified ocean, with its thin oxygenated layer produced by phytoplankton activity above an anoxic deep ocean (Slack & Cannon, 2009). The post impact oceans were much more homogenous and suboxic.

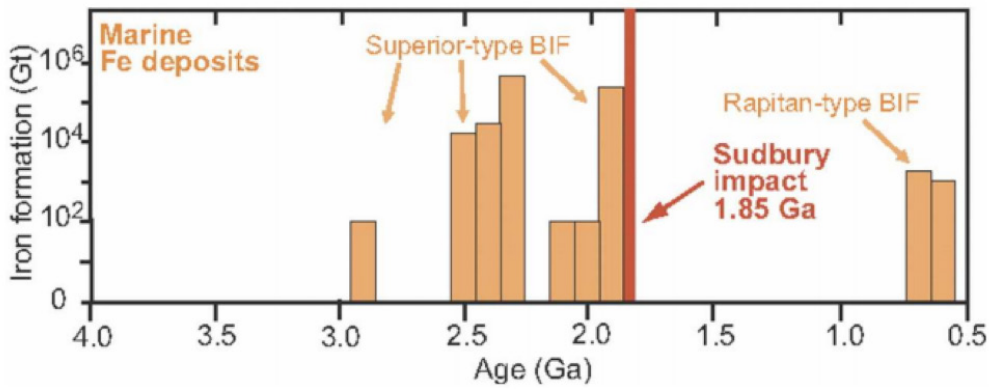

Figure 1: Histogram showing the mass of Superior and Rapitan BIF deposits formed in the Pre-Cambrian. The large hiatus between Superior and Rapitan deposits correlates with the Sudbury impact event (Slack & Cannon, 2009).

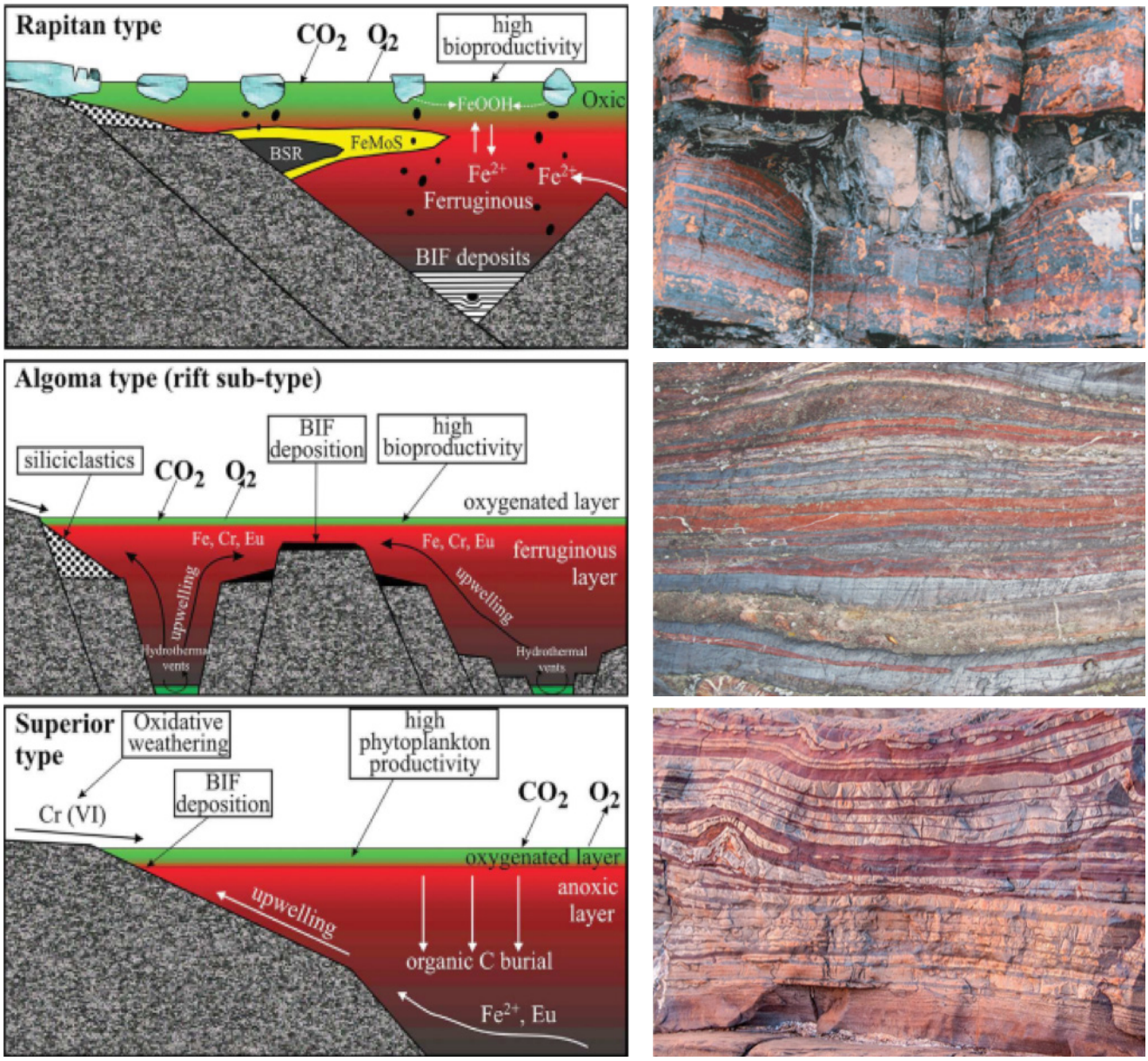

Figure 2: Hypothesises for the formation of the Rapitan, Algoma and Superior type BIF deposits (Sial, 2015). These models all rely on a high bio-productivity producing an oxygenated layer in which dissolved iron precipitates. Images on the right show characteristic properties of BIFs of these types. Top: layers of jasper and magnetite deformed beneath a glacial drop stone (Photo credit – P. Hoffman). Middle: Layers of chert, jasper and magnetite from the Soudan Iron-Formation (Photo credit – J. St.John) Bottom: Laterally continuous beds of hematite and jasper from Dales Gorge (Photo credit – G. Churchard).

Between Timmins and Cobalt, most BIF deposits are of the Algoma type (Sabina, 2000; Diekrup et al., 2018). BIF deposits in this area include:

- Sherman Mine: Bands of grey quartzite, jasper and chert, chloritic and tremolitic tuff, and finely granular magnetite. The jasper ranges from a bright crimson to a brownish red colour. Minor minerals present include hematite, pyrite (including up to 5 cm diameter nodules), stilpnomelane (phyllosilicate mineral associated with blue/greenschist facies metamorphism) and chlorite.
- Mattarrow mine: Banded iron formation with veinlets containing galena, sphalerite, pyrite and pyrrhotite.
- Tommy Burns mine: Alternating bands of hematite, chert and magnetite cut by quartz veins containing pyrite and gold.

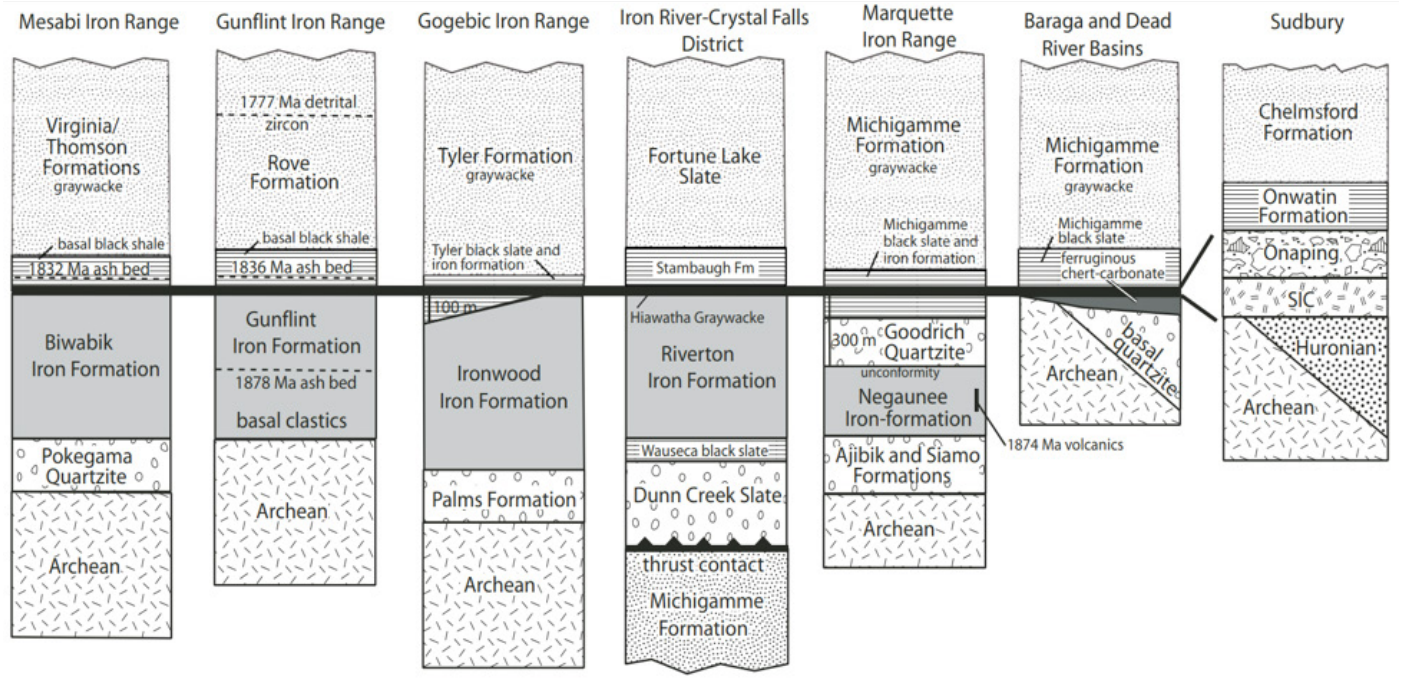

Figure 3: Correlation of the stratigraphy in and near the iron ranges of the Lake Superior region. The Sudbury impact layer (heavy black line) that formed at 1850 Ma shows the end of large scale BIF deposits across the region (Cannon et al., 2009).

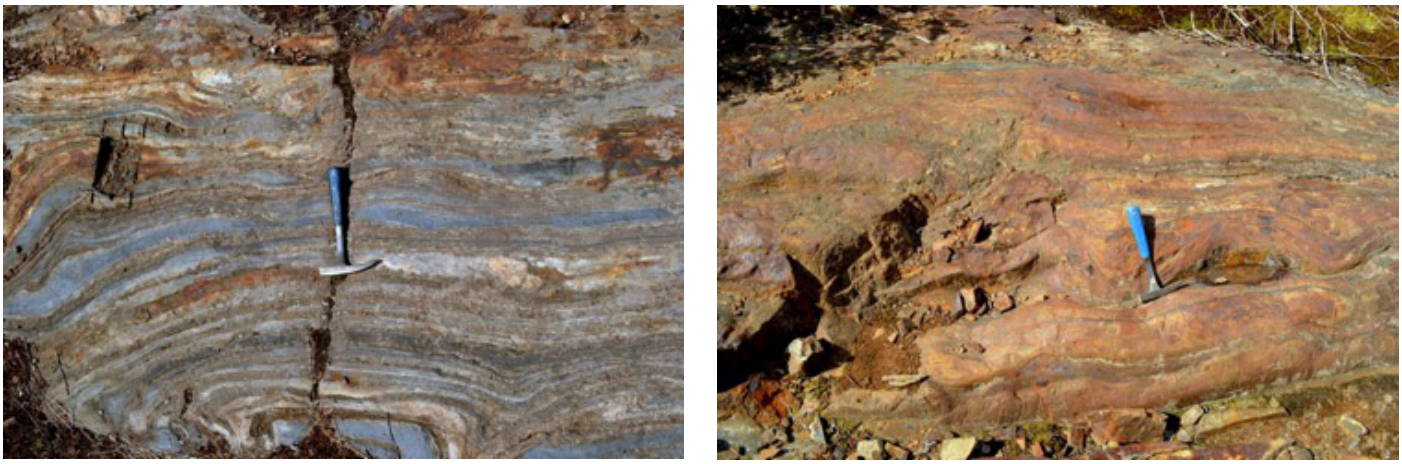

Figure 4: Two examples of algoma type banded iron formation outcrops, only a few hundred meters apart, observed in the Timmins area. The relative abundances of iron and silica vary significantly across the exposed outcrops, as is typical for an algoma type deposit. Silica is significantly more abundant in the left image forming thick pale bands. The right image is more iron rich, with thinner and less abundant chert layers. Fe concentrations varied between 30 and 60% in this locality. Photos: K. Bulcewicz

References

Baldwin, G. J., Turner, E. C., and Kamber, B. S. (2012): A new depositional model for glacigenic Neoproterozoic iron formation: Insights from the chemostratigraphy and basin configuration of the Rapitan iron formation. Can. J. Earth Sci. 49, 455–476. doi: https://doi.org/10.1139/e11-066

Cannon, W. F., Schulz, K. J., Horton Jr. J. W., and King, D. A. (2009): The Sudbury impact layer in the paleoproterozoiciron ranges of northern Michigan, USA. Geological Society of America Bulletin; 122 (1-2): 50-75. doi: https://doi.org/10.1130/B26517.1

Diekrup, D., Hannington, M. D., Strauss, H., and Ginley, S. J. (2018): Decoupling of Neoarchean sulfur sources recorded in Algoma-type banded iron formation. Earth and Planetary Science Letters; 489: 1-7. doi: https://doi.org/10.1016/j.epsl.2018.02.022.

Frei, R., Gaucher, C., Stopler, D., and Canfield D. E. (2013): Fluctuations in late Neoproterozoic atmospheric oxidation — Cr isotope chemostratigraphy and iron speciation of the late Ediacaran lower Ar-

royo del Soldado Group (Uruguay). Gondwana Research; 23(2): 797-811. doi: https://doi.org/10.1016/j.gr.2012.06.004

Holland, H. D. (2006): The oxygenation of the atmosphere and oceans. Phil. Trans. R. Soc. B; 361: 903-915. doi: https://10.1098/rstb.2006.1838

Houlé, M.G., Ayer, J. A., Baldwin, G., Berger, B. R., Dinel, E., Fowler, A.D., Moulton, B., Saumur, B.-M. and Thurston, P.C. (2008): Field trip guidebook to the stratigraphy and volcanology of supracrustal assemblages hosting base metal and gold mineralization in the Abitibi greenstone belt, Timmins, Ontario; Ontario Geological Survey, Open File Report 6225, 84p.

Martin, H. (1965): Beobachtungen zum Problem der jung-präkambrischen Glazialen Ablagerungen in Südwestafrika (Observations concerning the problem of the late Precambrian glacial deposits in South West Africa): Geologische Rundschau, 54: 115-127, doi: http://dx.doi.org/10.1007/BF01821173

Sabina, A. P. (2000): Rocks and Minerals for the Collector (2000). Geological Survey of Canada Miscellaneous Report 57

Sial, A. N. (2015). Chemostratigraphy of Neoproterozoic banded iron formation (BIF): types, age and origin. In M. Ramkumar, Chemostratigraphy, Concepts, Techniques and Applications. 433-449. Elsevier.

Slack, J. F., and Cannon, W. F. (2009): Extraterrestrial demise of banded iron formations 1.85 billion years ago. Geology; 37 (11): 1011-1014. doi: https://doi.org/10.1130/G30259A.1

Trendall, A. (2013): SEDIMENTARY ROCKS | Banded Iron Formations, Editor(s): Richard C. Selley, L. Robin M. Cocks, Ian R. Plimer, Encyclopedia of Geology, Elsevier, 2005, Pages 37-42, doi: https://doi.org/10.1016/B0-12-369396-9/00440-8.

Zhu, X. –Q., Tang, H. –S., and Sun, X. –H. (2014): Genesis of banded iron formations: A series of experimental simulations. Ore Geology Reviews; 63: 465-469. doi: https://doi.org/10.1016/j.oregeorev.2014.03.009.

XIII The Cadillac-Larder Lake Fault: fluid flow and gold mineralization

Michael Schirra

Introduction to orogenic gold deposits

Gold is one of the most important metals for humans and has been mined throughout history from various geological types of ore deposits formed in different tectonic settings (Figure 1). More than 75% of the total gold ever recovered comes from orogenic gold deposits, which are, hence, the most important source of this strategic commodity (Phillips, 2013). They are hydrothermally formed, quartz-vein hosted, economic anomalies of gold in greenschist to lower amphibolite facies rocks along second or third order faults associated to regional-scale structures that can reach mantle depths. In contrast to many other gold-bearing deposits, orogenic-type mineralization contains exclusively gold as recoverable commodity. They commonly form in the mid- to shallow crust (5 to 15 km) in compressional settings, facilitating ascent of hot, gold-bearing fluids along major shear zones (Goldfarb et al., 2005; Phillips and Powell, 2009; Figure 1). Main features of this deposit type include: (a) very late to post-peak metamorphic timing, (b) located within a metamorphosed fore- or back-arc setting, (c) thermal equilibrium between fluid and host rock, (d) addition of K, S, CO_2, Si, and Au by hydrothermal fluids but lack of base metals, and (e) low- to moderate-salinity, CO_2-CH_4-N_2-H_2S bearing fluids that might have undergone phase separation (Goldfarb and Groves, 2015). Orogenic gold deposits formed from the Paleoarchean to the present. Archean deposits are thereby hosted in greenstone belts including sub-volcanic intrusions, banded iron formations and minor amounts of clastic sedimentary-rock sequences, while the younger ones formed during the Phanerozoic are mainly associated with clastic sediments (Goldfarb and Groves, 2015). Gold lode deposits are present in all Archean shield areas with prominent examples like the Yilgran craton in Australia, the Kaapvaal and Zambian Craton in Africa and the Superior Province in Canada (Roberts, 1997).

Understanding the processes that lead to the formation of these deposits is essential for further exploration and the continuous supply of gold. Despite intense research on orogenic-type gold deposits, however, main mechanisms like the transport of gold in hydrothermal solutions and the trigger of precipitation as well as the source of the fluid and gold remain speculative. In the following sections, the genesis of orogenic gold deposits will be reviewed with focus on the ones formed along the Cadillac-Larder Lake Fault Zone (CLLFZ) in the Abitibi Subprovince, Canada.

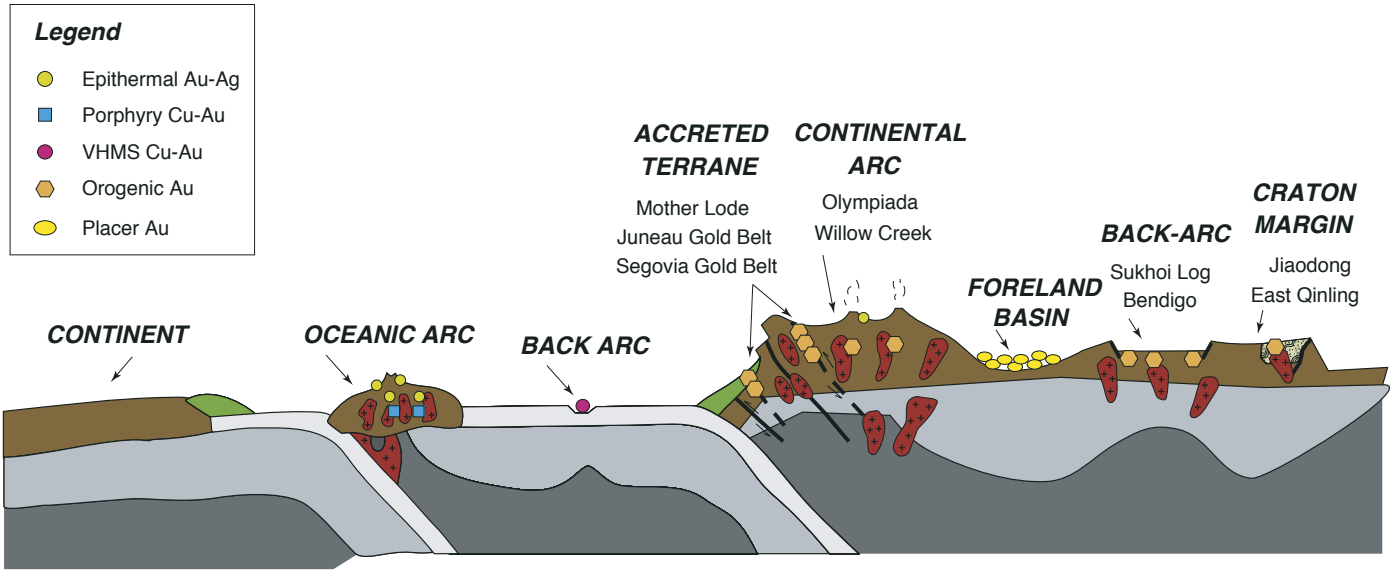

Figure 1: Tectonic setting of different gold-bearing ore deposit types; from Goldfarb and Groves (2015). Orogenic gold deposits are most commonly associated with fore- and back-arc regions of active convergent margins (Rabeau et al., 2013).

Regional geology of the Cadillac-Larder Lake Fault Zone

The Abitibi Subprovince is an Archean greenstone belt composed of volcano-sedimentary sequences metamorphosed at greenschist facies conditions and separated by large granodioritic plutons. The Pontiac Subprovince to the south is comprised of highly folded and deformed turbiditic sediments showing amphibolite grade metamorphism. The Cadillac-Larder Lake Fault Zone (CLLFZ), an east-trending 250 km long sub-vertically to the north dipping regional fault (Figure 2), separates both domains and can be subdivided into four segments from west to east: (1) Rouyn, (2) Joannes, (3) Malartic, and (4) Val-d'Or. Each segment displays different styles of deformation, strike, and associated smaller-scale faults (Robert, 1989; Bedeaux et al., 2017). Multiple phases of ductile to brittle deformation, metamorphism, and alteration indicate activity of the CLLFZ over long periods of time (Simard et al., 2013). Ductile deformation is characterized by continuous offset of markers and mylonites, while brittle deformation can be recognized by abrupt offset of markers and the development of faults and breccias. Development of fabrics typical for a brittle-ductile shear zone is shown in Figure 3. The most recent structural evolution model of the CLLFZ includes four different deformation events, starting with north-south shortening, followed by extension that reactivated the fault zone, a subsequent deformation event leading to local S-shaped minor faults, and finally a late northwest-southeast shorting produced by dextral strike-slip movements (Bedeaux et al., 2017). The first deformation event (D1) is recorded by a well-developed, E-trending and vertically N-dipping schistosity. Reactivation of the CLLFZ during extension and uplift (D2) is evident by contrasting metamorphic grades between the Abitibi and Pontiac Subprovinces along the CLLFZ. The subsequent deformation event (D3) is of minor importance and developed only locally a northwest-trending cleavage and folds, probably during local shorting along secondary fault planes. Ultimately, northwest-southeast shortening (D4) caused dextral strike-slip movements along east-trending fault planes marked by a recurrent northeast-trending cleavage. The largely mineralized Porcupine-Destor Fault Zone to the North displays a comparable structural evolution (Legault et al., 2005).

Mineralization along the fault zone

Three different types of gold deposits are associated with the different lithological units and deformation events: (1) volcanogenic massive sulfide (VMS) deposits that formed during active volcanism, (2) syenite-type magmatic-hydrothermal systems associated with the emplacement of plutonic complexes during D2, and (3) orogenic gold deposits during and after peak metamorphism of D4 (Nadeau, 2019). Most gold deposits are associated with the CLLFZ, which structurally controlled fluid flow and pluton emplacement. In total, more than 2000 tons of gold have been extracted from the deposits along the CLLFZ up to date (Rabeau et al., 2013). In general, ore is hosted in

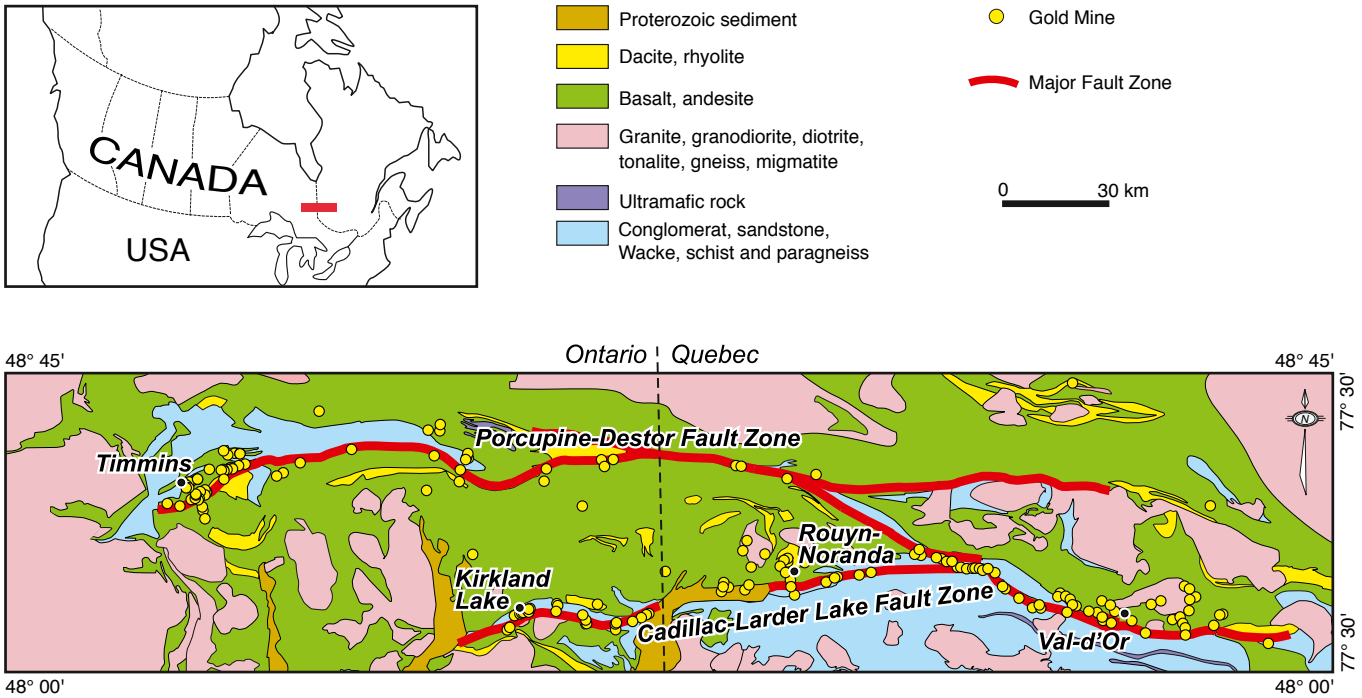

Figure 2: Simplified geological map of the CLLFZ and associated gold deposits and mines; from Rabeau et al., (2013).

a network of tabular, sub-vertical veins consisting of quartz and carbonates (typically ferroan dolomite) with variable amounts of tourmaline and minor presence of opaque minerals such as pyrite, pyrrhotite, and arsenopyrite (Roberts, 1997). Gold is hosted within these veins or disseminated in the adjacent altered host rock and usually associated with iron-sulfides. The geometry of the vein systems and, hence, of the mineralized zones depends on local structural features with veins parallel to C and S foliations shown in Figure 3 (Roberts, 1997). However, vein geometry can be complicated by sequential vein formation as deformation progresses.

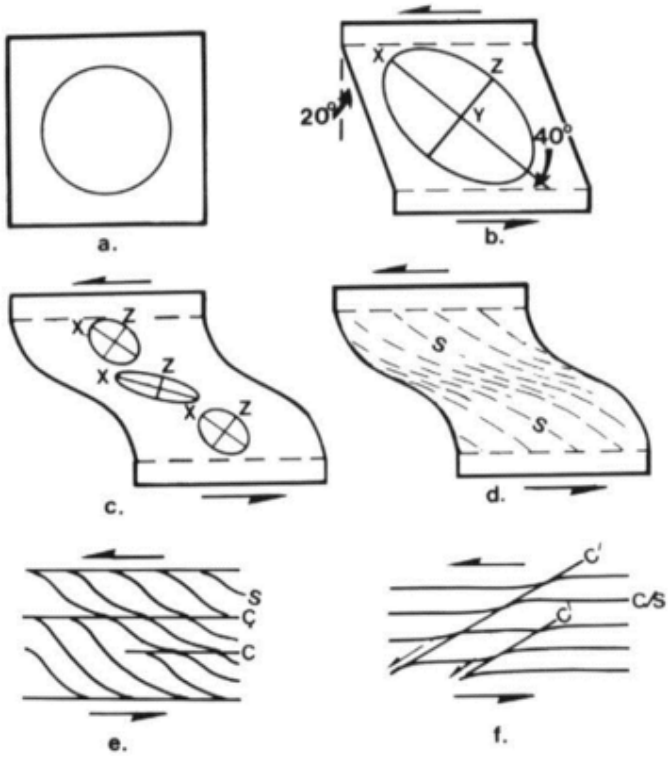

Figure 3: Development of foliations by simple shear in a ductile shear zone. a) undeformed state. b) Strain ellipsoid under homogeneous simple shear strain. c) and d) Variations of the strain ellipsoid and foliation (S) through a shear zone under low strain conditions by heterogeneous simple shear. e) and f) Heterogeneous simple shearing under high strain conditions leading to a spaced foliation (C) parallel to the walls or shear banding (C') transecting earlier foliations (Roberts, 1997).

Although any lithological unit is capable of hosting gold mineralization, felsic porphyry intrusions are used as exploration tool in the Superior Province since more than 90% of the major gold deposits are either hosted by or adjacent to such intrusions (Hodgson & MacGeehan, 1982). Mineralization is mainly hosted by the Piché Group, consisting of mafic to ultramafic rocks of upper greenschist to lower amphibolite facies rocks that are highly strained and altered (Simard et al., 2013). Hydrolysis and carbonatization due to addition of mainly CO_2, K, S, and H_2O produced various alteration styles including potassic (biotite + K-feldspar), chloritic (chlorite + calcite) and carbonate alteration (Fe-rich dolomite + sericite + pyrite + quartz; Roberts, 1997). Chlorite alteration is of regional extent while carbonate alteration is most intense around individual veins but can be extensive within the vein systems due to overlapping alteration selvages.

World-class orogenic gold deposits associated with the Cadillac-Larder Lake Fault Zone

The Lapa deposit is located in the eastern part of the CLLFZ within the major fault zone and hosts gold mineralization within fine-grained, foliated rocks of the Piché Group along the contact with sedimentary rocks of the Cadillac Group. Strongly dismembered and folded carbonate-rich veinlets are associated with mineralized rocks. Gold mineralization occurs as auriferous assemblages of arsenopyrite-pyrrhotite ± pyrite and native gold disseminated in biotite-carbonate altered host rock associated with native gold-bearing quartz ± dolomite-calcite veins. Sb-bearing minerals such as stibnite (Sb_2S_3), aurostibnite (AuSbS) and gudmundite (FeSbS) are associated with gold mineralization. Based on petrographic observations three mineralization stages are described during which the gold was first precipitated as auriferous arsenopyrite and later remobilized and deposited as native gold grains (Simard et al., 2013).

The Canadian-Malartic deposit is located in the Pontiac Subprovince, immediately South of the CLLFZ, hosted by meta-sedimentary and intrusive rocks belonging to the Pontiac Group and structurally controlled by east-striking south-dipping secondary order faults (Perrouty et al., 2017). It is a large-tonnage but low-grade deposit. Vein-hosted and disseminated gold is mainly associated with pyrite in dominantly potassic-altered rocks (Helt et al., 2014). In contrast to other orogenic gold deposits, mass gains in silver, tellurium, bismuth, molybdenum, lead, antimony and tungsten have also been described, which might indicate a magmatic fluid source (Helt et al., 2014; De Souza et al., 2016). Gold mineralization is indeed associated with quartz-monzodioritic intrusions, probably facilitating the propagation of secondary faults along rheological contrasts and hence enabling multi-stage fluid flow from the main CLLFZ into local second order structures (Perrouty et al., 2017). Based on Re-Os dating of molybdenite, an absolute age of 2664

± 11 Ma is assumed for ore formation (De Souza et al., 2016).

The Sigma-Lamaque deposit (Chapter X) contains more than 100 t of gold in multiple generations of quartz-carbonate-tourmaline veins spatially associated with shear zones and porphyritic intrusions and pyrite-rich altered volcanoclastic wall rocks. In addition to gold, pyrite, rutile, chlorite, muscovite, pyrrhotite, chalcopyrite, galena, and bismuth tellurides are present within the vein system. Native gold grains are rare and most gold occurs as inclusions or along fractures in pyrite, tourmaline and quartz, alloyed with significant amounts of silver (up to 17 wt.%). Aqueous-carbonic fluid inclusions of low salinity (< 8 wt.% $NaCl_{eq}$) and oxygen isotopes of quartz-tourmaline pairs suggest formation temperatures between roughly 300° and 400°C (Olivo et al., 2006).

The Kerr-Addison deposit is a major Archean lode gold deposit in the Abitibi greenstone belt, localized immediately to the south of the CLLFZ and hosted by originally mafic to ultramafic rocks metamorphosed at greenschist-facies conitions and overprinted by chlorite-carbonate alteration. Gold is associated with pyrite in quartz-carbonate veins and disseminated pyrite preferentially concentrated at the interface between of carbonate-muscovite and carbonate-albite alteration, indicating that lateral variations of fluid chemistry, probably due to pH gradients, led to gold accumulation (Kishida & Kerrich, 1987).

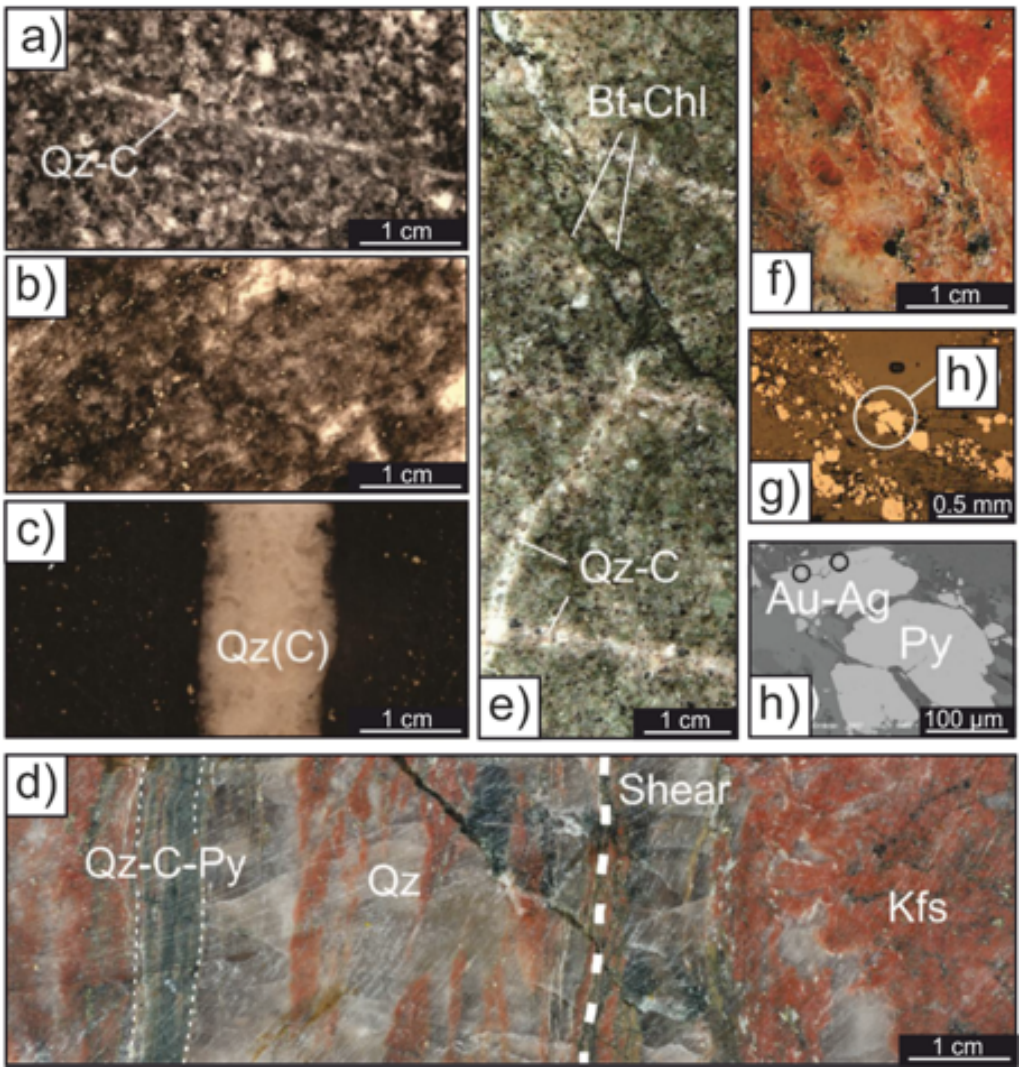

Vein and alteration petrography of several orogenic gold deposits from the Abitibi greenstone belt (modified from Nadeau, 2019). a) Altered porphyryitic texture of granodiorite with quartz-carbonate veinlets. b) Altered quartz monzonied with disseminated pyrite. c) Mineralized meta-sediments cut by quartz-carbonate vein. d) Sheared syenite with hematized K-feldspar, quartz and quartz-carbonate-pyrite veins. e) Chloritized porphyry showing quartz-carbonate veinlets crosscut by biotite-chlorite veinlets. f) Fluid flow channel cutting through K-Fe-altered protolith with quartz, carbonate, and fine pyrite. g) Reflected light image of gold-rich pyrite close to carbonates. h) BSE image of pyrite grains encircled in g) showing tiny gold and silver inclusions hosted by the pyrite.

Source of fluid and gold

In general, there are two potential sources for the gold in orogenic-type deposits: (a) devolatilization of rocks during metamorphism and (b) felsic-intermediate magmas emplaced at lower to mid crustal levels (Tomkins, 2013). The main argument for the metamorphic origin is the close spatial relationship of orogenic gold deposits with regional-scale fault zones, while the presence of magmatic intrusions is not document from all deposits of this type and age constraints are lacking. In contrast, the magmatic-hydrothermal model is based on the common spatial association of intrusions with gold mineralization combined with alteration-types and fluid compositions typical for magmatic-derived fluids. Recent studies combine both models and assume mixing of primarily magmatic fluids from the mantle or lower crust with metamorphic fluids in the upper crust (e.g. De Souza et al., 2016; Nadeau, 2019). Fluid migration and focusing via shear zones and hydraulic fractures is common to all the different models.

The metamorphic devolatilization model

For most deposits a metamorphic fluid and gold source is favored (Goldfarb et al., 2005; Phillips & Powell, 2010), with the most fertile fluid generated by pyrite-bearing carbonaceous rocks (Tomkins, 2010). Biogenic and diagenetic pyrite is thereby assumed to be the most important source of gold, which was primarily scavenged from oxidized seawater and subsequently released during later metamorphism (Tomkins, 2013). Gold in seawater might be enriched by leaching of oceanic basalts in form of magmatic sulfides that are remobilized by the seawater (Roberts, 1997). This source is certainly a valid option for orogenic gold deposits that formed in sedimentary rock sequences during the Phanerozoic after the great oxidation event but older Archean lode gold deposits, like the ones in the Abitibi greenstone belt, must have had a different source of gold, which might have been the basaltic to andesitic volcanoclastic rock sequences (Goldfarb & Groves, 2015). Required amounts of carbon-rich fluid to transport sufficient amounts of Fe, S, and Au are produced during metamorphic devolatilization of hydrated carbonated rocks primarily across the greenschist-amphibolite facies boundary (Figure 5; Phillips & Powell, 2010). Gold is thereby released during the same devolatilization event and not leached from lithologies along the fluid pathway (Goldfarb & Groves, 2015). In the CLLFZ the main ore forming event is assumed to be temporally correlated to the major shortening (D1) and the late strike-slip event (D4; Bedeaux et al., 2017, and references therein). Metamoprhic fluids used the CLLFZ as conduit to rise towards the surface, where they were channeled into second- and third-order shear faults. Despite a few exceptions, most gold deposits are spatially associated with such higher order fault zones.

The magmatic-hydrothermal model

In the Abitibi greenstone belt many gold deposits are spatially associated with magmatic intrusions (e.g. Sigma-Lamaque, Canadian-Malartic, Duquesne, Dolodau, and Lac Shortt; Helt et al., 2014; De Souza et al., 2016; Nadeau, 2019), indicating a potential role of magmatic-hydrothermal fluids in ore genesis, which was obscured by later deformation and remobilization (Mériaud & Jébrak, 2017). Igneous rocks associated

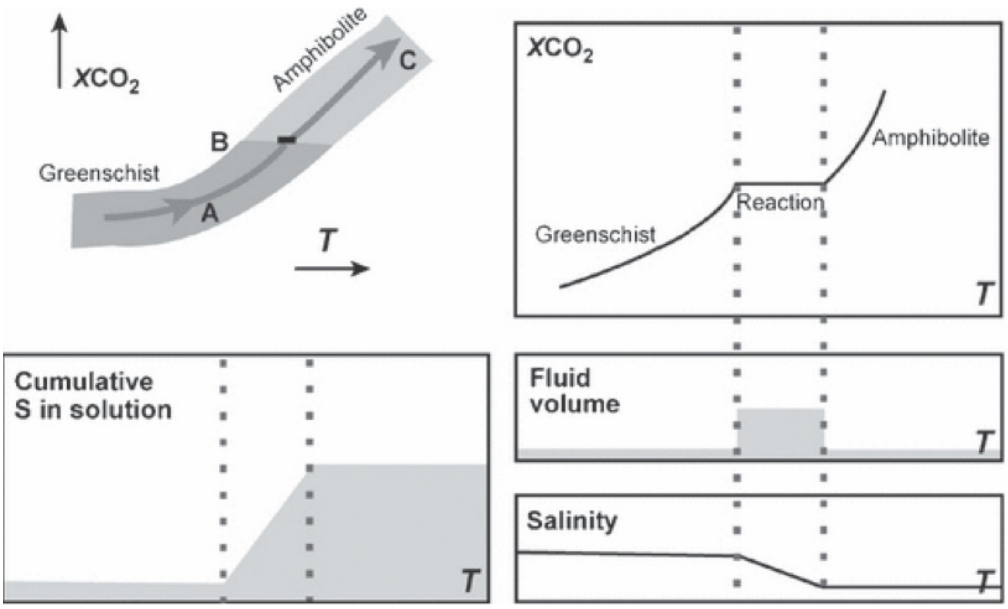

Figure 5: Qualitative representation of the transition from greenschist to amphibolite facies of mafic rocks (Phillips & Powell, 2010). Within a small temperature interval of tens of degrees, chlorite-carbonate dominated mineral assemblages are changed to hornblende-plagioclase, thereby releasing carbonate-rich sulfur-bearing fluids. The CO2/H2O ratio is buffered by the mineral assemblage to a more or less constant value during mineral transformation.

with gold mineralization are syenites, lamprophyres and carbonatites containing primary magmatic carbonates. Trace elements, stable ($\delta^{13}C$ and $\delta^{18}O$) and radiogenic isotopes ($^{87}Sr/^{86}Sr$) from magmatic and hydrothermal carbonates might provide crucial insights into fluid sources (Nadeau, 2019). Consistently high Sr/Mn and Sr/Ba ratios as well as the isotopic $^{87}Sr/^{86}Sr$ signature of the carbonates from various orogenic gold deposits point toward a mantle source (high Sr) of the fluids and subsequent mixing with upper crustal metamorphic fluids (low Sr; Figure 6; Nadeau, 2019). Especially values above 0.714 indicate carbonate precipitation from fluids that have interacted with reservoirs marked by very high Rb/Sr ratios, such as clay-rich sedimentary units in the upper part of the crust. Variable amounts of fluid mixing from the different reservoirs might have been responsible for gold precipitation. Consequently, magmatic-derived fluids might play an important role, at least in the formation of some orogenic gold deposits in the Abitibi greenstone belt (Figure 7; De Souza et al., 2016; Nadeau, 2019). Interestingly, elements enriched in typical orogenic gold deposits, namely Au, As, Sb and S, are characteristic elements enriched in vapor-like fluids from magmatic-hydrothermal systems, such as porphyry copper deposits.

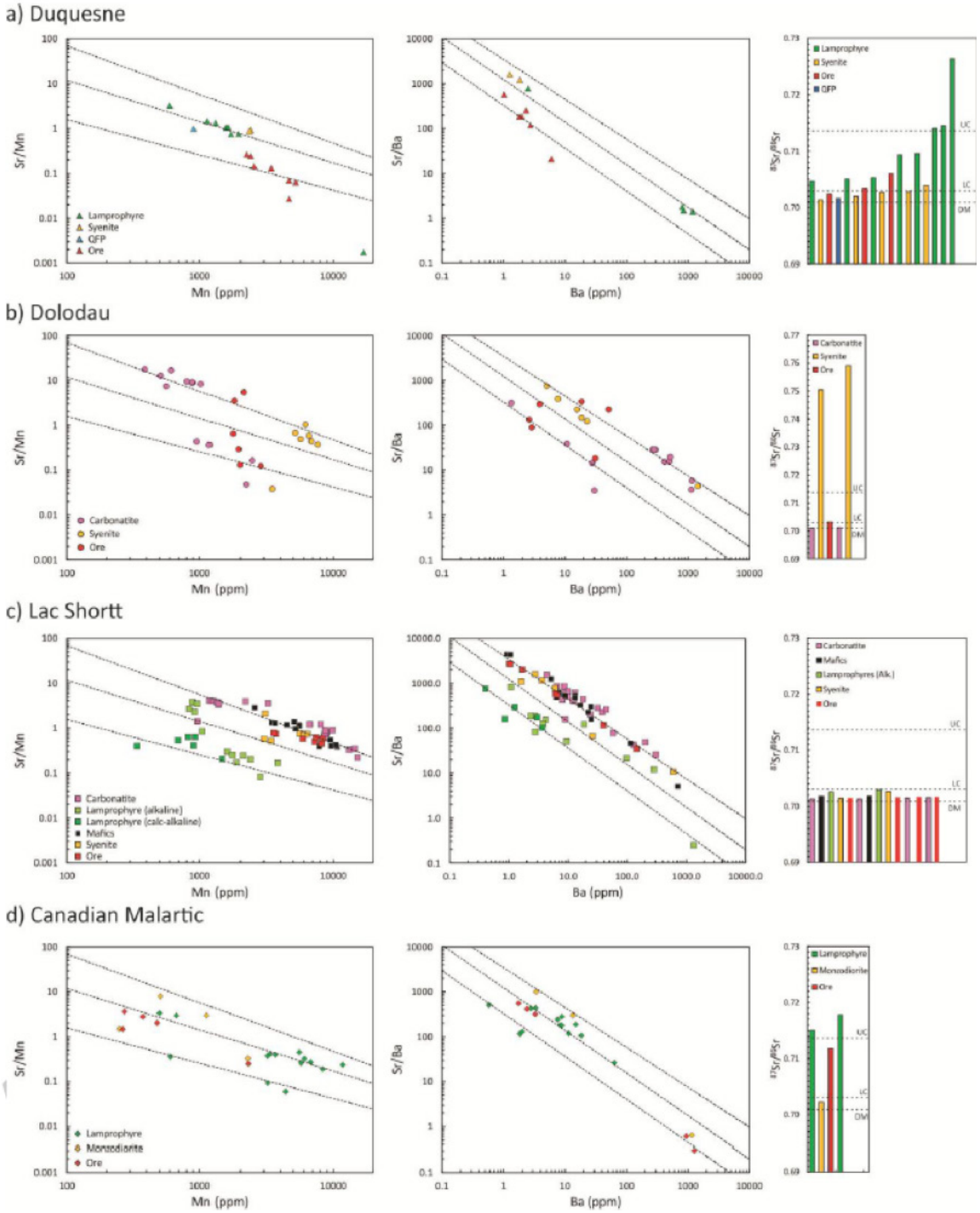

Figure 6: Sr/Mn vs Sr, Sr/Ba vs Ba and Sr isotope signatures of four different orogenic gold deposits within the Abitibi greenstone belt associated with intrusions. Low to high Sr isotope ratios and inversely correlated low to high Sr concentrations indicate three potential source regions of the hydrothermal fluid: the depleted mantle (DM, low Sr isotope ratio, high Sr concentrations), the lower crust (LC; medium Sr isotope ratio and concentrations) and the upper crust (UC; high Sr isotope ratios, low Sr concentrations).

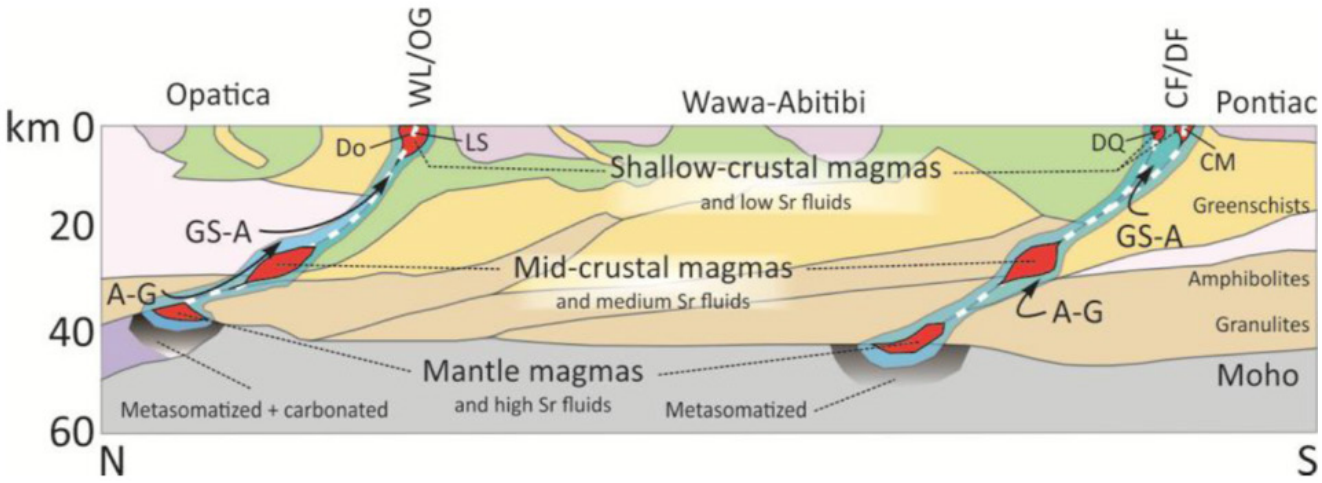

Figure 7: Conceptual model for the genesis of Archean lode gold deposits in the Abitibi greenstone belt (Nedeau, 2019). Fluid flow is channeled along the Wedding-Lamarck/Opawica-Guercheville (WL/OG) and the Cadillac-Larder Lake/Destor-Porcupine (CF/DF) suture zones. Along these suture zones magmatic fluids from partially melted mantle material and metamorphic fluids produced at the amphibolite-granulite (A-G) and greenschist-amphibolite (GS-A) transitions.

Fluid characteristics and gold precipitation

The age of many orogenic gold deposits and the assumed long fluid flow paths coupled to the long lifespan of the hydrothermal systems limit the informative value of fluid inclusions and isotopic studies. However, comparison of fluid inclusion assemblages from many orogenic gold deposits indicate that a H_2O-NaCl-CO_2 ± CH_4 low salinity (3 to 7 wt.% $NaCl_{eq}$), H_2S-bearing fluid with near-neutral pH (~5.5) at moderate temperatures (220° to 450 °C) and pressures (10 to 50 MPa) is responsible for ore formation (Ridley amd Diamond, 2000; Garofalo et al., 2014). Generally, gold might be transported by hydrosulfide complexes $(Au(HS)^{2-}$ and AuHS) in weakly-oxidized fluids (Roberts, 1997; Phillips & Powell, 2010; Tomkins, 2013). Destabilization of these complexes will accordingly result in gold precipitation. In addition to rapidly decreasing temperature and pressure during fluid ascent, mechanisms like boiling (Weatherley and Henley, 2013), fluid mixing (Bateman and Hagemann, 2004), fluid-rock interactions (Evans et al., 2006) and chemisorption on pyrite and arsenopyrite surfaces (Möller and Kersten, 1994) were identified as potential triggers of ore formation. Buffering of the hydrothermal solution at an optimal pH by weak acids such as H_2CO_3 might be very important, indicating that a spontaneous change in pH due to boiling, fluid mixing and fluid-rock interactions is indeed a main precipitation trigger (Evans et al., 2006; Phillips and Powell, 2010). Fluid reduction by carbon-bearing host rocks and resulting precipitation of pyrite also destabilizes gold complexes and lead to precipitation (Phillips and Powell, 2010).

Impressions from the field

Several deformation features that represent the tectonic events (D1 to D4), which created the Cadillec-Larder Lake Fault zone, were visible during the field trip and some examples are shown in this chapter (Figures 8-10).

Figure 8: Boudinaged quartz vein in greenschist facies metamorphosed rock, indicating extension during the D2 deformation event. Photo: M. Schirra

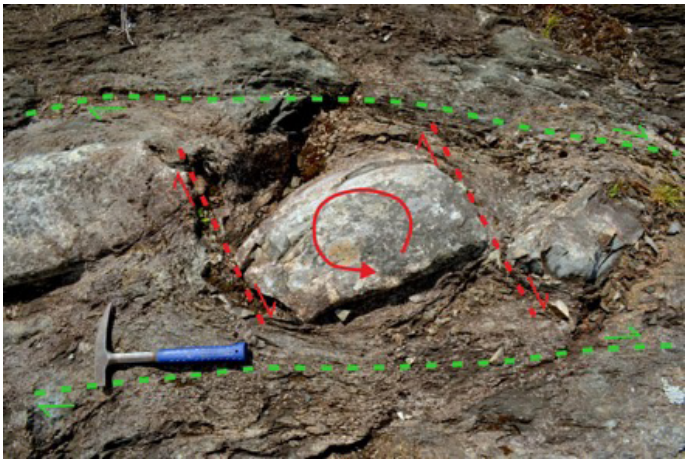

Figure 9: Rotation of a block between two local shear bands caused by dextral strike-slip movements during the transpressional D4 deformation event. Photo: M. Schirra

Figure 10: Different generations of barren quartz veins crosscut by late sulfide-bearing ankerite veinlets in highly altered greenschist. Locally, such quartz vein systems can host economic accumulation of gold. Photo: M. Schirra

References

Bateman, R., and Hagemann, S. (2004): Gold mineralization throughout about 45 Ma of Archaean orogensis: Protracted flux of gold in the Golden Mile, Yilgran craton, Western Australia. Mineralium Deposita 39, 536-559.

Beaudoin, G., and Pitre, D. (2005): Stable isotope geochemistry of the Archean Val-d'Or (Canada) orogenic gold vein field. Mineralium Deposita 40, 59-75.

Bedeaux, P., Pilote, P., Daigneault, R.,and Rafiniy S. (2017): Synthesis of the structural evolution and associated gold mineralization of the Cadillac Fault, Abitibi, Canada. Ore Geology Reviews 82, 49-69.

De Souza, S., Dubé, B., McNicoll, V.J., Dupuis, C., Mercier-Langevin, P., Creaser, R.A., and Kjarsgaard, I.M. (2016): Geology, hydrothermal alteration, and genesis of the world-class Canadian Malartic stockwork-disseminated Archean gold deposit, Abitibi, Quebec. Reviews in Economic Geology 19, 263-291.

Evans, K.A., Phillips, G.N., and Powell, R. (2006): Rock-buffering of auriferous fluids in altered rocks associated with the Golden Mile-style mineralization, Kalgoorlie gold field, Western Australia. Economic Geology 101, 805-817.

Garofalo, P.S., Fricker, M.B., Günther, D., Bersani, D., and Lottici, P.P. (2014): Physical-chemical propteries and metal budget of Au-transporting hydrothermal fluids in orogenic deposits. Geological Society, Lodon, Special Publications 402, 71-102.

Goldfarb, R.J., and Groves, D.I. (2015): Orogenic gold: Common or evolving fluid and metal sources through time. Lithos 233, 2-26.

Goldfarb, R.J., Baker, T., Dube, B., Groves, D.I., Hart, C.J.R., and Gosselin, P. (2005): Distribution, character, and genesis of gold deposits in metamorphic terranes. Economic Geology 100, 407-450.

Groves, D.I. (1993): The crustal continuum model for late-Archaean lode-gold deposits of the Yilgran Block, Western Australia. Mineralium Deposita 28, 366-374.

Groves, D.I., Goldfarb, R.J., Gebre-Mariam, M., Hagemann, S.G., and Robert, F. (1998): Orogenic gold deposits: a proposed classification in the context of their crustal distribution and relationship to other gold deposit types. Ore Geology Reviews 13, 7-27.

Helt, K.M., Williams-Jones, A.E., Clark, J.R., Wing, B.A., and Wares, R.P. (2014): Constraints on the genesis of the Archean oxidized, intrusion-related Canadian Malartic Gold Deposit, Quebec, Canada. Economic Geology 109, 713-735.

Kishida, A., and Kerrich, R. (1987): Hydrothermal alteration zoning and gold concentration at the Kerr-Addison Archean lode gold deposit, Kirkland Lake, Ontario. Economic Geology 82, 649-690.

Legault, M., Goutier, J., Beaudoin, G., and Aucoin, M. (2005): Synthèse métallogénique de la Faille Porcupine-Destor, Sous-Province de l'Abitibi. Ministère des Resources naturalles et de la Faune, 1-35.

Mériaud, N., and Jébrak, M. (2017): From intrusion-related to orogenic mineralization: The Wasamac deposit, Abitibi greenstone belt, Canada. Ore Geology Reviews 84, 289-308.

Möller, P., and Kersten, G. (1994): Electrochemical accumulation of visible gold on pyrite and arsenopyrite surfaces: Mineralium Deposita 29, 404-413.

Nadeau, O. (2019): Sources of fluids in Archean hydrothermal stockwork-disseminated gold deposits of Abitibi, Canada: insights from Duquesne, Dolodau,

Lac Shortt abd Canadian Malartic. Ore Geology Reviews, accepted manuscript.

Olivo, G.R., Chang, F., and Kyser, T.K. (2006): Formation of the auriferous and barren North Dipper Veins in the Sigma Mine, Val-d'Or, Canada: Constraints from structural, mineralogical, fluid inclusion, and isotopic data. Economic Geology 101, 607-631.

Perrouty S., Gaillard, N., Piette-Lauzière, N., Mir, R., Bardoux, M., Olivo, G.R., Linnen, R.L., Bérubé, C.L., Lypaczewski, P., Guilmette, C., Feltrin, L., and Morris, W.A. (2017): Structural setting for Canadian Malartic style of gold minerlization in the Pontiac Subprovince, south of the Cadillac Larder Lake deformation zone, Québec, Canada. Ore Geology Reviews 84, 185-201.

Phillips, G.N. (2013): Australian and global setting for gold in 2013, in Proceedings World Gold 2013, Brisbane, Australia: The Australian Institute for Mining and Metallurgy, 15-21.

Phillips, G.N., and Powell, R. (2010): Formation of gold deposits: A metamorphic devolatilization model. Journal of Metamorphic Geology 28, 689-718.

Rabeau, O., Royer, J.J., Jébrak, M., and Cheilletz, A. (2013): Log-uniform distribution of gold deposits along major Archean fault zones. Mineralium Deposita 48, 817-824.

Ridley, J.R., and Diamond, L.W. (2000): Fluid chemistry of orogenic lode gold deposits and implications for genetic models. Reviews in Economic Geology 13, 141-162.

Simard, M., Gaboury, D., Daigneault, R., and Mercier-Langevin, P. (2013): Multistage gold mineralization at the Lapa mine, Abitibi Subprovince: insights into auriferous hydrothermal and metasomatic processes in the Cadillac-Larder Lake Fault Zone: Mineralium Deposita 48, 883-905.

Tomkins, A.G. (2010): Windows of metamorphic sulfur liberation in the crust: Implications for gold deposit genesis. Geochimica et Cosmochimica Acta 74, 3246-3259.

Tomkins, A.G. (2013): A biogeochemical influence on the secular distribution of orogenic gold: Economic Geology and the Bulletin of the Society of Economic Geologists 108, 193-197.

Weatherley, D.K., and Henley, R.W. (2013): Flash vaporization during earth-quakes evidenced by gold deposits. Nature Geoscience 6, 294-298.

XIV Canadian Malartic Mine

Taraneh Roodpeyma

Abstract

The Canadian Malartic deposit as an Archean gold system is consisting 1 to 5 % disseminated pyrite associated with fine native gold and free grains in stockworks and veins hosted by diorite porphyry and altered Pontiac Group metasediments. These host assemblages are intruded by a number of intermediate to felsic porphyritic bodies having highly variable geometries and occurring on the property as dykes, sills, etc. Dominant alteration in the metasediments is potassic metasomatism consisting of biotite-K-feldspar-carbonate, and biotite and K-feldspar are directly related to gold mineralization. The Canadian Malartic General Partnership in 2018 produced 697,200 oz Au and 873,420 oz of Ag from about 20 Mt of ore grading 1.20 g of Au per ton and 1.8 g of Ag per ton.

Introduction

Malartic, the town next to the Malartic River in northwestern Quebec, Canada, in the La Vallée-de-l'Or Regional County Municipality is located about 80 km east of the centre of Rouyn-Noranda along Quebec Route 117 and the Canadian National Railway.

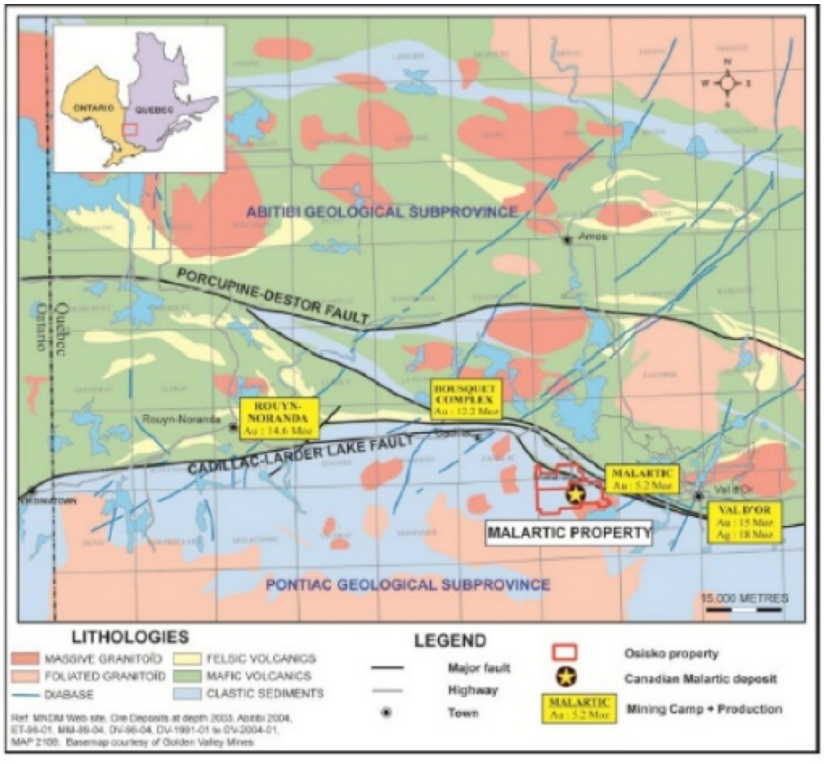

Figure 1: Regional geology of Quebec's southern Abitibi greenstone belt, including location of the Canadian Malartic deposit (Wares, 2013).

Canadian Malartic (Figure 1) is the largest operating open-pit gold mine in Canada. Gouldie Brothers in 1923 discovered gold in the Malartic area for the first time. From 1935 to 1983 it was mined –in gold mines named Canadian Malartic, Sladen Malartic, East Malartic and Barnat, mostly from underground operations. After having different owners from 1983, Osisko Mining Corp started owning the mine in 2004 and in 2005 drilled the first hole at the western extremity of the deposit. In May 2011 its commercial production started. In June 2014, Agnico Eagle and Yamana Gold created the Canadian Malartic General Partnership by acquiring Osisko Co. and the mine along it by having 50% share for each company. The mine is developed to feed the mill at a nominal rate of 55,000 t of ore per day and will be in production with the same rate until at least 2026 with ongoing extension studies, and the rate will be decreased until 2028. The ongoing project of extending the Canadian Malartic pit consists of mining the Barnat deposit and the Jeffrey pit to the East, both located in the territory of the town of Malartic. These new prospects are shown in Figure 2 together with other productive zones. The final pit's dimensions will be about 3500m along strike and 920m wide, with a final depth of 410m and the closure year of the mine is planned to be around 2030. A hydrogeological study is ongoing by the Golder Associates Ltd. to verify if the Canadian Malartic pit suitable to provide a hydraulic trap and contain the tailings with minimal environmental risk or not (Gervais et al., 2014; Wares, 2013; Agnico Eagle Mines Limited, 2018).

Geologic setting

The Canadian Malartic gold deposit is hosted by clastic metasedimentary rocks of the Pontiac Group and subalkaline porphyritic quartz monzodiorite and granodiorite with the ages of 2677 and 2678 Ma, respectively. They are located immediately south of the Larder Lake–Cadillac Fault Zone (Figure 1). The Au-Te-W-Bi±Ag metallic signature of the ore and the potassic component of the alteration assemblages (biotite+muscovite and K-feldspar) are key features that can also be applied in geochemical prospecting. It was suggested that D2 faults,

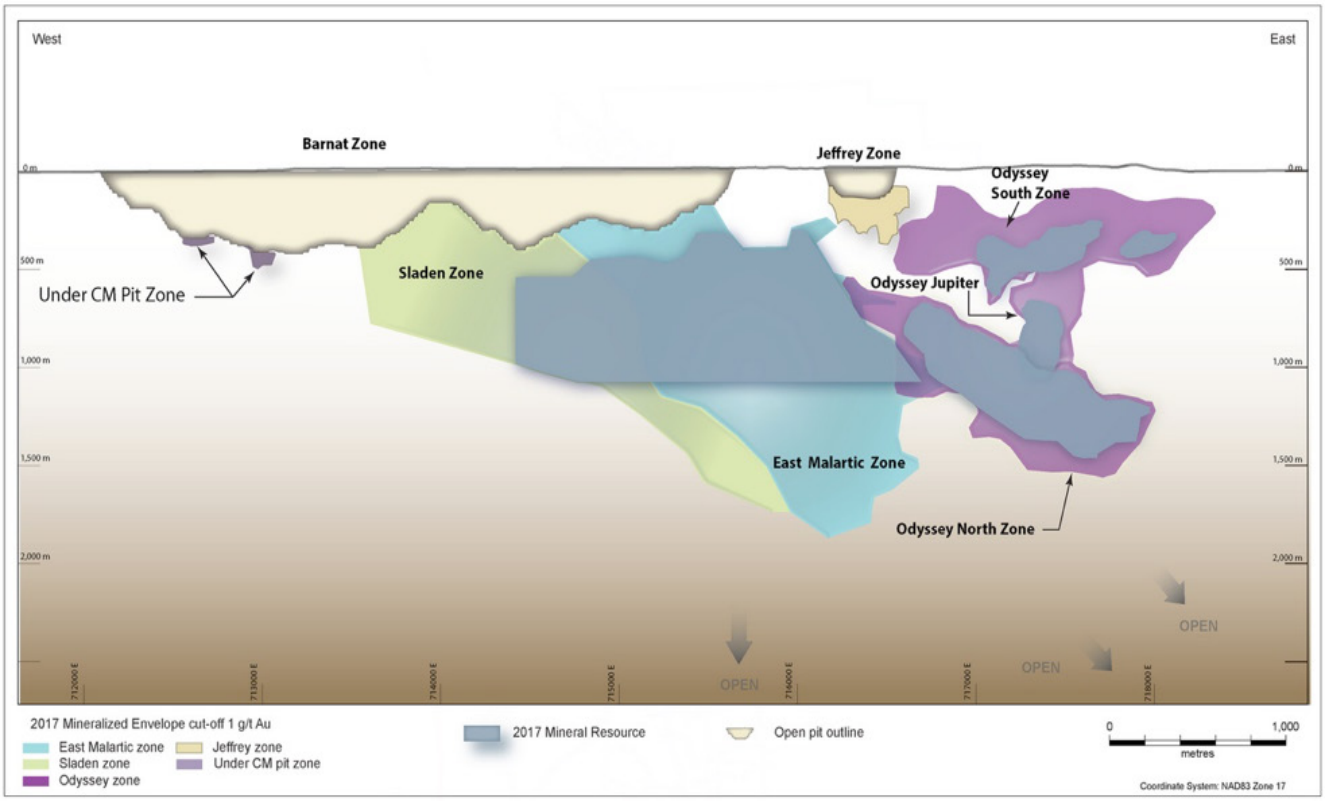

Figure 2: Composite longitudinal section (Agnico Eagle – Geological maps).

shear and high-strain zones developed in the hinge zone of F2 folds, and the Sladen Fault controlled gold mineralization and its distribution. Neither the northwest-southeast and east-west distribution of the ore zones, nor the interpreted chronology of mineralization relative to deformation and magmatism can be explained by a simple magmatic-hydrothermal model (De Souza et al., 2015).

Mining methos and machinery, economic and environmental aspects

Due to its low grade, profitable ore extraction from the Canadian Malartic mine is only possible by conventional open pit mining methods. Thus, without its location at shallow depths, the Canadian Malartic mine would be uneconomic at present gold prices. In the pit they are using large-scale equipment to increase the productivity and decrease the number of units operating in the pit. The mine plan is designed in a way to minimize the transportation distance and optimize cost by locating the ramp entry, the mill site and waste-dump areas. The entry ramp has an 8% to 10% decline with a maximum width of 35 m so that the trucks have access. The strip ratio in the pit is 2.40:1 (waste:ore) on average, the mine's payable production in 2018 was 697,200 oz of Au and 873,420 oz of Ag from about 20 Mt of ore grading 1.20 g/t Au and 1.8 g/t Ag. The mine processed on average 56,120 t per day in 2018, which was higher compared to 55,774 t per day in 2017 because of the mill optimization, additional crushed ore from the portable crusher and mill stability.

The mining operations done by these machines cause a lot of noise so that noise-suppression devices were installed on the larger vehicles, noise-barrier walls were constructed, etc. Regarding improving the air quality, the pit's loading surfaces, roadways and ramp are being sprinkled by water to help reduce dust. They also control the blast-induced vibrations and noise pressure on the town of Malartic during drilling and blasting activities and implemented some restriction for blasting when winds blow toward the town. The tailings are also treated to reduce cyanide levels before they are discharged into containment cells in tailings and sedimentation pond areas from the previous mines that once occupied the same site (Gervais et al., 2014; Agnico Eagle Mines Limited, 2018; Noble, 2015; Wares, R., 2013).

Geology and ore genesis

At the southern margin of the eastern portion of the Abitibi Subprovince, an Archean greenstone belt spanning across the Ontario–Quebec border in Canada, the Malartic property is located. The east-west trending Cadillac-Larder Lake Fault Zone (Chapter XIII) is a major fault, which marks the contact between the Pontiac Subprovince and the Abitibi greens-

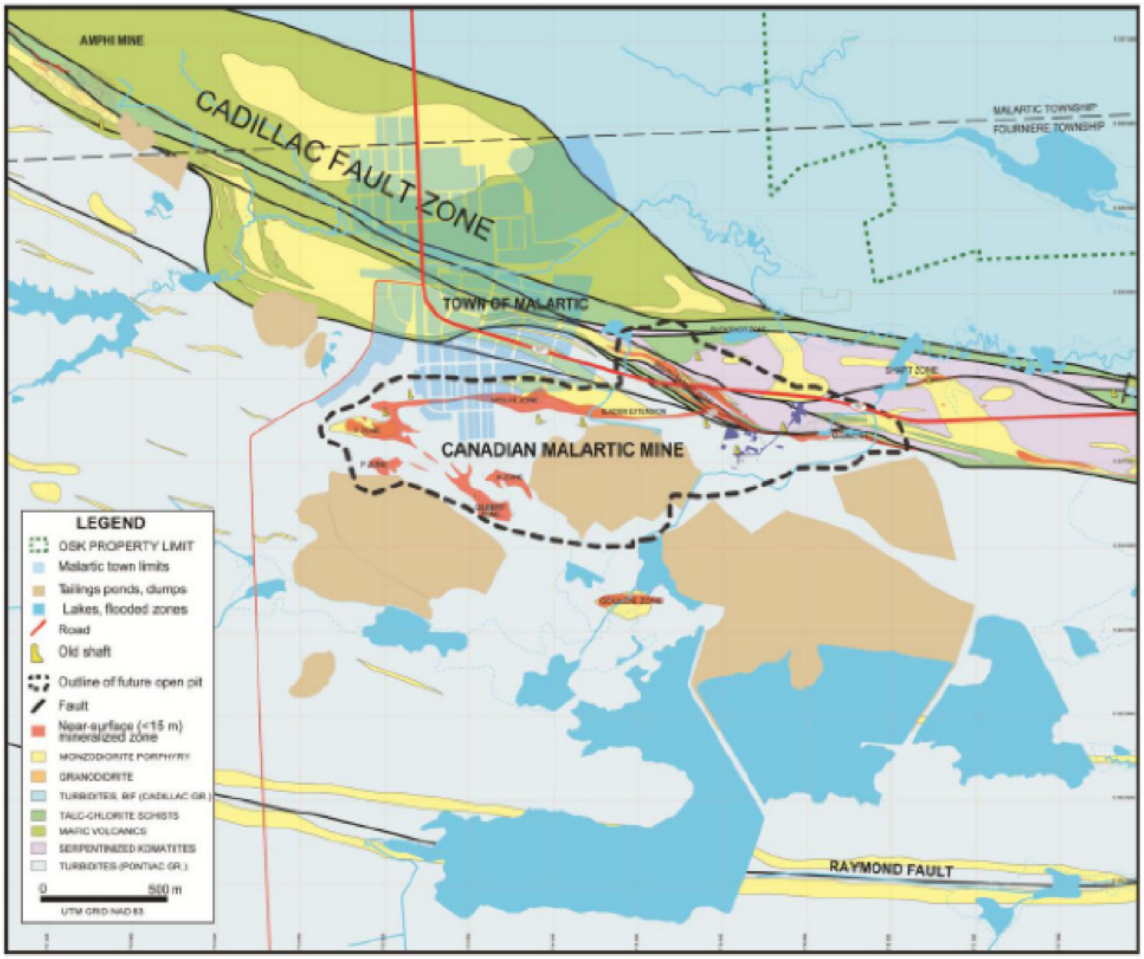

Figure 3: Local geology of the Malartic area with surface features and outline of gold mineralized zones (Wares, 2013).

tone belt (Chapter IV; Figure 1). Immediately south of the Cadillac Fault Zone, the majority of the Canadian Malartic property is underlain by meta-sedimentary units of the Pontiac Group (Figure 3). Small outcrops of the Piché Group, consisting of bluish-grey, pervasively foliated ultramafic metavolcanic rocks are present within the mining district (Wares, 2013). These rocks show evidence for hydrothermal activity as they contain many talc-carbonate veinlets. Less altered variants are aphanitic to fine-grained, serpentinized ultramafic rocks.

Meta-sedimentary rocks of the Pontiac Group host the mineralization of the Canadian Malartic mine. Rocks are composed of biotite, muscovite, oligoclase, chlorite, and epidote, and a maximum age of ca. 2685 Ma is suggested by U-Pb dating (De Souza et al., 2015). Compositionally different intermediate to felsic dykes, sills and intrusive rocks including porphyritic quartz monzodiorite and granodyorite and also lamprophyre dykes have cut the metasedimentary rocks at the mine site. They are hydrothermally altered and, at least locally, host ore-grade Au mineralization. The main mineralized intrusive phase is the quartz monzodiorite, which is magnetite- and titanite-bearing and consisting of perthitic orthoclase phenocrysts (Figure 4), located in the northern and western parts of the deposit (De Souza et al., 2015). Although the intrusive rocks are compositionally variable, magmatic event(s) centered in the Malartic area are restricted in time and dated to be syn-Timiskaming (2678–2676 Ma).

The gold occurs as less than 20 µm large, free grains in stockwork veins and as inclusions in pyrite (Figure 4c). Minor amounts of chalcopyrite, sphalerite, molybdenite as well as gold-silver and silver tellurides are also associated with pyrite (Fallara et al., 2000; De Souza et al., 2015), which occurs as disseminated grains in the altered host rocks (Figure 4d). The mineralization follows mainly E-W and NW-SE trends defined by fault zone parallel to the Cadillac – Larder Lake Fault Zone (Figure 5).

De Souza et al. (2015) subdivided the different vein types occurring in the gold deposit based on mineralogy, texture and cross-cutting relationships into five groups: the first vein generations V1 (quartz-dominated veins with low Au contents, interpreted to pre-date the main mineralization event), V2 (stockwork vein

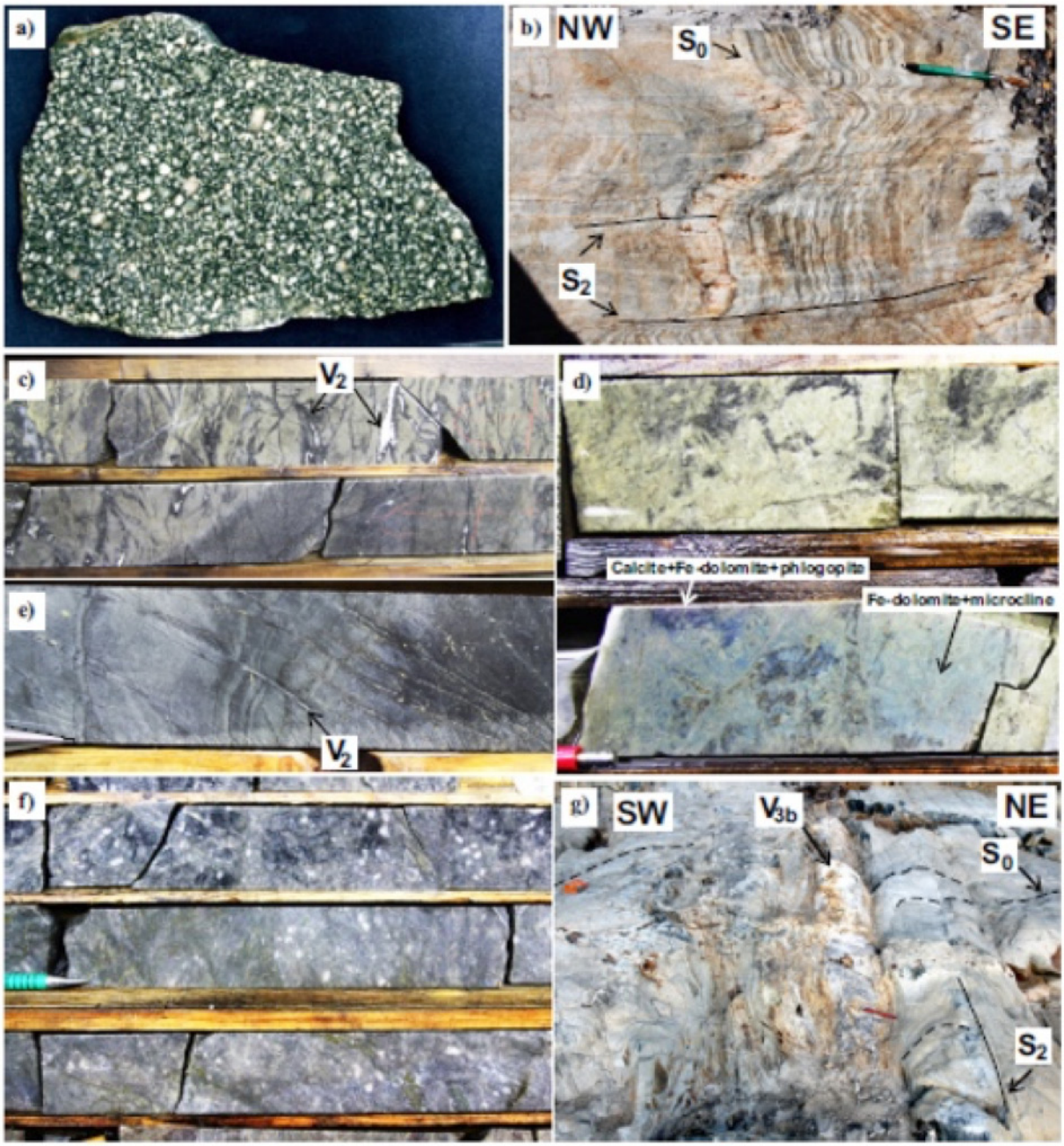

Figure 4: Sample photographs. (a) Least-altered quartz monzodiorite of the Sladen zone. (b) F2 folds in massive to laminated greywacke and mudstone of the Pontiac Group showing S2 pressure-solution cleavage. Younging direction is to the northwest. (c) Stockwork of V2 veinlets and disseminated gold mineralization in altered greywacke. (d) Proximal alteration in greywacke with ferroan dolomite coloured blue using carbonated staining technics. Notice the local presence of calcite (pinkish/purple) in biotite-rich zones. (e) V2 quartz veinlets with biotite-rich pyritized selvages in a distal alteration zone in sedimentary rocks. Veinlets are formed perpendicular to bedding. (f) Proximal alteration zone in quartz monzodiorite, footwall of the Sladen Fault. (g) High-grade laminated V3b quartz vein in D2 high-strain zone cutting the stratification at a high-angle (De Souza et al., 2015).

system including variable proportions of quartz, calcite, ferroan dolomite, biotite, microcline, albite, chlorite, pyrite, and ankerite), and V3 (cutting V2, can be further divided into 3 distinct subtypes) are related to auriferous hydrothermal alteration. In contrast, V4 and V5 are barren and hence post-date mineralization (De Souza et al., 2015).

The major amount of gold (~ 70 %) is hosted by altered clastic sediments of the Pontiac Group, which are overlying an epizonal monzodioritic porphyry intrusion pinching out in the eastern portion of the deposit. Disseminated mineralization keeps on in the strongly altered metasdiments, forming the Sladen Extension, a subvertical tabular body, truncated by the Cadillac fault. The South Barnat Zone of the current Canadi-

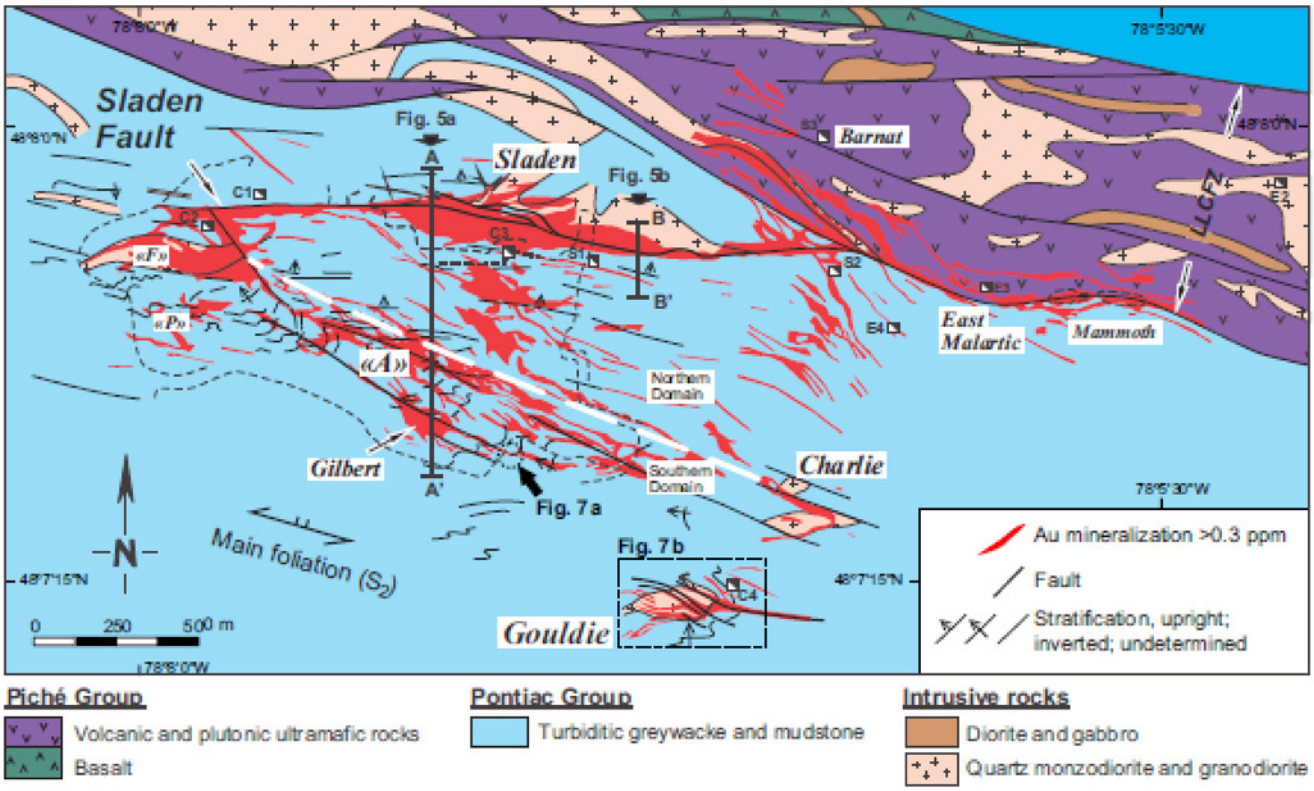

Figure 5: Geological map of the Canadian Malartic open pit gold mine. Mineralized zones (≥0.3 g/t Au) are shown in red. The outline of the open pit mine, as of September 2012, is shown as a dashed line. The approximate limit between the northern and southern structural domains is identified by a white dashed line. Names of the main mineralized ore zones are identified in italic font. Location of the shafts of the closed mines: C = Canadian Malartic, E = East Malartic, S = Sladen-Barnat (De Souza et al., 2015).

an Malartic Mine is this truncated portion of the deposit along with additional mineralization within the Piché Group rocks north of the fault. The other 30 % also occur in the upper portions of the porphyry body underlying the host metasediments (Figure 6;Wares, 2013).

A magmatic-hydrothermal model defining the deposit type was proposed, explaining the gold mineralization of the Canadian Malartic mine. Exsolution of an ore-forming fluid from monzodioritic magma at mid-crustal levels is playing a role during its ascent to potassically alter, carbonatize, sulphidize and locally silicify the host rocks and deposit gold. The contacts of the host rocks with Pontiac greywacke and Piché mafic and ultramafic rocks provided the competency contrasts that helped focus the mineralizing fluids (Gervais et al., 2014).

According to the other studies, as a result of D2 deformation and gold-bearing hydrothermal fluids invading D2 structures, widespread brittle and brittle-ductile structures, which are associated with at least part of the alteration assemblages, disseminated orebodies, and vein networks, have formed. The widespread car-

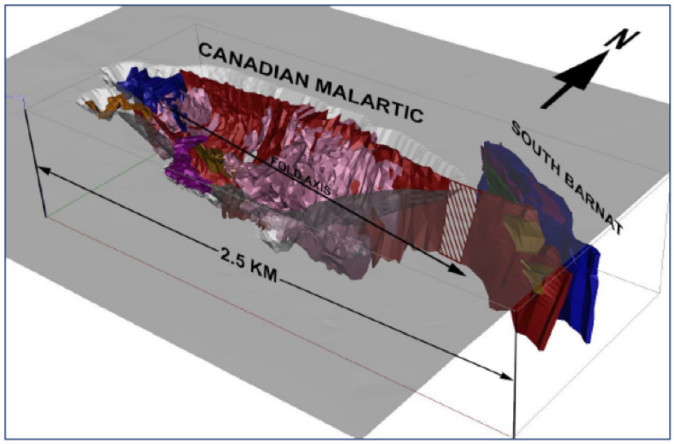

Figure 6: 3D projection of the Canadian Malartic deposit and adjacent South Barnat deposit. All colored domains, except for light pink, grade more than 1 g/t Au and define a synformal structure plunging toward the ESE in the Canadian Malartic deposit . The light pink domain represents a diffuse shell of low grade (0.3 to 1.0 g/t Au) mineralization along the hinge of the synform. The northern limb of the synform extends into the Cadillac fault zone (Sladen Extension, hatched), where it is dismembered and, along with subvertical, tabular, porphyry-hosted mineralization north of the fault, forms the South Barnat deposit (Wares, 2013).

bonate alteration typifying many gold deposits along the Larder Lake-Cadillac and Destor-Porcupine fault zones in the Abitibi greenstone belt is related to D2 deformation (Dubé and Gosselin, 2007; De Souza et al., 2015).

Syn-D2 deformation gold (ca. 2670–2660 Ma) superimposed onto, or partly remobilized from, an early gold-bearing magmatic/hydrothermal system related to Timiskaming-age porphyritic intrusions emplaced along a major fertile fault zone could explain the main characteristics of the Canadian Malartic deposit. In addition, common features of Archean orogenic gold deposits include a combination of widespread carbonate alteration, overall low Cu, Bi, Zn and Pb contents, CO_2, K_2O, Na_2O, and S hydrothermal metasomatism, and the spatial association with brittle-ductile faults and shear zones (Goldfarb et al., 2005; De Souza et al., 2015). Also, one of the pivotal roles in forming the Canadian Malartic deposit is belonging to the Sladen Fault through which gold-bearing hydrothermal fluid(s) could rise (De Souza et al., 2015).

Open pit mine visit

Figure 7: Canadian Malartic Mine from west to east sides. The holes observed on the ground were going to be blasted. Photo: T. Roodpeyma

References

Agnico Eagle Mines Limited (2018): A New Era Begins: 2018 Annual Report.

De Souza, S., Dubé, B., McNicoll, V. J., Dupuis, C., Mercier-Langevin, P., Creaser, R. A., and Kjarsgaard, I. M. (2015): Geology, hydrothermal alteration, and genesis of the world-class Canadian Malartic stockwork-disseminated Archean gold deposit, Abitibi, Quebec. In: Targeted Geoscience Initiative 4: Contributions to the Understanding of Precambrian Lode Gold Deposits and Implications for Exploration, (ed.) B. Dubé and P. Mercier-Langevin; Geological Survey of Canada, Open File 7852, 113–126.

Dubé, B., and Gosselin, P. (2007): Greenstone-hosted quartz-carbonate vein deposits, In: Mineral Deposits of Canada: A Synthesis of Major Deposit Types, District Metallogeny, the Evolution of Geological Provinces and Exploration Methods, (ed.) W.D. Goodfellow; Geological Association of Canada, Mineral Deposits Division, Special Publication No. 5, 49–73.

Fallara, F., Ross, P.-S., and Sansfaçon, R. (2000): Caractérisation géochimique, pétrographique et structurale: Nouveau modèle métallogénique du camp minier de Malartic; Ministère des Ressources Naturelles du Québec, MB 2000-15, 41 p.

Gervais, D., Roy, C., Thibault, A., Pednault, C., and Doucet, D. (2014): Technical Report on the mineral resource and mineral reserve estimates for the Canadian Malartic property, 460p.

Goldfarb, R. J., Baker, T., Dubé, B., Groves, D. I., Hart, C. J. R., Robert, F., and Gosselin, P. (2005): World distribution, productivity, character, and genesis of gold deposits in metamorphic terranes, In: One Hundredth Anniversary Volume, (ed.) J. W. Hedenquist, J. F. H. Thompson, R. J. Goldfarb, and J. P. Richards; Society of Economic Geologists, 407–450.

Noble, R. (2015): Canadian Malartic mine puts small Quebec Town on the international map. Canadian mining journal.

Wares, R. (2013): The Canadian Malartic Mine, Southern Abitibi Belt, Quebec, Canada: Discovery and Development of an Archean Bulk-Tonnage Gold Deposit.

XV Lamaque Mine

Milos Velojic

Overview

The Lamaque property is part of the Val-d'Or mining camp of the southern Abitibi Greenstone Belt. Genetically it is part of the Val-d'Or formation, which belongs to the southeast zone of the Abitibi belt (Dimroth et al., 1982). The property hosts three major orogenic lode gold deposits, which consist of quartz-tourmaline(-carbonate) veins closely associated with shear zones. The property is owned by Eldorado Gold, and an underground mine is currently being developed at the Triangle prospect.

Geological setting

The Lamaque property is located in the Val-d'Or mining district near the city of Val-d'Or in northwestern Quebec, around 500 km northwest of Montreal (Perrault et al, 1984). The Val-d'Or district comprises the Malartic and Louvicourt groups, which formed at 2714-2611 Ma (e.g. Scott et al., 2002; Figure 1). The Malartic group consists of komatiites and tholeiitic basalts, which formed in a mantle plume-dominated extensional environment, whereas the Louvicourt group consists of mafic to felsic volcanic rocks of a volcanic arc (Scott et al., 2002). Common rock types include volcanoclastics (breccias, lappilli and tuffs), andesitic lavas and hypabyssal porphyry intrusives, most notably the Bourlamaque Pluton (Figure 1).

The lithologies of the Val-d'Or district were metamorphosed at Greenschist facies conditions and exposed to three major deformation events (Taner & Trudel, 1991). Notably, the D2 deformation is expressed in tight and isoclinal folds, subvertical E-W-trending foliation, faults, and shear zones that host the auriferous veins (e.g. Robert, 2001).

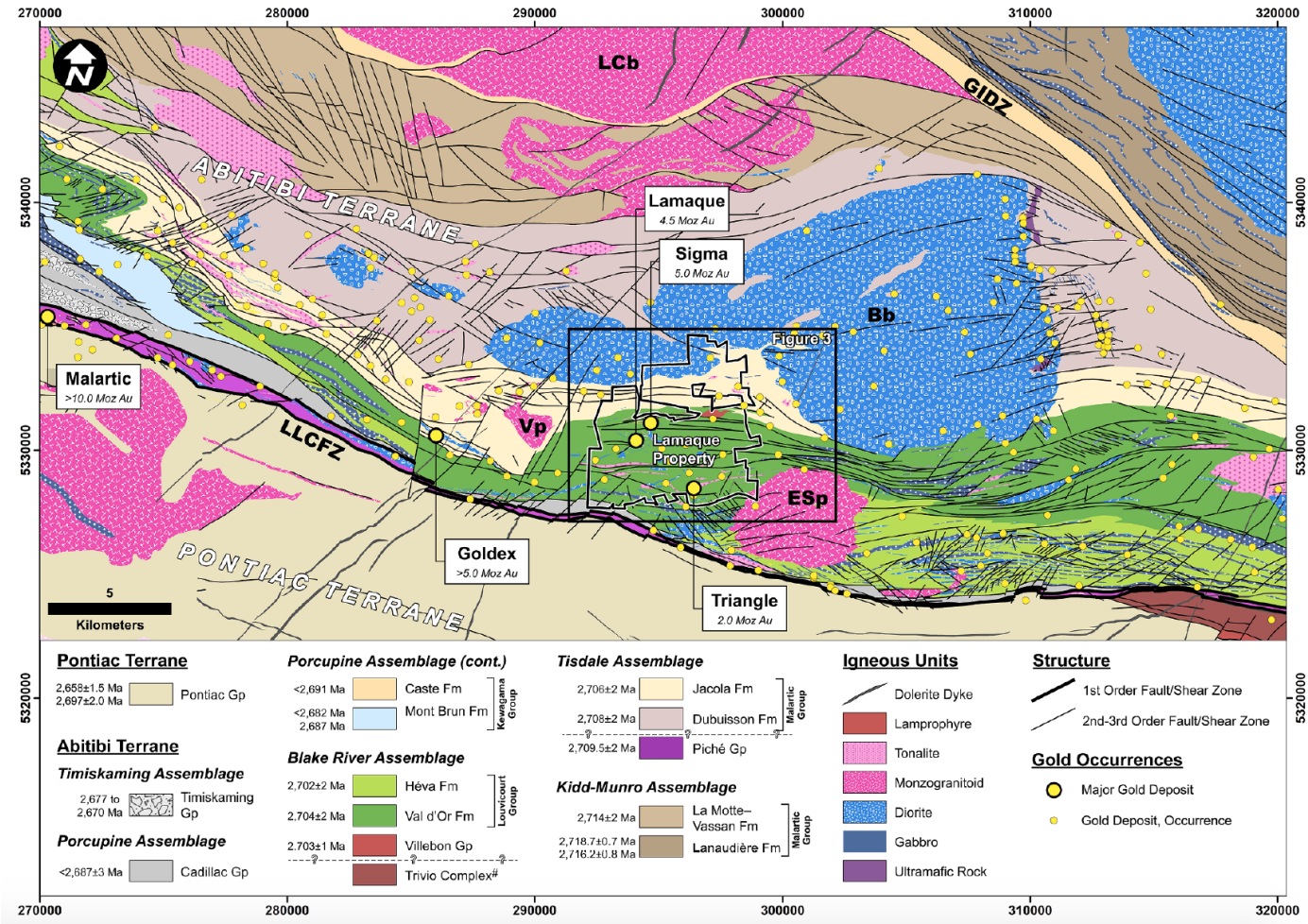

Figure 1: Geological map of the Val-d'Or district from Kreuzer et al. (2019); Lamaque property outlined in black. LLCZ = Larder-Lake-Cadillac fault zone, GIDZ = Garden Island deformation zone, Bp = Bourlamaque pluton, ESp = East Sullivan pluton, Vp = Valentin pluton.

Mining at the Lamaque property

The Lamaque property comprises the Sigma, Lamaque, and Triangle gold prospects (Keogh et al., 2018). All three prospects have in common: (a) a position within a steeply dipping intrusive body intruded in the Val-d'Or formation and (b) a close relationship with faults and shear zones of the regional D2 deformation event at ca. 2672-2665 Ma.

According to Keogh et al. (2018), the first gold discovery at the Lamaque property happened in 1923, followed by the construction of the first mine shaft in 1933 and ore extraction starting in 1935. The Lamaque mine was active between 1935-1985 and 2010-2012. The Sigma mine (Figure 2) was active between 1936-1999 and 2007-2008 and an underground mine and between 1999-2000, 2002-2003, and 2004-227 as an open pit mine (Keogh et al., 2018). Production from both deposits totalled ca. 9.5 Moz Au at a grade of ca. 5.3 g/t Au (Keogh et al., 2018).

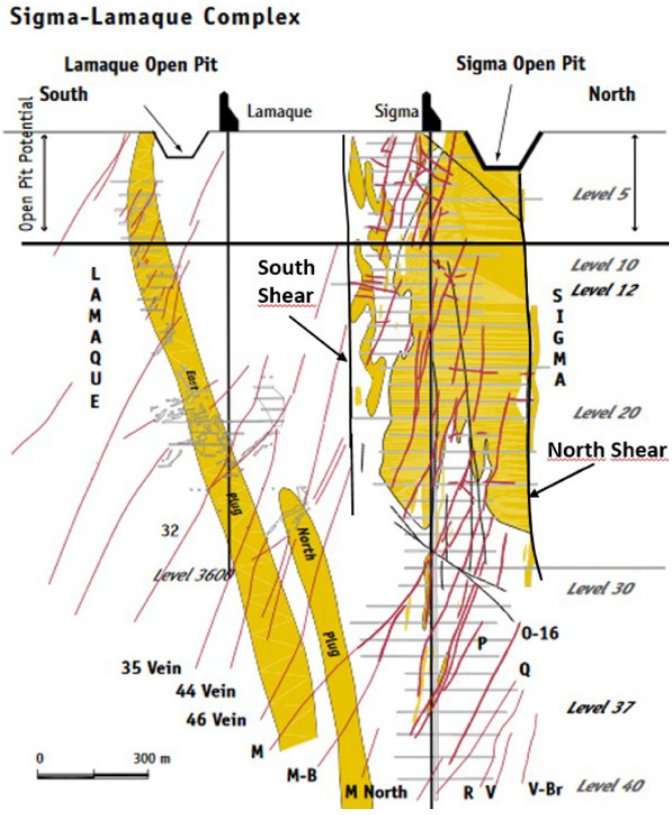

Figure 2: Cross-sections of the Lamaque and Sigma deposits; from Integra Gold Corp (2017).

The Lamaque deposit (Figure 2) consists of two main ore bodies: East and West plug, which are located within the main tonalite-diorite intrusives (Perrault et al., 1984). At the Sigma deposit, most of the mineralized veins are located in a deformed andesitic block of the Val-d'Or formation, intruded by a body of porphyritic diorite and several east-west trending feldspar porphyry dikes. The vein network of the Sigma deposit is limited by two vertical shear zones called North and South shear (Figure 3; Robert & Brown, 1986).

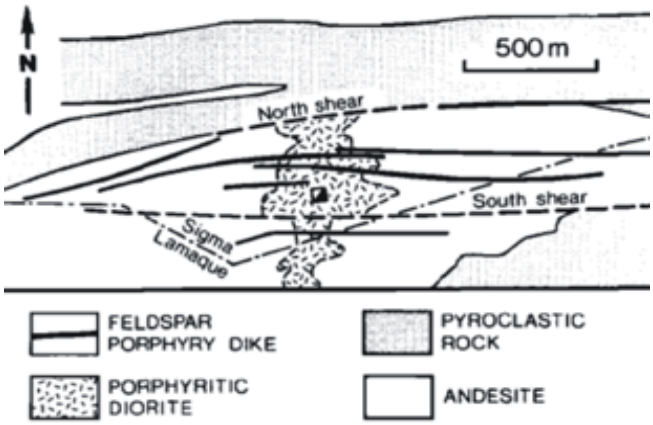

Figure 3: Simplified geology of the Sigma mine area with marked borders of porphyritic diorite; from Robert & Brown, 1986).

In 2011 Integra Gold discovered the Triangle gold deposit (Figure 4) and in 2015 restarted production in the Lamaque area. In 2017 Eldorado Gold Corporation acquired Integra Gold and changed the name to Eldorado Gold Lamaque. Today's Lamaque property consists of the recently-discovered Triangle gold deposit located just 2.5km south of the historical Lamaque and Sigma mines, as well as No. 4 Plug and Parallel. The total measured and indicated resources of the three deposits amount to ca. 1.3 Moz Au at a grade of ca. 8.5 g/t Au (Keogh et al., 2018).

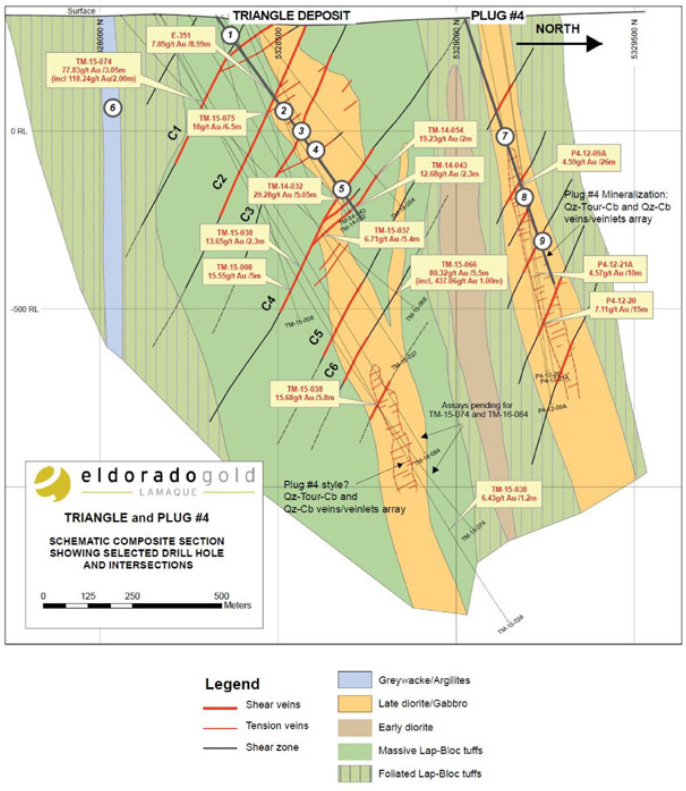

Figure 4: Cross-sections of the Triangle and Plug No. 4 deposits; from Keogh et al. (2018).

Like the other mineralizations at Lamaque, Triangle is also a typical orogenic gold deposit. Gold is located in quartz-tourmaline-carbonate veins in sub-vertical shear zones centered around a steeply plunging (around 70°) porphyry diorite ("Triangle Plug"), which intrudes the mafic volcanics of the Val d'Or formation. Gold bearing veins are on average 4-5m thick; and the thickest veins are hosted by east-west trending, 50-70° dipping reverse faults (Kreuzer et al., 2019).

Mining at the Triangle deposit will be performed using a haulage ramp system to the surface. The predominant mining technique will be long-hole retreat (stoping) and minor room-and-pillar mining (Keongh et al., 2018).

Most recent brownfield exploration was performed between 2015-2017, employing drilling and geophysical surveying (Keogh et al., 2018). In addition, the Lamaque property launched a crowdsourcing competition for gold exploration in 2015 to further prospecting in the area (Kreuzer et al., 2019).

Auriferous veins

Four types of auriferous veins were recorded on the Lamaque property (Olivo et al., 2006): (1) steeply to moderately dipping fault-fill veins accommodated by shear zones, (2) subhorizontal extensional veins, (3) subhorizontal veins within the porphyry dikes, and (4) extensional shear veins with moderate dip to the north. Veins consist of quartz-tourmaline(-carbonate) and minor pyrite, chalcopyrite, and scheelite (Olivo et al., 2006). The veins produced alteration haloes of white mica, carbonate, and pyrite and cross-cut all rock types. Fluid inclusion evidence suggests that Au was transported by a CO_2-bearing aqueous fluid and precipitated upon mixing with H_2O-rich fluids (Olivo et al., 2006).

There are still some uncertainties related to the genesis (fluid and metal sources) of these deposits. Isotopic and noble gas data are inconsistent between different deposits. There are three genetic models of fluid sources of orogenic gold deposits in general (Goldfarb & Groves, 2015): (1) magmatic-hydrothermal source-from granitic intrusions, (2) metamorphic crustal fluids, and (3) sub-crustal fluid source (from subducting slabs).

Impressions of the mine visit

Figure 5: Sample from Lamaque mine, containing a quartz-tourmaline vein with pyrite and native gold. Photo: M.Velojic

Figure 6: Vein in underground outcrop. Photo: E. Gagnon

References

Dimroth, E., Imreh, L., Rocheleau, M., and Goulet, N. (1982): Evolution of the south-central part of the Archean Abitibi belt, Quebec. Part I: Stratigraphy and paleogeographic model. Canadian Journal of Earth Sciences 19, 1729-1758.

Goldfarb, R. J., and Groves, D. I. (2015): Orogenic gold: Common or evolving fluid and metal sources through time. Lithos 233, 2-26.

Integra Gold Corp (2017): Ni-43 101 technical report on the spring 2017 mineral resource estimate update for the Lamaque project.

Keogh, C., Simoneau, J., Juras, S., Utiger, M., and Chabot, F. (2018): Technical Report Lamaque Project, Québec, Canada. 322p.

Kreuzer, O. P., Buckingham, A., Mortimer, J., Walker, G., Wilde, A., and Appiah, K. (2019): An integrated approach to the search for gold in a mature, data-rich brownfields environment: a case study from Sigma-Lamaque, Quebec. Ore Geology Reviews, 102977.

Olivo, G. R., Chang, F., and Kyser, T. K. (2006): Formation of the auriferous and barren North Dipper Veins in the Sigma Mine, Val d'Or, Canada: constraints from structural, mineralogical, fluid Inclusion, and isotopic data. Economic Geology 101, 607-631.

Perrault, G., Trudel, P., and Bedard, P. (1984): Auriferous halos associated with the gold deposits at Lamaque mine, Quebec. Economic Geology 79, 227-238.

Robert, F., and Brown, A. C. (1986): Archean gold-bearing quartz veins at the Sigma Mine, Abitibi greenstone belt, Quebec; Part I, Geologic relations and formation of the vein system. Economic Geology, 81, 578-592.

Robert, F. (2001): Syenite-associated disseminated gold deposits in the Abitibi greenstone belt, Canada. Mineralium Deposita 36, 503–516.

Scott, C. R., Mueller, W. U., and Pilote, P. (2002): Physical volcanology, stratig- raphy, and lithogeochemistry of an Archean volcanic arc: Evolution from plume-related volcanism to arc rifting of SE Abitibi greenstone belt, Val d'Or, Canada. Precambrian Research 115, 223–260.

Taner, M. F., and Trudel, P., (1991): Gold distribution in the Val-d'Or Formation and a model for the formation of the Lamaque–Sigma mines, Val-d'Or, Quebec. Canadian Journal of Earth Sciences 28, 706-720.

Field stops: Sudbury Structure

Shirley Péloquin

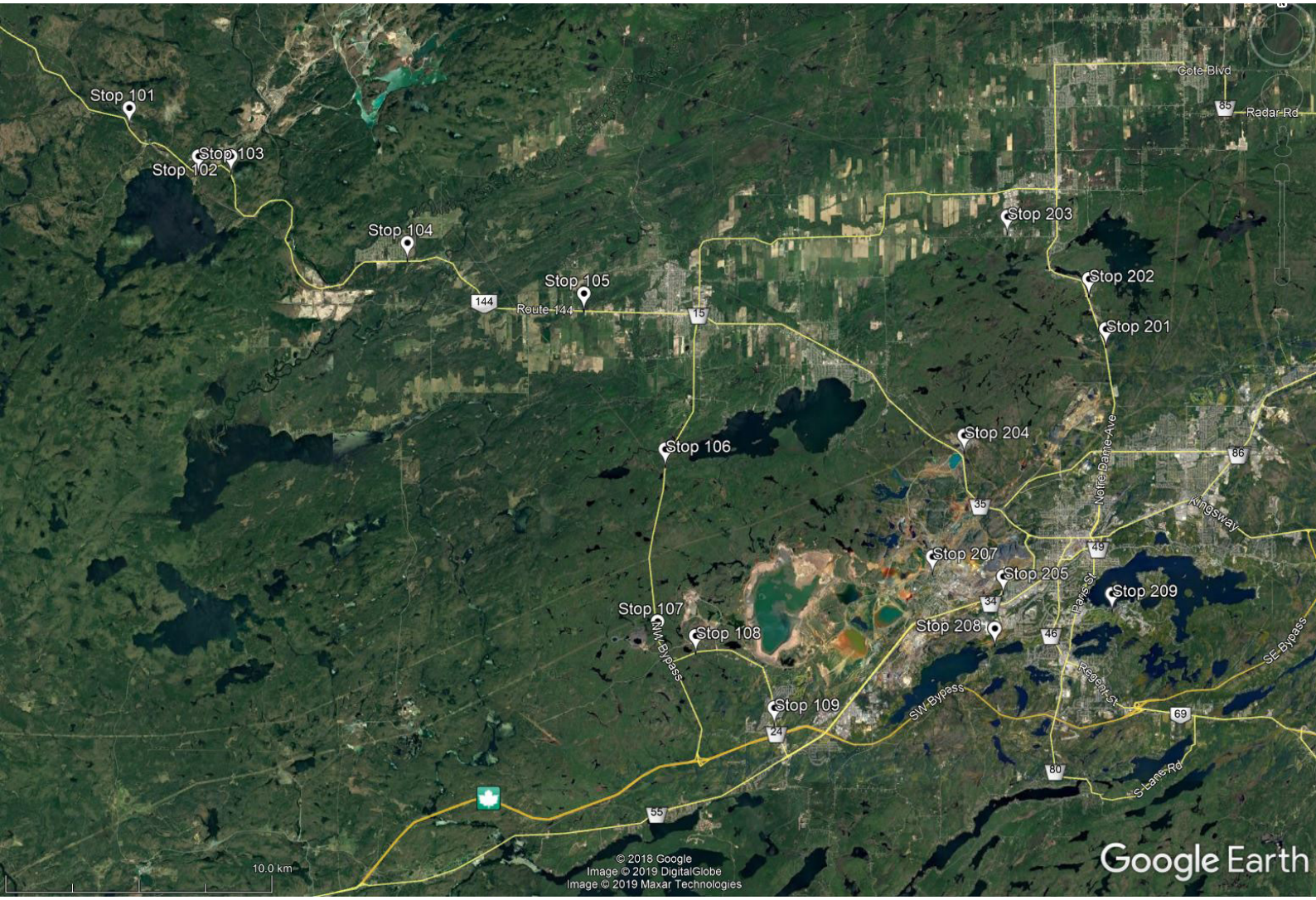

Figure 1: Overview over the field stops focusing on the Sudbury Structure

Day 1

Stop 101 – Levack Gneiss Complex with Matachewan dyke and Sudbury Breccia
Highway 144 North of Windy Lake; 464631E, 5164306N

Stop 102 – Quartz Gabbro and Granophyre
Regional Road 8 at Highway 144; 468456E, 5162763N

Stop 103 – Onaping Formation, Whitewater Group
Across Highway 144 from the AY Jackson Lookout on High Falls; 467233E, 5162488N

Stop 104 – Onwatin Formation – Whitewater Group
Highway 144 east of Dowling; 475069E, 5159227N

Stop 105 – Chelmsford Formation, Whitewater Group
Highway 144 west of Chelmsford. 481688E, 5157320N

Stop 106 – Sheared Onaping Formation
Highway 144 Bypass between Chelmsford and Lively; 484730E, 5151486

Stop 107 - Fragment-rich base of South Range Norite
Highway 144 - 484424E, 5145048N

Stop 108 – Creighton pluton, Matachewan dike and Sudbury Breccia
South side of Highway 24 between the 144 Bypass and Lively; 485850E, 5144510N

Stop 108 - Pseudotachylite "Sudbury Breccia"
Tom Davies Community Centre – 488793E, 5141811N

Day 2

Stop 201 - South Range Norite
Regional Road 80: 501270E, 5155943N

Stop 202 – Sudbury Igneous Complex Quartz Gabbro and Sudbury Dike
Regional Road just south of McCrea Heights; 500640E, 5157821N

Stop 203 – Scenic View: Corner of Valleyview and Belisle Drive. 497579E, 5160158N

Stop 204 – Discovery Site
495941E, 5151977N

Stop 205 – The Big Nickel at Dynamic Earth: Sudbury breccia – Mckim Formation
122 Big Nickel Drive

Stop 206 – Contact Between Creighton Pluton and Elsie Mountain Formation –
Intersection of Godfrey Drive and Cliff Street, Copper Cliff; 494743E, 5147449N

Stop 207 – Copper Cliff Offset, Behind the Emergency Service Building.
494762E, 5146819N

Stop 208 – Sudbury Breccia
Southview Drive; 497075E, 5144757N

Stop 209– Shatter Cones
Ramsey Lake Rd., 1.4 km east of Paris St.; 501482E, 5146044N

All coordinates: UTM NAD 83, Zone 17

Field stops: Cadillac - Larder Lake - Fault

Pierre Bedeaux

Table 1: Overview over the field stops focusing on the Cadillac - Larder Lake Fault.

Location	Day	Geological setting	Themes	Coordinates
Astoria showing	1-am	Cadillac Fault and Piché	Mineralization and deformation	48°11‘39.24“ N 79°02‘02.29“ W
McWatters trench	1-am	McWatters Formation	Deformation	48°12‘38.84“ N 78°54‘23.39“ W
Landry trench	1-am	Piché Formation	Volcanology	48°13‘51.72“ N 78°27‘35.38“ W
Malartic Lake Shore Showing	1-pm	Riviere-Heva Fault Zone	Mineralization and deformation	48°13‘53.95“ N 78°09‘07.88“ W
Pan Canadian old mine	2-am	Cadillac Fault and Piché	History, mineralization and deformation	48°10‘51.91“ N 78°13‘39.55“ W
Timiskaming outcrops	2-am	Timiskaming Fm.	Sedimentology related to mineralization	48°11‘37.21“ N 78°12‘48.82“ W

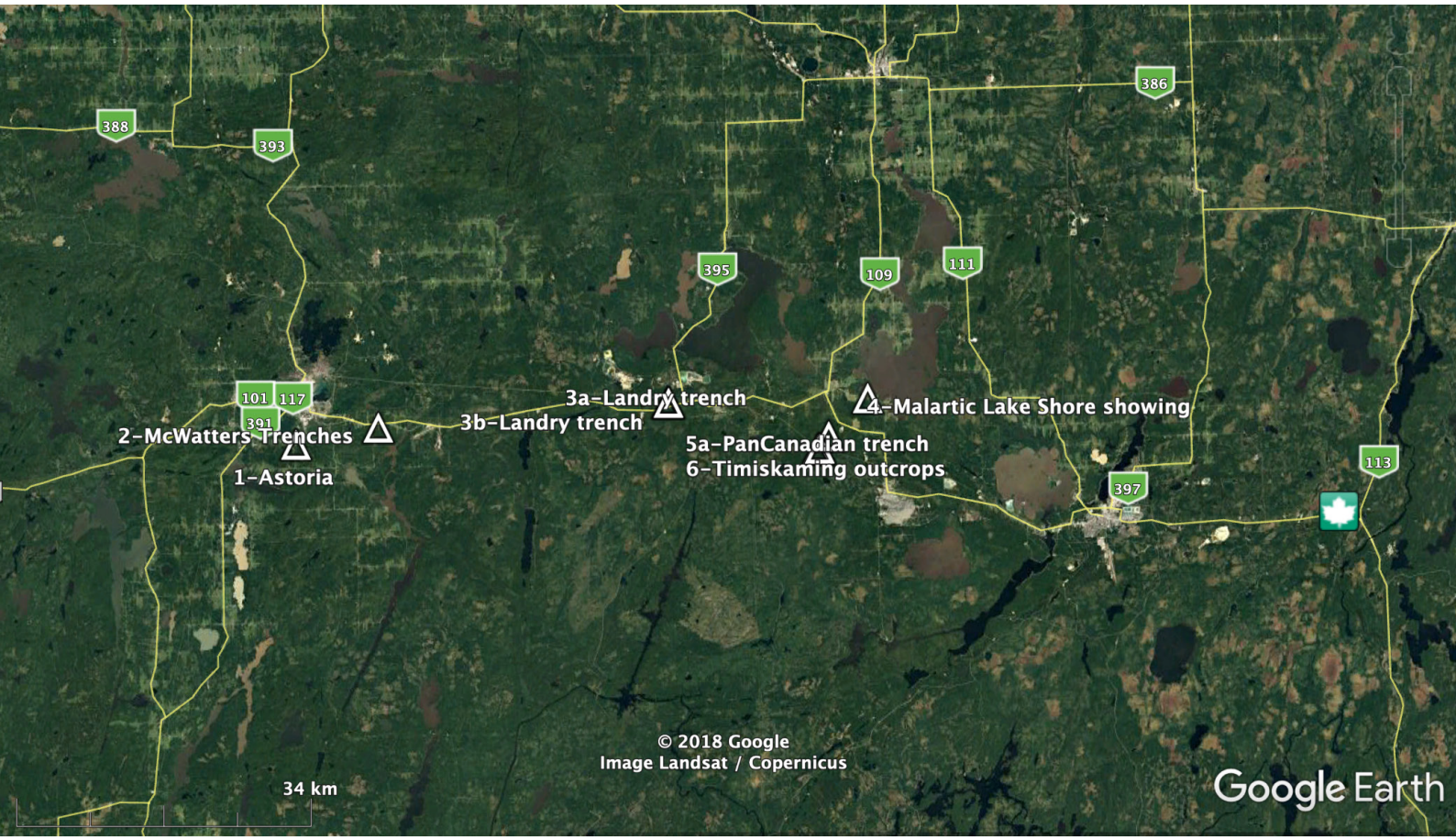

Figure 1: Overview over the field stops focusing on the Cadillac - Larder Lake Fault.

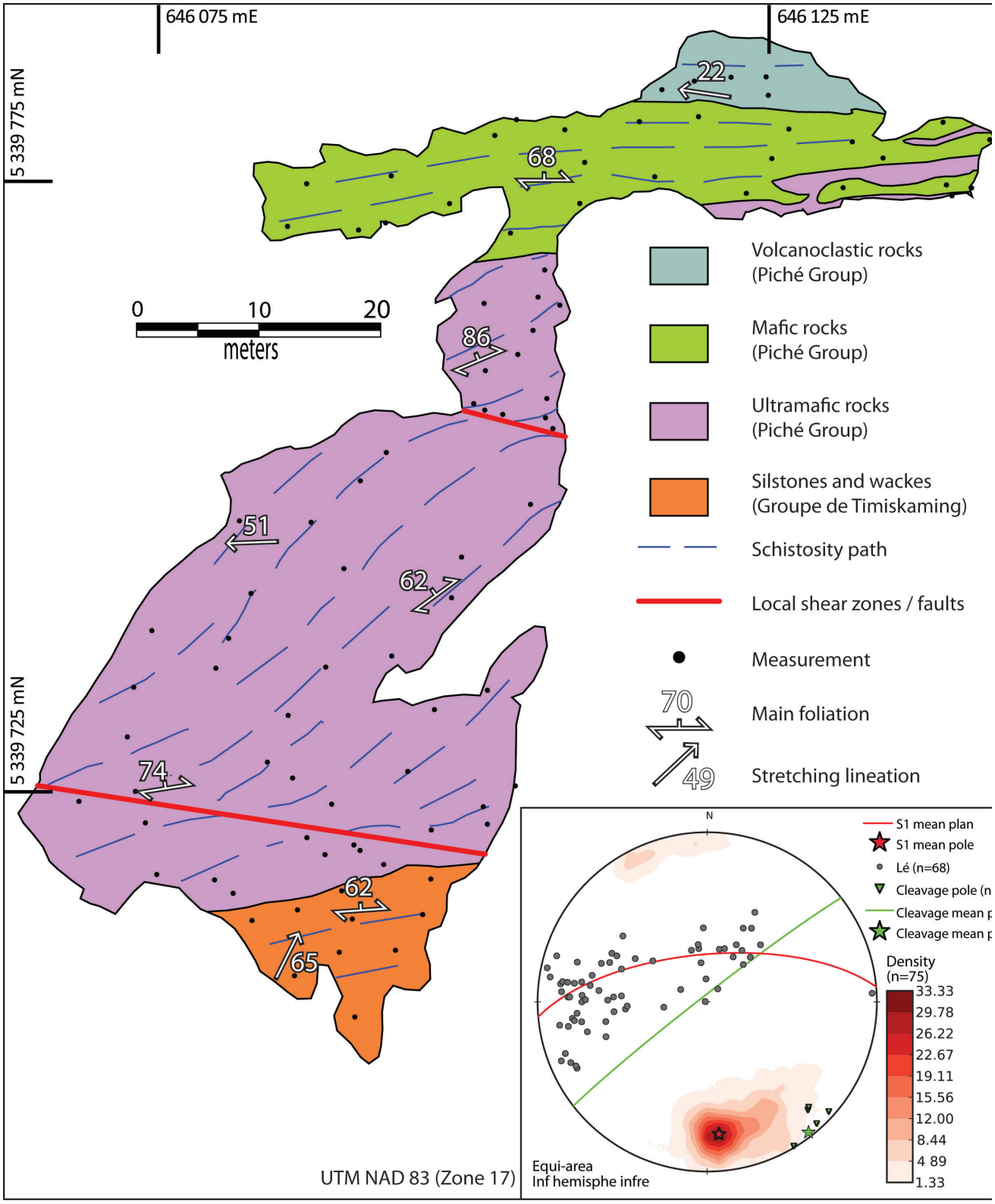

Figure 2: Astoria showing

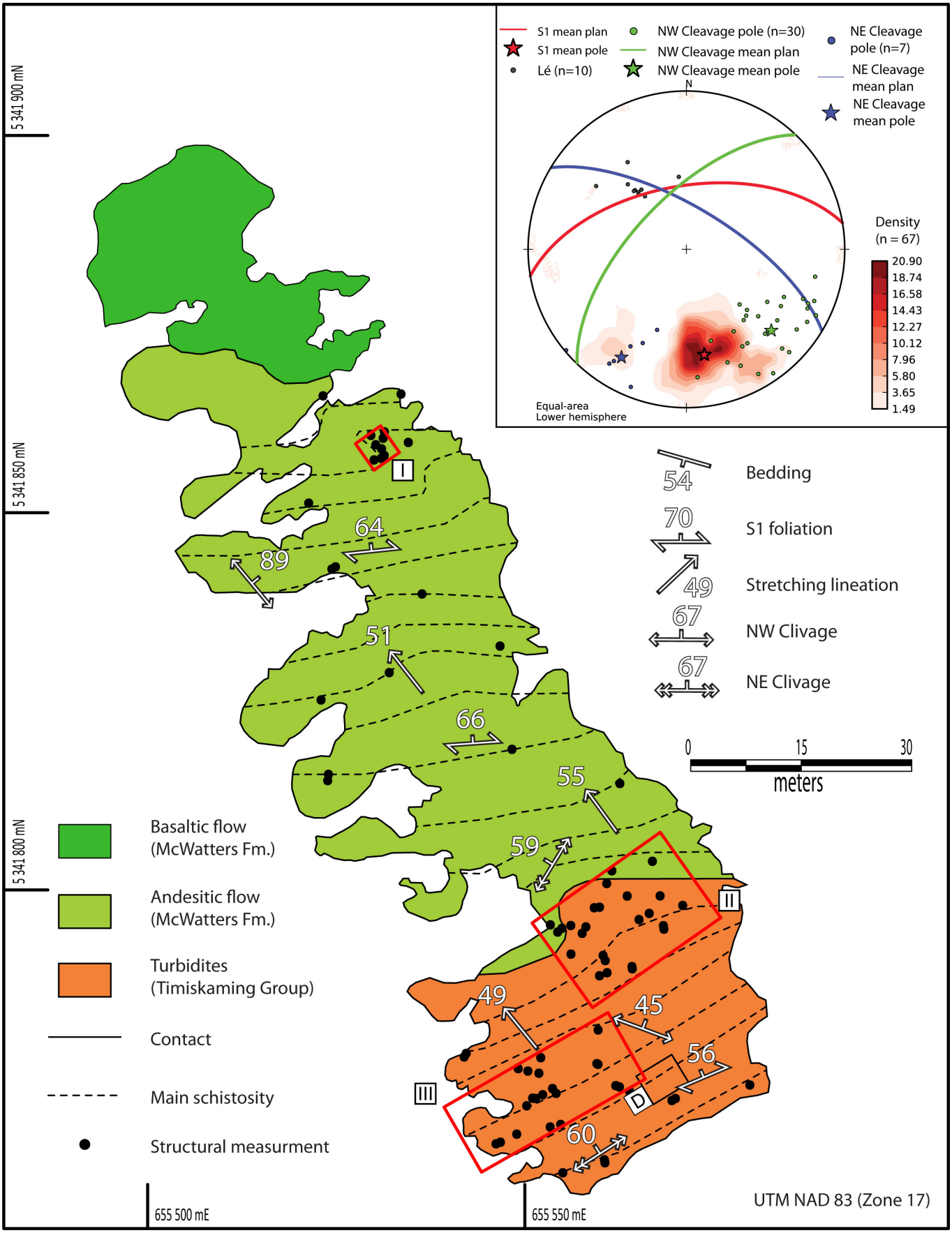

Figure 3: McWatters trench

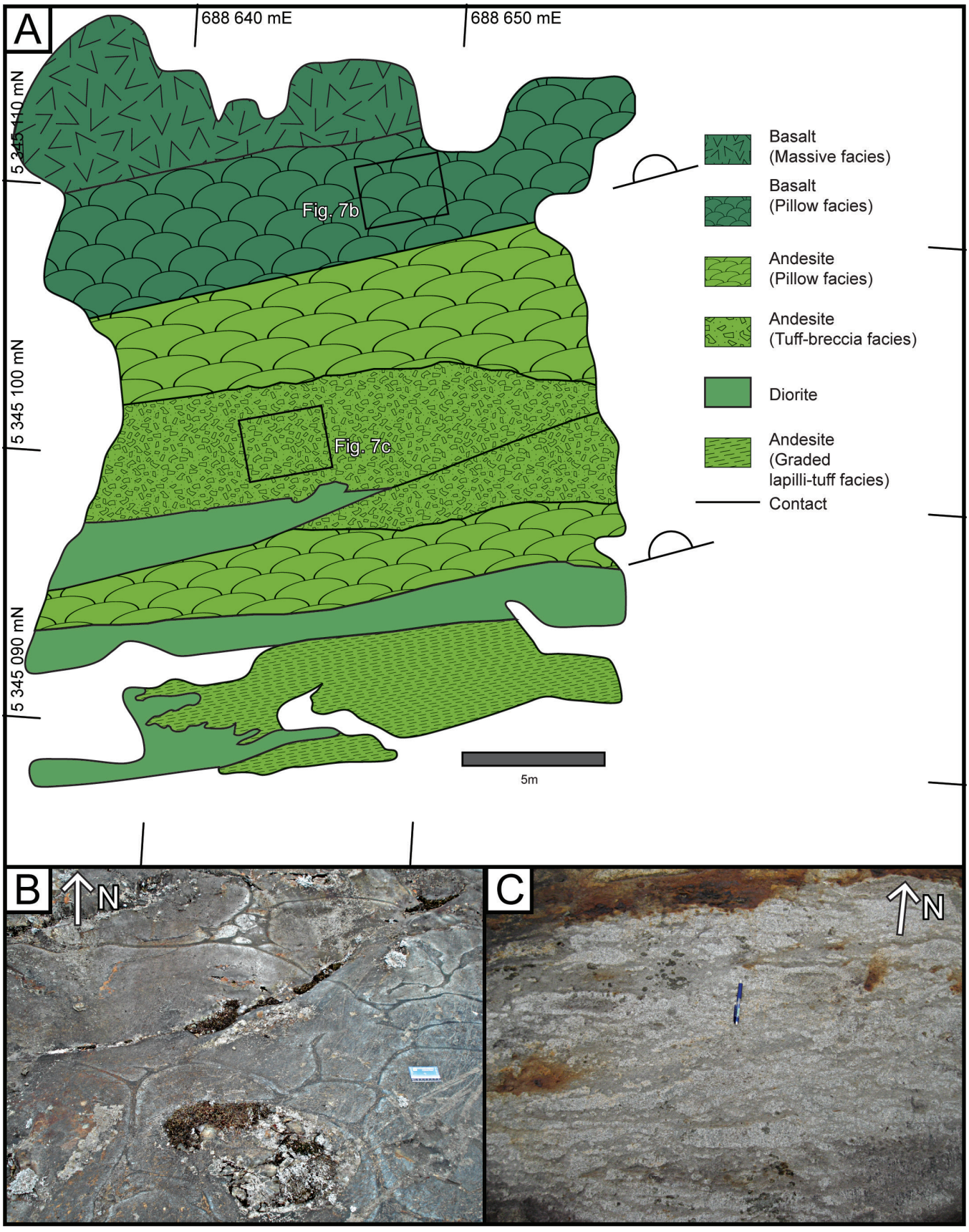

Figure 4: Landry trench

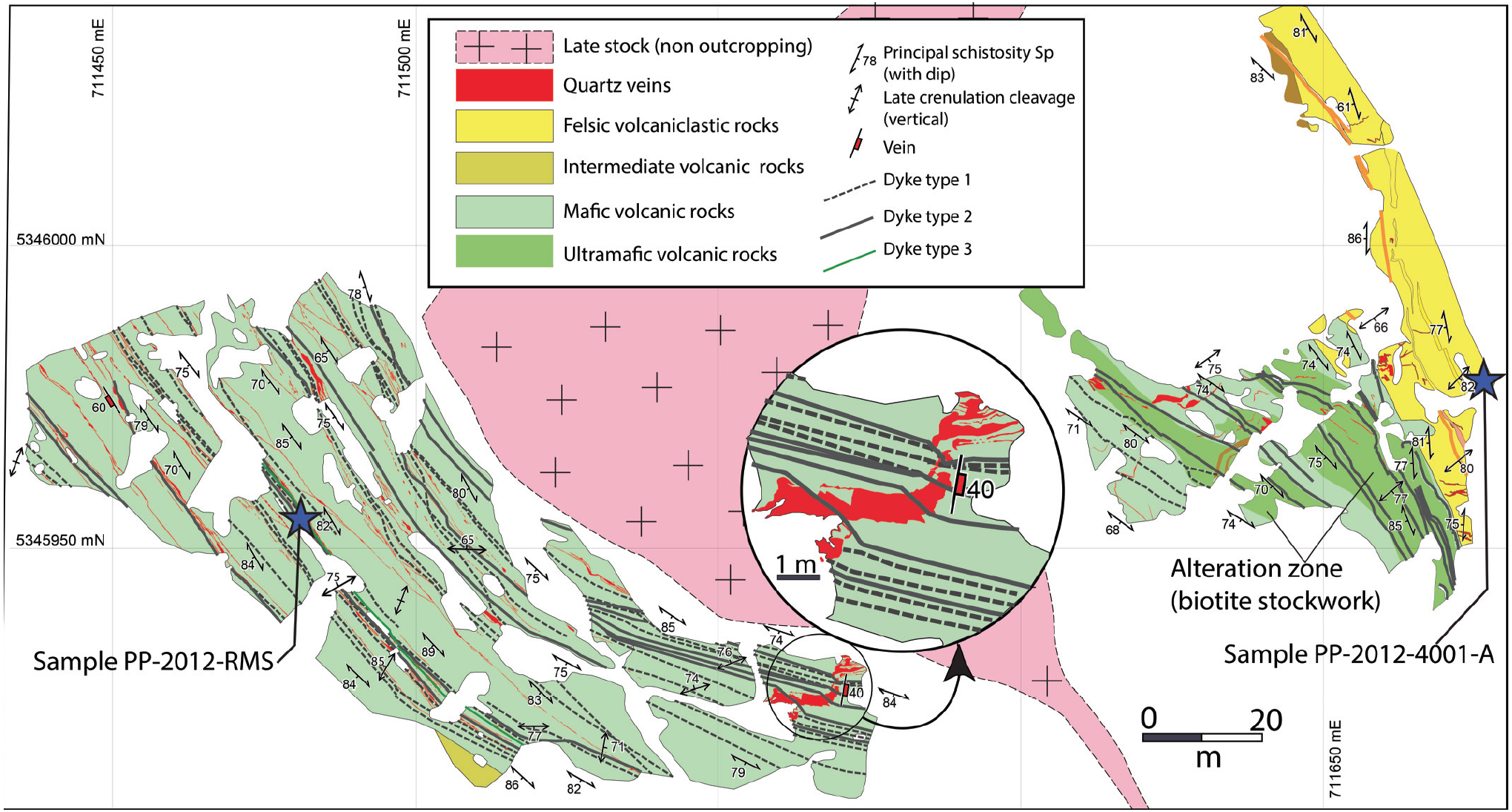

Figure 5: Malartic Lake Shore showing; from Guay et al. (2018).

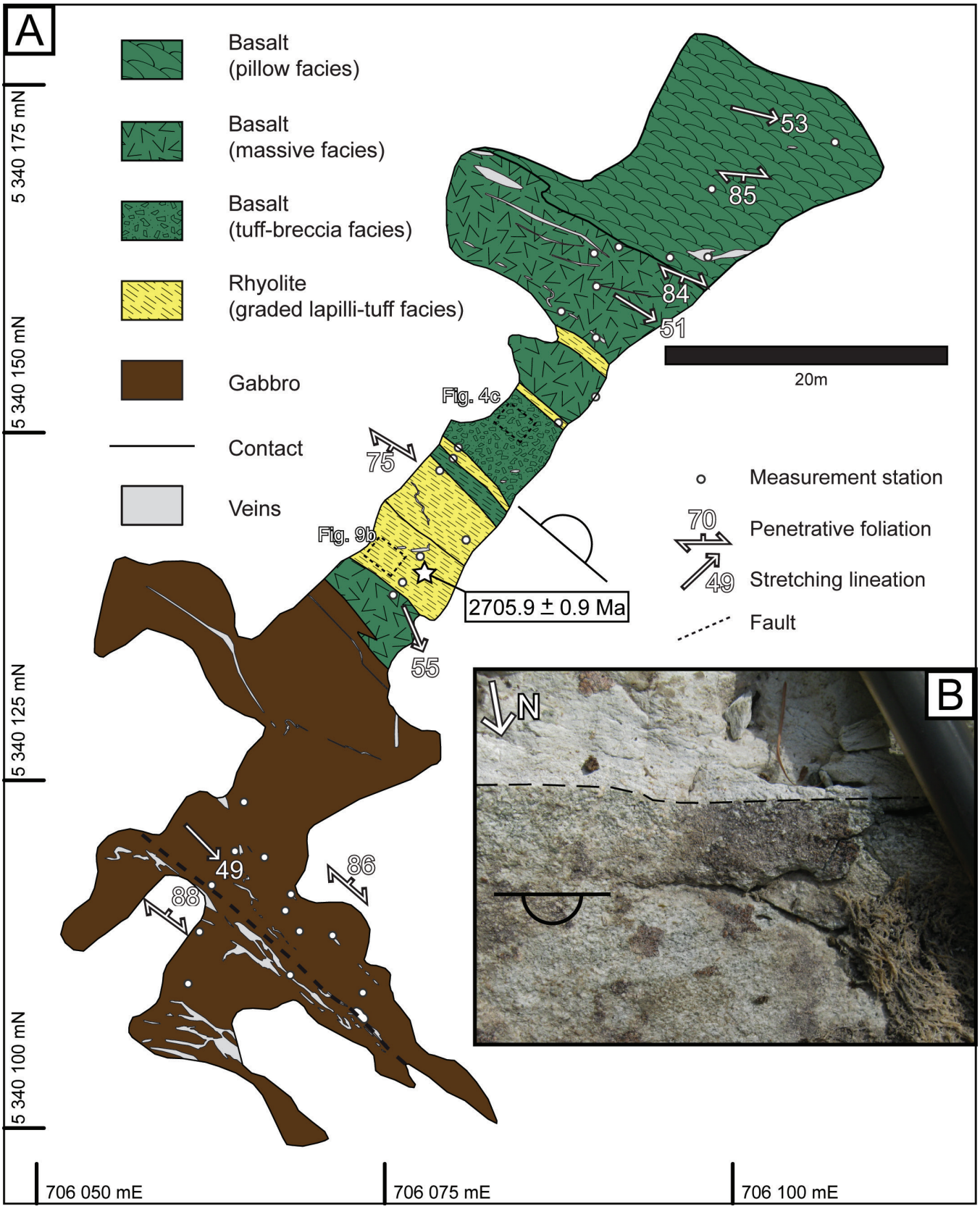
A
Basalt
(pillow facies)
Basalt
(massive facies)
Basalt
(tuff-breccia facies)
Rhyolite
(graded lapilli-tuff facies)
Gabbro
Contact
Veins
Measurement station
Penetrative foliation
Stretching lineation
Fault
20m
Fig. 4c
Fig. 9b
2705.9 ± 0.9 Ma
53
85
84
51
75
55
49
86
88
B
N
5 340 175 mN
5 340 150 mN
5 340 125 mN
5 340 100 mN
706 050 mE
706 075 mE
706 100 mE

Minerals

albite	$NaAlSi_3O_8$
arsenopyrite	FeAsS
aurostibnite	AuSbS
calcite	$CaCO_3$
chalcopyrite	$CuFeS_2$
chlorite	$(Mg,Fe^{2+})_5Al(Si_3Al)O_{10}(OH)$
cubanite	$CuFe_2S_3$
dolomite	$CaMg(CO_3)_2$
epidote	$Ca_2Al_2Fe^{3+}(SiO_4)(Si_2O_7)O(OH)$
galena	PbS
gudmundite	FeSbS
hematite	Fe_2O_3
magnetite	Fe_3O_4
millerite	NiS
pentlandite	$(Fe,Ni)_9S_8$
pyrite	FeS_2
pyrrhotite	$Fe_{(1-x)}S$
quartz	SiO_2
sphalerite	ZnS
stibnite	Sb_2S_3
stilpnomelane	$K(Fe^{2+},Mg,Fe^{3+})_8(Si,Al)_{12}(O,OH)_{27} \cdot n(H_2O)$
tourmaline	$(Ca,K,Na,\square)(Al,Fe,Li,Mg,Mn)_3(Al,Cr,Fe,V)_6(BO_3)_3(Si,Al,B)_6O_{18}(OH,F)_4$
tremolite	$Ca_2MgSi_8Si_{22}(OH)_2$

Some impressions of the field trip

INTERNATIONAL CHRONOSTRATIGRAPHIC CHART

IUGS

www.stratigraphy.org

International Commission on Stratigraphy

v 2018/08

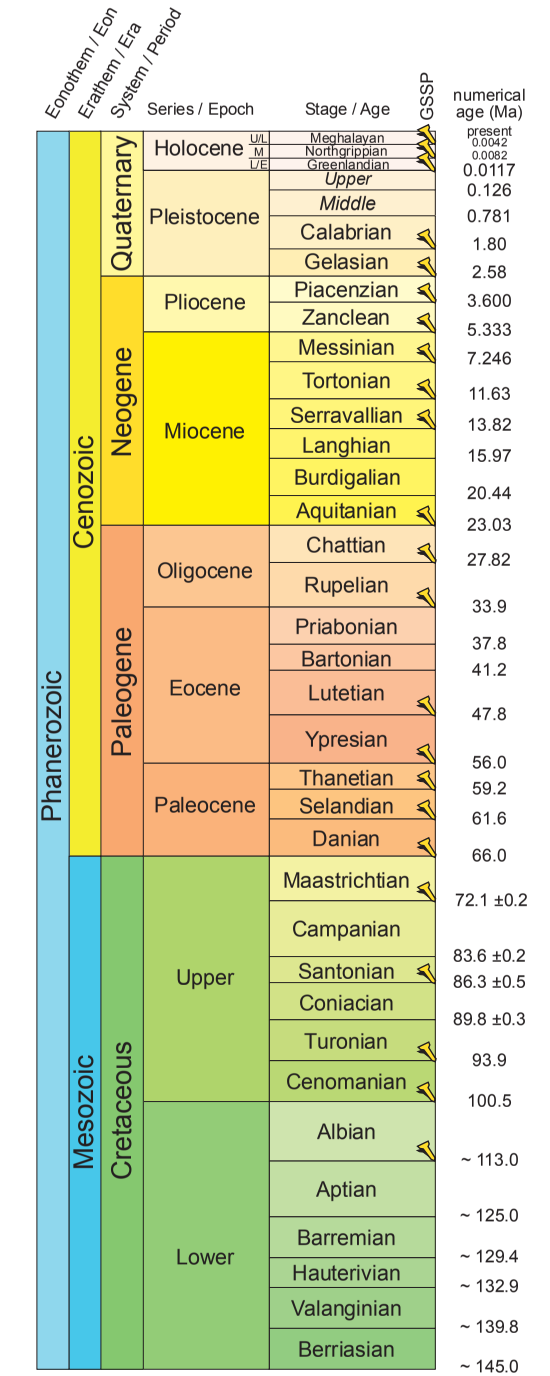

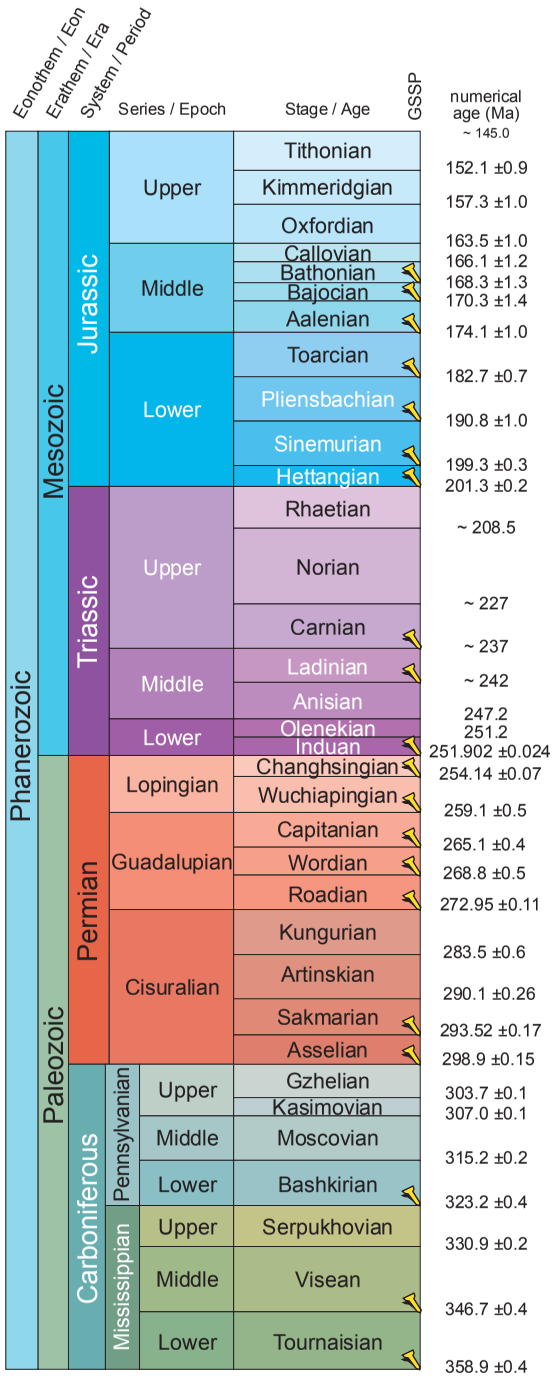

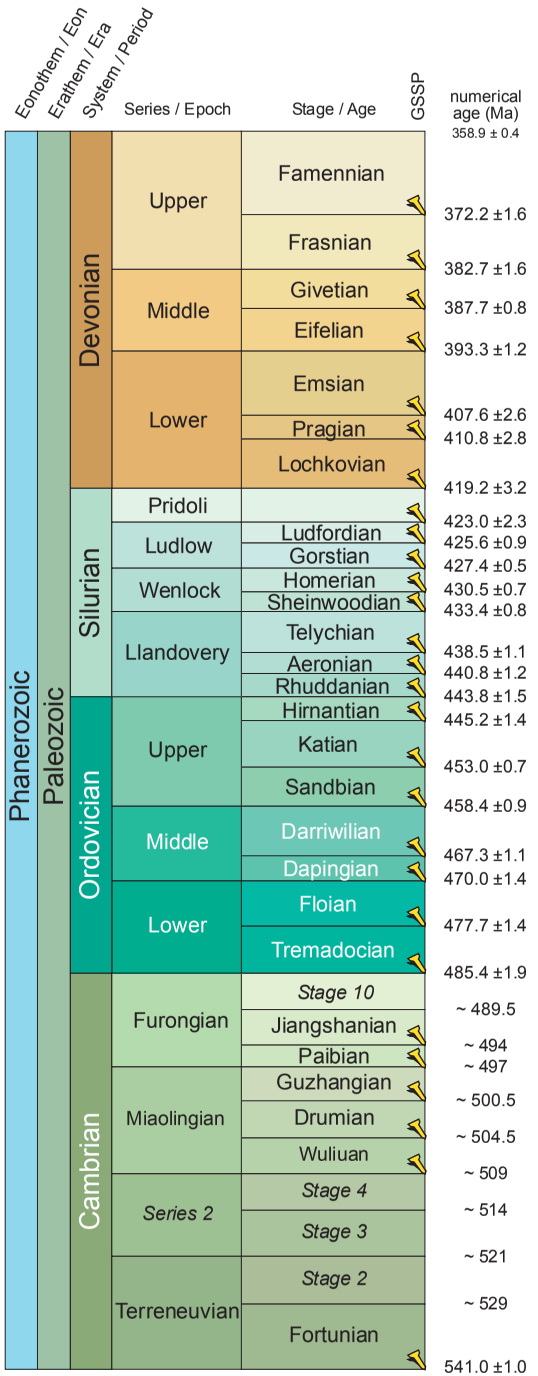

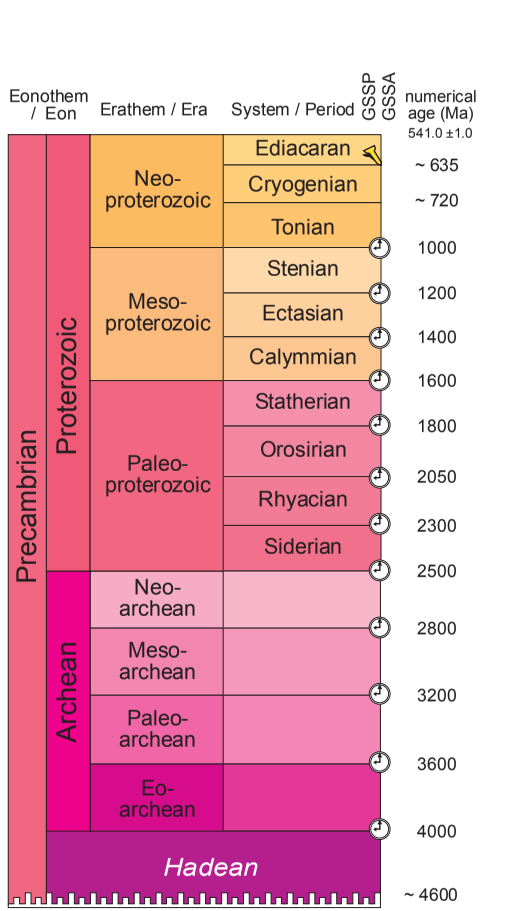

Units of all ranks are in the process of being defined by Global Boundary Stratotype Section and Points (GSSP) for their lower boundaries, including those of the Archean and Proterozoic, long defined by Global Standard Stratigraphic Ages (GSSA). Charts and detailed information on ratified GSSPs are available at the website http://www.stratigraphy.org. The URL to this chart is found below.

Numerical ages are subject to revision and do not define units in the Phanerozoic and the Ediacaran; only GSSPs do. For boundaries in the Phanerozoic without ratified GSSPs or without constrained numerical ages, an approximate numerical age (~) is provided.

Ratified Subseries/Subepochs are abbreviated as U/L (Upper/Late), M (Middle) and L/E (Lower/Early). Numerical ages for all systems except Quaternary, upper Paleogene, Cretaceous, Triassic, Permian and Precambrian are taken from 'A Geologic Time Scale 2012' by Gradstein et al. (2012), those for the Quaternary, upper Paleogene, Cretaceous, Triassic, Permian and Precambrian were provided by the relevant ICS subcommissions.

Colouring follows the Commission for the Geological Map of the World (http://www.cgmw.org)

Chart drafted by K.M. Cohen, D.A.T. Harper, P.L. Gibbard, J.-X. Fan

To cite: Cohen, K.M., Finney, S.C., Gibbard, P.L. & Fan, J.-X. (2013; updated) The ICS International Chronostratigraphic Chart. Episodes 36: 199-204.

URL: http://www.stratigraphy.org/ICSchart/ChronostratChart2018-08.pdf